The Effect of Cooling Rate on the Microstructure and its Influence on Toughness of two Types of Tool Steels Studied by High Resolution Techniques

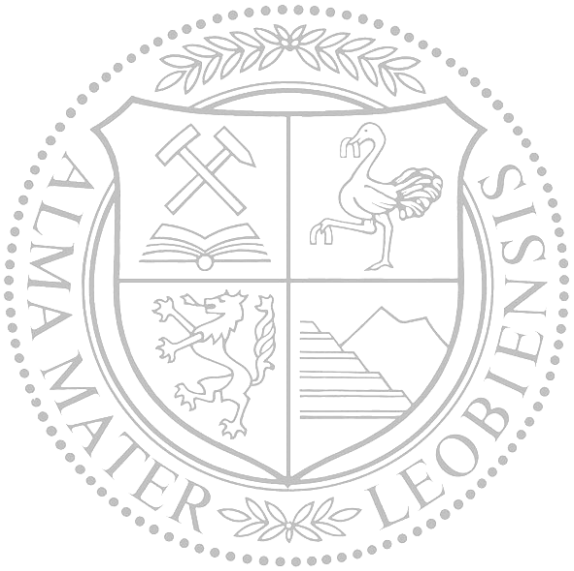

Doctoral thesis

Dipl.-Ing. Christoph Lerchbacher

Accomplished at the Department of Physical Metallurgy and Material Testing of the University of Leoben.

Leoben, April 2013

Affidavit

I declare in lieu of oath, that I wrote this thesis and performed the associated research myself, using only literature cited in this volume.

Leoben, April 2013 Christoph Lerchbacher

Acknowledgments

A lot of persons accompanied me in the last 3 years and have contributed to successfully finish this thesis. Some of them have earned special thanks:

I would like to thank Univ.-Prof. Dipl.-Ing. Dr. mont. **Helmut Clemens**, head of the Department Physical Metallurgy and Materials Testing, for giving me the chance to conduct this thesis on his department.

Most of all, I want to thank my supervisor, Dr. **Harald Leitner**, who gave me the opportunity to work on this research topic in his Christian Doppler Laboratory "Early Stages of Precipitation": Thank you for always supporting me in all fields belonging the thesis and I am sure that your way of guidance positively developed my character. Best wishes for your new challenge in Kapfenberg.

The present thesis has been funded by the company Böhler Edelstahl GmbH & Co KG. I want to thank Dipl.-Ing. **Silvia Zinner** for the productive cooperation. Your friendliness made the trips to Kapfenberg really enjoyable.

Thanks to all my **colleagues** on the department, especially the steel group including the non-scientific staff and some "Thinfilm- and TiAl-friends", for providing such a friendly and helpful atmosphere over the last years.

My student co-workers, **Christina Hofer**, **David Lang** and **Christin Aumayr**, who supported my experimental work, are acknowledged for their help.

Special thanks go to my friends from the "Castle-land" (Burgenland), **Matthias Nöhrer**, **Manfred Schlögl** and **Christopher Pöhl**. A deep friendship developed during the last 10 years being together in Leoben. Thank you for making the whole time really enjoyable, on good days as well as on bad days. I will miss the soccer-events in the "Admiral". In the style of the Musketeers: *"One for All, All for One!"*

My final and special thanks go to my **family** for their everlasting support throughout all my life. Without their encouragement it would have never been possible to finish this thesis.

Contents

Publication III	Retained Austenite Decomposition and Carbide Formation During Tempering a Hot-Work Tool Steel X38CrMoV5-1 Studied by Dilatometry and Atom Probe Tomography
Publication IV	Direct or indirect: Influence of type of retained austenite decomposition during tempering on the toughness of a hot-work tool steel
Publication V	Evidence of pro-eutectoid cementite formation and its influence on impact toughness of the plastic mould steel X38CrMo16

Section A

1. Introduction

In an era where the human being is affected by rapid innovation and the associated technical as well as technological progress, tools are of essential importance. High sophisticated structural components can more or less easily be designed on a paper, but the realisation of such ideas and the feasibility depends on the use of appropriate tools. The wide range of technical components goes hand in hand with a wide range of required tool materials' properties. Therefore, the so-called tool steels cover a variety of carbon and alloyed steels which are suitable for being used as tools. Typical required properties are, amongst others, wear resistance, strength and fracture toughness. One sub group of the tool steel family is the hot-work tool steel group. As already indicated by the group's name, these steels are used for applications at elevated temperatures. Typical applications are the use as die casting equipment mainly for the light alloy processing, forming dies, die inserts or plastic moulding dies. Chromium hot-work tool steels are most frequently used for high-temperature applications. Although hot-hardness is lower compared to molybdenum or tungsten hot-work tool steels, their high toughness and shock resistance make them so attractive for most applications [1]. Martensitic stainless chromium steels are very similar providing increased corrosion resistance which is required for the processing of chemically aggressive plastics.

Beneath a well-balanced chemical composition, a high micro-cleanness and a well-defined heat treatment process determine the outstanding characteristics of these steels. High quality chemical composition and micro-cleanness have been established by improving metallurgical processes in the last decade. Beneath preceding solidification, forging, normalizing and annealing processes, the finalising hardening and tempering treatments control the material properties. Figure 1 schematically depicts the heat treatment steps for hot-work tool steels. Before the hardening treatment a stress relieve procedure with subsequent slow cooling is applied to the tool. The microstructure at that stage consists of a ferritic matrix with coarse spheroidised embedded carbides. Then the tool geometry can be finalised. Several preheating stages are recommended during heating the tool to austenitisation temperature. After a certain dwell time at austenitisation temperature, the tool is rapidly cooled in order to produce a martensitic microstructure. The high alloyed hot-work tool steels provide a good hardenability which also provides a martensitic microstructure at relatively low cooling rates. Air-quenching, oil-quenching or salt-bath quenching is commonly used in industrial processes. The choice of austenitisation parameters as temperature and dwell time is optimized by considering required materials properties and depends on material and application. High austenitisation temperature and long times cause on the one hand an enhanced dissolution of carbides which increases elemental contents within the austenite and allows for an increased

potential for secondary hardening during tempering. On the other hand, austenitic grain size is increased which reduces nucleation sites for the martensitic transformation, hence, leads to a coarser microstructure which negatively influences toughness and strength. Additionally, the higher solute carbon content of the austenite lowers the martensite start temperature which can cause higher amounts of undesired retained austenite within the hardened microstructure. However, the following quenching procedure should be in general fast enough in order to fully transform into martensite. After that, the as-hardened microstructure consists of a supersaturated martensitic matrix with amounts of retained austenite and some primary carbides which have not been dissolved during austenitisation. Low toughness properties caused by the high super-saturation of the martensite lead to the need of a following tempering procedure. Beneath the relaxation of the martensite, tempering leads to the precipitation of high-temperature resistant secondary hardening carbides from the matrix and from the retained austenite. These carbides increase the strength of the material and are responsible for the outstanding high-temperature properties of hot-work tool steels. At least two tempering steps are recommended as after the first tempering step some retained austenite might transform into new untempered martensite which again could lower toughness [2]. However, hardening and tempering parameters have to be assigned individually for each material in combination with its destined application.

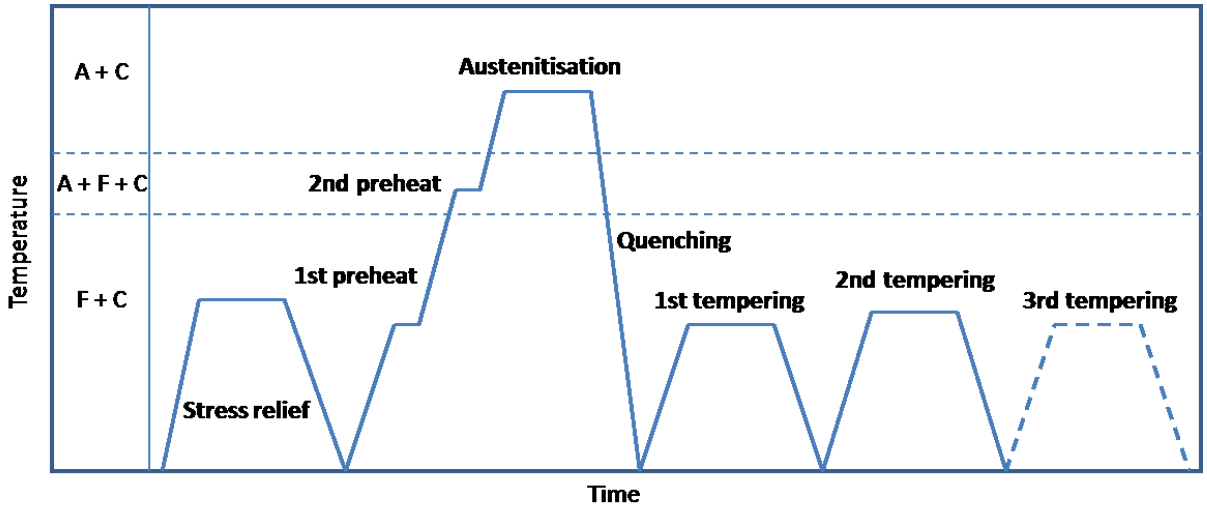

Figure 1: Schematic diagram of tool steel heat treatment steps for final hardening and tempering treatment. Letters A, F, and C correspond to Austenite, Ferrite and Carbide, respectively. After references [1] **and** [3].

A very interesting and promising heat treatment strategy in order to improve mechanical properties is a cryogenic heat treatment after commercial hardening. Nirmal et al. [4] give a review about the investigations on this topic over the last decades. Improvements of hardness, fatigue resistance, toughness and wear resistance are reported. The transformation of retained austenite into martensite during cryogenic treatment plays a major role beneath the precipitation of a fine and homogeneous distribution of secondary carbides. Molinari et al. [5]

could show that a deep cryogenic treatment improves both toughness and wear resistance of a hot-work tool steel AISI H13 which is supported by the work of Konoshlou et al. [6].

However, this is the fabulous theory of heat treatment, not considering technological and process-related difficulties. In order to provide “perfect” material properties just a narrow range of heat treatment parameters is available. In case of large tools, cooling rates and therefore microstructures are not adjustable in any order, which complicates the adjustment of required material properties.

2. Motivation and Background

The demand for larger tools and enhanced material properties by the tool manufacturing industry forces the tool steel producers to improve their materials and processes. As already mentioned, the heat treatment of large blocks does not allow for fast cooling rates during hardening. For tools which have to resist high cycling loads the resistance against crack propagation is the key property. It radically influences tool life which goes hand in hand with costs. Therefore, providing sufficient impact toughness is a major factor in producing tool steels. Tool producers observe heavy losses in toughness at lowered cooling rates during the hardening procedure. Several investigations demonstrated this issue [7–10]. Pro-eutectoid carbide formation and/or the formation of bainite are thought to be responsible for this issue. Corresponding research studies have been conducted, e.g. [11]. A theoretically simple approach to avoid this problem is highest cooling rate during quenching. But this is not achievable for large tools with sections of different cross sections and complicated geometries. Simulations and experiments show the broad temperature distribution and corresponding microstructure distribution within a block during quenching from austenitisation temperature [12]. For a block of 400 x 400 x 400 mm^3 the cooling rate decreases from 29.5 K/s at the block surface to 7.5 K/s in the core, respectively, during quenching with nitrogen at 9 bar [13]. This strong discrepancy in cooling conditions makes one sense that also the microstructure locally varies. Thus, the aim of the present thesis is the identification of those cooling rate dependent microstructural distinctions and their correlation with impact toughness properties.

A first strategy to analyse this problem is the identification of the microstructure related factors which influence the onset and growth of cleavage fracture within steels. These factors are: nucleation of cracks at twins as well as at carbide particles and the grain size. Twins do not play a major role within the investigated steels because the relatively low carbon content leads to the formation of lath martensite which is almost free of twins [14]. The former austenite grain size determines the maximum size of martensitic packets and blocks [15], hence, the toughness controlling “effective grain size” [16]. The low-carbon lath-martensite consists of packets which can be divided into blocks. These blocks are built up by sub-blocks which consist of the single laths. This classification is based on the crystallographic orientation [17]. Morito et al. [18] could show for an Fe-Ni alloy, that the packet size and block thickness decrease with increasing cooling rate during quenching which is a first indication for cooling-rate dependent toughness properties. As the microstructure of tempered medium carbon martensites contains a lot of carbide particles, those are meant to play the major role for the toughness behaviour. In fact, so-called tempered martensite embrittlement

is correlated to the existence of carbides within the microstructure, e.g. [19]. Additionally, grain boundary carbides precipitated during cooling from austenitisation temperature which reduce toughness are reported, e.g. [9]. All these phenomena build the starting point for the route of experimental work and investigations in the present study.

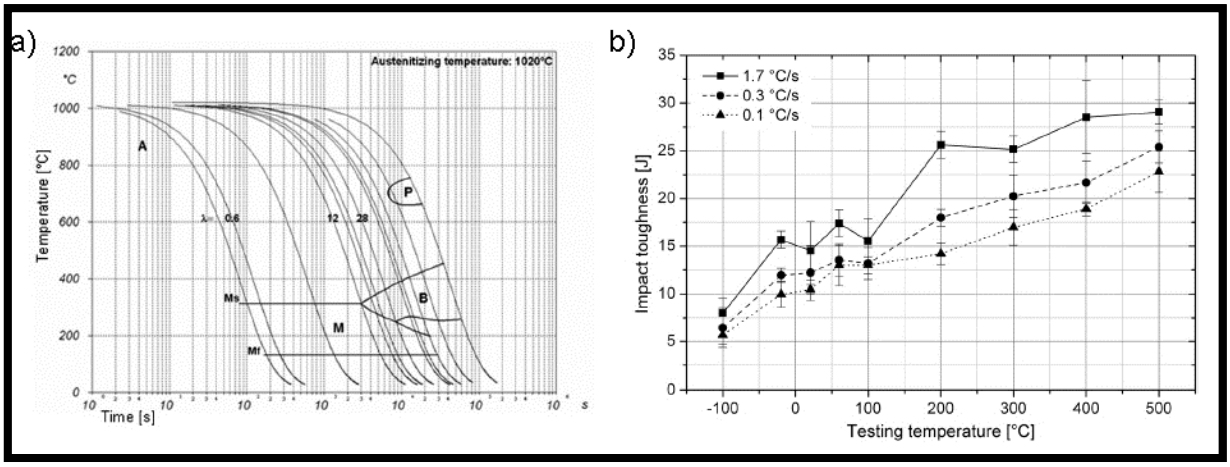

Figure 2: TTT diagram of the hot-work tool steel X38CrMoV5-1. The letters stand for austenite (A), pearlite (P), martensite (M), bainite (B), martensite start temperature (Ms), and martensite finish temperature (Mf) (a); Impact toughness versus testing temperature corresponding to different cooling rates used prior tempering (b). Cooling rates 1.7, 0.3 and 0.1 °C/s correspond to λ values 0.6, 12 and 28, respectively. The graphs have been taken from [10].

Time-Temperature-Transformation-diagrams (TTT) are very useful for the estimation of amounts of microstructural contributions which form during continuous cooling. Figure 2a depicts the TTT-diagram corresponding to the hot-work tool steel X38CrMoV5-1 [10]. The cooling rates are indicated by parameter λ. This parameter is defined as the cooling time from 800°C to 500°C divided per hundred in seconds and is commonly used in heat treatment factories because it simulates the real cooling paths within a part in a more accurate way. The diagram demonstrates the high hardenability of this steel as the transformation during hardening is purely martensitic up to a cooling rate $\lambda = 12$. However, even in the martensitic range, cooling rate dependent impact toughness values are observed, showing lower values at low cooling rates as demonstrated in Figure 2b [10].

The aim of the present work is the identification of the microstructural origin of this cooling rate dependent material behaviour within the purely martensitic range. After identification, approaches for solving the problem should be offered and evaluated. For this, two different tool steels showing similar cooling rate dependent toughness behaviour have been investigated. First, chromium hot-work tool steel X38CrMoV5-1, and second, plastic mould steel X38CrMo16 (0.27 wt% C and 0.1 wt% N). Therefore, cooling rate dependent microstructural distinctions after hardening and their influence on the following tempering behaviour have been investigated with the focus laid on the formation of early carbide structures. This issue is handled in Publications I-III and V. Publication IV deals with an approach to improve toughness on the basis of the results according to Publications I-III.

3. Microstructure-Toughness Relationship of Tool Steels

Tool steel producers and vendors provide in the datasheets corresponding to their products Time-Temperature-Transformation-diagrams in order to provide information for the customer on the microstructural changes of the material during the hardening process. From those, critical cooling rates can be determined. However, TTT-diagrams corresponding to the tool steels DIN 1.2343 (hot-work tool steel X38CrMoV5-1) and 1.2316 (plastic mould steel X38CrMo16), which have been investigated in the present thesis, of different suppliers show slight differences. These differences can be a result of varying elemental contents within the tolerances and of differing austenitisation temperatures and times. On the other hand, variations of data evaluation and misinterpretations can result in such differences. As an example, in case of the mentioned hot-work tool steel X38CrMoV5-1 all considered TTT-diagrams show the typical martensitic transformation at high cooling rates and the additional bainitic transformation at lower cooling rates [3, 20–22]. The start of the bainite formation ranges from cooling rates 1.5°C/s to 0.25°C/s. Additionally, some datasheets show dashed lines in the austenitic range indicating carbide precipitation during cooling [20–22]. The existence or non-existence of these carbides might play a significant role considering the toughness properties of the material. In case of the plastic mould steel X38CrMo16 all considered datasheets show the previously mentioned carbide precipitation [23–25], but the low-temperature transformation at low cooling rates is on the one hand determined to correspond to bainite [23] and on the other hand to so-called grain-boundary martensite [25]. The existence of this grain boundary martensite has been reported to form due to a preceding carbide precipitation at the grain boundaries during cooling of the austenite [26]. Due to the grain boundary carbides the grain boundary near regions are depleted in carbon, hence, lead to increased martensite start temperatures for these regions.

However, the intention to correlate toughness properties with the microstructure after the hardening process demands for a detailed knowledge of the formation and appearance of the microstructural components.

3.1. Formation and Appearance of the As-quenched Microstructure

The as-quenched sample state is defined as the microstructure after cooling from austenitisation temperature, hence, after the hardening process. Hardenability is often called a sign of quality concerning tool steels. A comprehensive definition says: “Hardenability is

usually defined as the capacity of a steel to transform partially or completely from austenite to some percentage of martensite at a given depth when cooled under some given conditions. Hardenability is, therefore, dependent upon the nucleation and growth of the non-martensitic products, the austenite grain size which affects the nucleation sites, and the effect of alloying elements on nucleation and growth" [27]. This implies that the desired microstructure, regarding strength, is predominantly martensitic. The microstructural evolution during hardening depends on the chemistry of the austenite during austenitisation and on the cooling conditions. Empirical equations describe the dependence of the martensite start temperature of the austenite composition for medium carbon steels [28]. During cooling there exists a competition between athermal martensitic transformation and diffusion controlled processes. For a given alloy and given austenitisation parameters, diffusional processes can only be suppressed by high cooling rates.

However, even when the transformation is "fully" martensitic, diffusion controlled processes take place during further cooling within the martensitic microstructure. This phenomenon, most likely observed for materials with high martensite start temperatures, is usually termed auto-tempering [15]. Carbon segregation, carbon cluster formation and carbide precipitation count for this. In the early comprehensive studies on martensite these carbon segregations have been predicted by conducting electrical resistivity and internal friction experiments [29].

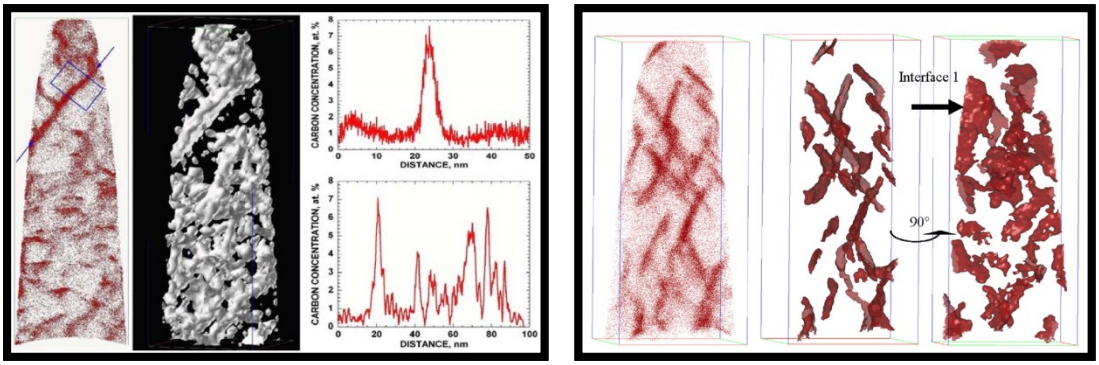

Figure 3: Carbon atom map and the corresponding 1.3 at% carbon iso-surfaces obtained by atom probe tomography from a high silicon martensitic medium carbon steel specimen quenched with 560 K/s and aged at 22°C (Left). Image taken from [30]**. Carbon atom map and carbide interfaces (rotated 90°) for a Fe-Ni-C alloy quenched from 1150°C into liquid nitrogen and tempered at room temperature (22°C) for 1000 h. The interfaces are defined by iso-surfaces of 4 at% C (Right). Image taken from** [31]**.**

High resolution analytical characterisation methods make such carbon segregations nowadays relatively easily and quantitatively measurable. Sherman et al. [30] showed carbon clusters within the microstructure of a martensitic medium carbon high silicon steel after quenching with cooling rates of 560 K/s and 25 K/s by means of atom probe tomography. The investigated steel X38CrMoV5-1 belongs to this steel group and those auto-tempering effects could also be demonstrated in the present study. Similar to that, several studies dealing with the carbon segregation during the early stages of tempering depict the presence of such features by means of atom probe tomography. Regarding these carbon features the early

stages of tempering of low Ms steels are equal to the as-quenched microstructure of steels with higher martensite start temperature. Studies on FeC martensites [32], FeNiC martensites [31,33], FeCMnSi TRIP steels [34,35] or FeCCrMo low alloy steels [36] report such carbon segregations. Wilde et al. [37] showed a 3-dimensional mapping of carbon around dislocations in iron and stated a carbon concentration of approximatley 8 at% in the core of the dislocations. Zhu et al. [31] demonstrated the formation of carbon rich clusters within a FeNiC and commercial AISI 4340 steel during low temperature aging and proposed carbon levels of 10 at% within those clusters. Figure 3 shows on the left hand side the carbon distribution in a martensitic matrix of a high silicon medium carbon steel after quenching with 560 K/s. Cluster formation is obvious over the full probed volume [30]. On the right hand side, carbon clusters are visualized corresponding to a FeNiC martensite tempered for 40 hours at 350°C. Preferred growth directions can be seen as well [31]. Hutchinson et al. [38] investigated the as-hardened microstructures of commercial steels containing 0.1 to 0.5 % of carbon. This work demonstrates that the carbon amount existing in solid solution is extremely small and independent of the overall carbon content of the alloy. Carbon redistribution to intra-lath dislocations and lath boundaries has been found to provide the major contribution to the materials' strength. This study does not account for retained austenite within the as-quenched microstructure. Beneath the comprehensively discussed auto-tempering effects carbon redistribution to the retained austenite takes place during the martensitic transformation. The retained austenite predominantly occurs as films between martensitic laths [39].

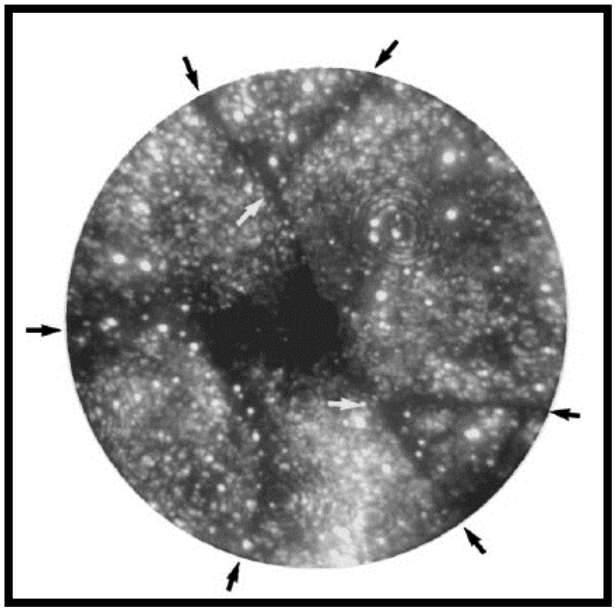

Figure 4: A neon field ion micrograph (FIM) of a FeCCrMo steel tempered for 40 h at 350°C. The dark bands across the images have been identified from atom probe analysis as being enriched in carbon, hence, being carbon enriched ultra-thin retained austenite films [36].

Carbon enriched ultra-thin films characterised by atom probe tomography have been reported for several steels [36,40,41]. Sherman et al. [30] reported a carbon concentration of approximately 6-7 at% within the retained austenite films in the as-quenched microstructure of a martensitic medium carbon high silicon steel. Such a film is shown on the left hand side of Figure 3, marked by the blue arrows. The corresponding carbon concentration profile reveals the 6-7 at%. In Figure 4 an image recorded by field ion microscopy demonstrates the occurrence of carbon enriched films within a FeCCrMo low alloy steel. These carbon enriched films again are attributed to ultra-thin interlath retained austenite films [36]. Figure 5 shows the carbon atom map corresponding to an as-quenched X38CrMoV5-1 steel sample investigated in Publication II of the present study. The carbon atom map is a typical representative for samples quenched with high cooling rates during hardening [42]. The inhomogeneous carbon distribution within the probed volume is obvious. Martensitic laths with different carbon segregation levels can be seen and the nanometric interlath retained austenite films have a carbon content of approximately 10 at%. In Publication II of the present thesis it is reported that the mean thickness of those films depends on the cooling rate during quenching [42]. Lower cooling rates lead to a higher amount of retained austenite [11] which goes hand in hand with a thickness increase of the interlath films. The demonstration of the thickness increase of the interlath retained austenite films and the evaluation of film-thicknesses for this steel at that cooling rate level has been done for the first time in the present study, as picked out as a central theme in Publications I and II [42,43]. The stabilisation of the retained austenite by carbon partitioning during cooling is a not welcome effect for this type of steels since the desired microstructure is fully martensitic. On the other hand, for some steels this effect is forced by a so-called quenching and partitioning treatment, e.g. [44]. Atom probe studies on those steels do also inform about distribution and carbon contents of the different phases within those steels [45–49]. However, cooling rate dependent mean levels of carbon segregation are expected, but a confirmation is nearly impossible due to the small volume probed by atom probe and, therefore, low statistics. Additionally, martensitic laths formed at different temperatures show different segregation levels, which complicate the definition of a segregation level corresponding to a special cooling rate.

Summarized, the as-quenched microstructure of martensitic medium carbon steels contains martensitic laths of varying carbon segregation levels, hence, varying levels of carbon in solution, depending on the temperature when they have been formed. The martensitic laths are surrounded by carbon enriched retained austenite films. The most significant cooling rate dependent microstructural change is an increase of the amount of the retained austenite which goes hand in hand with a thickness increase of the carbon enriched interlath films. This thickness increase has been shown in the present study.

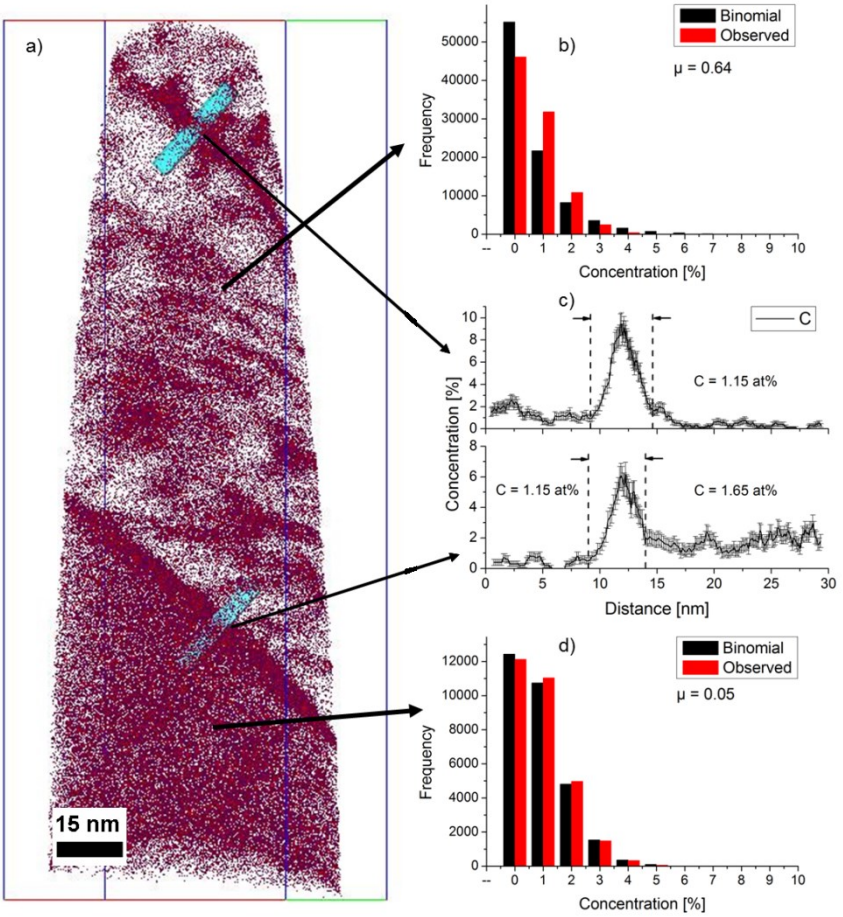

Figure 5: Carbon atom map of a hardened X38CrMoV5-1 sample quenched with cooling rate λ = 0.3 as a typical representative for fast quenched samples, recorded by atom probe tomography (a); Frequency distribution of carbon atoms corresponding to the heavily segregated region inside the probed volume (b); Carbon concentration profiles in the cubes' z-directions through the two interlath retained austenite films (c); Frequency distribution of carbon atoms corresponding to the homogeneous region inside the probed volume (d). Taken from Publication II [42].

3.1.1. Role of Silicon during Hardening

Hot-work tool steels are produced with varying silicon contents. In the last decades, the reduction of silicon has been implemented in order to improve toughness properties. Therefore, the role of silicon in hot-work tool steels regarding toughness is discussed.

Silicon has been long known to retard the cementite formation in low alloy medium carbon steels [50]. The reason for this retardation is the negligible small solubility of silicon in cementite. Formation energies for Fe_3C and its corresponding silicon substituted forms have been estimated using first-principles calculations [51]. The trapping of silicon is thought to reduce the driving force for precipitation. Trapping means that the cementite is forced to inherit the silicon present in the parent phase, which is hindered due to the low solubility [52]. Retardation becomes prominent at low temperatures where atomic mobility of silicon is limited, as it is the case for the auto-tempering range of the investigated tool steels. The low silicon variant of the hot-work tool steel X38CrMoV5-1 shows Fe_3C precipitates within the

as-quenched microstructure [11] in contrast to the high silicon variant where carbon clustering is observed as demonstrated in Figure 5. Atom probe experiments within the present study, which have not been published, confirm this. Due to the Fe_3C formation the matrix depletes more and more in carbon during the martensitic transformation. This fact might explain the lower amount of retained austenite within the microstructure of the low silicon variant as found in [11]. Contrary to that, Mesquita et al. [53] propose that the as-quenched microstructure is not influenced by the silicon content. This is due to the high quenching rates during hardening which they have used for their experiments. In this case also the high silicon variant shows a very low amount of retained austenite.

Summarized, high silicon contents lead to carbon cluster formation during auto-tempering. At low cooling rates, this causes higher amounts of retained austenite. This is due to a higher carbon supersaturation of the martensitic matrix compared to low silicon contents where Fe_3C precipitates are formed.

3.2. Tempering of FeC Martensites

The well-balanced mechanical properties of hardened and tempered steels lead to a voluminous set of investigations on the microstructural reactions occurring during tempering. Speich and Leslie [29] gave an extensive review on the work done on this subject before 1972. Basic tempering processes in iron-carbon martensites as carbon segregation, the precipitation of carbides, the decomposition of retained austenite and the recovery and recristallisation of the martensitic microstructure are discussed. Olsen and Cohen [54] critically assessed the experimental data on tempering kinetics obtained in literature by various experimental techniques such as X-ray diffraction, electrical resistivity measurements, transmission electron microscopy and atom probe tomography. Successful comparability of the results which have been gained by varying experimental parameters has become possible by introducing a normalized carbon diffusion time.

In accordance with newer studies, the isochronal tempering of iron-carbon martensites can be classified into the following stages [55]: Stage 0 tempering (-200°C – 100°C) is characterized by pre-precipitation processes like carbon segregation to dislocations, cluster formation and/or the formation of coherent transition carbides. Stage I tempering (80°C – 200°C) is the precipitation of transition carbides (Ɛ or ŋ carbide). Stage II (200°C – 350°C) comes along with the decomposition of retained austenite. Stage III (250°C – 350°C) is the transformation of transition carbides and carbon clusters into the more stable cementite. In case of alloyed steels, alloy carbide formation takes place at higher temperatures, called Stage IV. The martensitic matrix depletes in carbon and loses its tetragonality, hence, approaching a ferritc matrix during tempering.

Temperature ranges of the corresponding reactions depend on the elemental composition of the alloy and on the hardened martensitic microstructure. Plain carbon steels, which have martensite start temperatures considerably above room temperature, show tempering effects even during hardening, called auto-tempering. Those reactions are supressed during hardening in Fe-Ni-C martensites which have martensite start temperatures far below room temperature and which are preferably used for recent tempering studies.

The precipitation of transition carbides does not take place in steels with carbon contents lower than 0.2 wt% because this amount of carbon is trapped at dislocations and carbon clusters within the martensitic microstructure [29]. Transition carbides have been identified as both hexagonal Ɛ carbide [56] and also as orthorhombic ŋ carbide [57]. However, at present there are some uncertainties in the understanding of structural changes occurring in the first stages of tempering, especially the formation of transition carbides.

The decomposition of retained austenite, tempering Stage II, is often described as the transformation into ferrite and cementite [29], or into bainite [58]. Van Genderen et al. [59] proposed a preceding ferrite formation before the final transformation into ferrite and cementite takes place.

Stage III, the formation of cementite, predominantly takes place at the interface matrix/transition carbide, showing the common Bagaryatski orientation relationship. At higher temperatures the rod-shaped cementite coarsens and becomes spherical [15].

Alloying elements influence the appearance of the tempering reactions and transfer them to higher temperatures. Additionally, carbide forming elements as chromium, molybdenum or vanadium form secondary carbides at elevated temperatures which are responsible for the outstanding mechanical properties of hardened and tempered steels.

Figure 6 examplarily shows the tempering reactions of an FeC martensite recorded by differential scanning calorimetry (DSC) [59]. In the corresponding study, the carbon redistribution processes are divided into two successive ways (Stages I and II). The formation of transition carbides (Stage III), the decomposition of retained austenite (Stage IV) and the precipitation of cementite (Stage V) are clearly visible. Tempering reactions obviously can overlap, which might complicate their accurate determination.

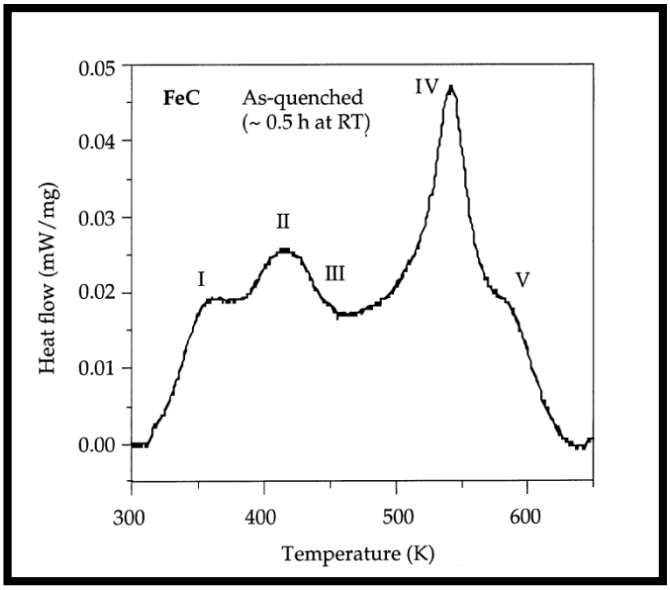

Figure 6: DSC curve of an as-quenched FeC (4.31 at% C) martensitic specimen (heating rate = 10 K/min). Stage I: carbon enrichment; Stage II: periodic arrangement of enrichments; Stage III: ε/η precipitation; Stage IV: decomposition of retained austenite; Stage V: cementite formation from transition carbides. Taken from Ref. [59].

3.2.1. Tempering of Hot-Work Tool Steels and Secondary Hardening

In high alloyed steels tempering is not only used for increasing toughness but also for the formation of a dispersion of stable alloy carbides which increase hardness, referred to as secondary hardening, and which are resistant to coarsening during exposure to high temperatures [1]. The precipitation behaviour is traditionally demonstrated by plotting the hardness over the tempering temperature. Figure 7 exemplarily depicts the hardness curve corresponding to the hot-work tool steel X38CrMoV5-1 as it is given in the BEG (Böhler Edelstahl GmbH & Co KG) product brochure [3]. The hardness increase comes from the formation of secondary carbides during the 2 x 2 hours tempering treatment. Due to the low diffusivity of the substitutional carbide forming elements, the formation of precipitates only takes place at elevated temperatures (approximately 400 to 600°C). Typical nucleation sites are pre-existing cementite particles, dislocations within the matrix and grain boundaries such as former retained austenite grain boundaries and martensite (ferrite) lath boundaries. The strong carbide formers as molybdenum, tungsten, chromium or vanadium lead to characteristic precipitation sequences. Molybdenum and tungsten do predominantly form fine rod-shaped hexagonal M_2C precipitates which are replaced by coarser cubic M_6C carbides at higher temperatures. The face centred cubic vanadium carbide VC is typical for vanadium alloyed steels. Small VC platelets which nucleate on dislocations within the martensitic (ferritic) matrix produce a marked secondary hardening effect. In chromium steels the precipitation sequence is as follows: $(Fe,Cr)_3C \rightarrow Cr_7C_3 \rightarrow Cr_{23}C_6$. The hexagonal Cr_7C_3 precipitates at the F_3C/α interface. Due to the higher diffusivity of chromium compared to

vanadium or molybdenum these precipitates coarsen more rapidly. The formation of $Cr_{23}C_6$ at higher temperatures takes place by separate nucleation and growth at the expense of Cr_7C_3, predominantly at former austenite grain boundaries and at ferrite lath boundaries. In complex alloy steels the corresponding precipitates do also contain contributions of the other carbide forming elements [15].

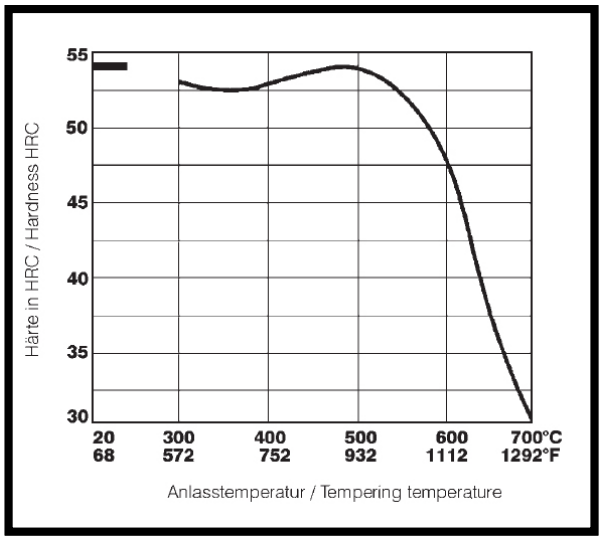

Figure 7: Tempering chart corresponding to the hot-work tool steel X38CrMoV5-1 after tempering 2 x 2 hours. Hardening temperature was set to 1020°C. Taken from Ref. [3].

A lot of such information originates from several studies which focus on the investigation of the precipitation behaviour of high speed steels during tempering by means of high resolution techniques such as transmission electron microscopy, small angle neutron scattering and atom probe tomography, e.g. [60–66].

Mayer [11] found round MC (3-7 nm), elliptical M_2C and facetted M_7C_3 (25-37 nm) precipitates after 2 x 2 hours tempering at 610°C in a hot-work tool steel X38CrMoV5-1, the alloy investigated in the present thesis. Delagnes et al. [67] propose the sequence of precipitation in AISI H11 steel, which is equivalent to the X38CrMoV5-1 steel grade. After hardening they found MC, $M_{23}C_6$ and M_3C, probably not dissolved during austenitisation. After tempering at 550°C four types of carbides have been identified: facetted hexagonal CrFe-carbides (M_7C_3 type), large globular face centred cubic (fcc) CrFe-carbides ($M_{23}C_6$ type), elongated orthorhombic FeCr-carbides (M_3C type) and small globular fcc V-carbides (MC type). After a second tempering sequence, at temperatures above the maximum hardness peak, two populations of carbides could be identified: small carbides in the size range of 6 nm including mainly vanadium carbides and a smaller quantity of chromium carbides, and a population in the size range of 20-40 nm including both chromium and vanadium carbides and a few iron carbides.

However, beneath the secondary carbide precipitation, the decomposition of retained austenite plays an important role for the final appearance of the microstructure. In Publication III of the present thesis [68] it was shown by conducting dilatometry and atom probe tomography experiments that no transition carbide formation takes place during isochronal heating to tempering temperature of X38CrMoV5-1 steel and that cementite precipitation occurs in the temperature range from 450°C to 550°C. The corresponding reaction is indicated by a volume decrease of the sample during heating to tempering temperature as depicted in the red heating curve in Figure 8a. At lower temperatures, no reaction does exist which comes along with a volume decrease, and therefore, might correspond to epsilon carbide formation. Although it cannot be seen in the dilatometer curve, alloy carbide formation and accompanying carbon depletion of the retained austenite takes place during heating to tempering temperature, as demonstrated in Publication III [68]. Figure 8b depicts the relative length change during subsequent tempering at 610°C. In the first 25 minutes carbide formation within the matrix and within the retained austenite takes place, indicated by a volume decrease. After that, the retained austenite decomposes into ferrite and cementite, coming along with a volume increase, with its extent depending on the amount of retained austenite. This is discussed in Publication IV of the present thesis [69]. From these results the tempering of hot-work tool steels has to be critically discussed. Similar experiments on high speed steels showed that the retained austenite transforms into martensite during cooling after the first tempering step [26]. From that, the more-step tempering procedure has been established in order to temper the newly formed martensite. Due to the similarity within the tool steel family, this procedure is applied to a wide range of tool steels. The results of the present study, showing that retained austenite decomposition occurs already during tempering, give reason to individually check the tempering behaviour of each steel type in order to optimize the tempering parameters, hence, the performance of the tool.

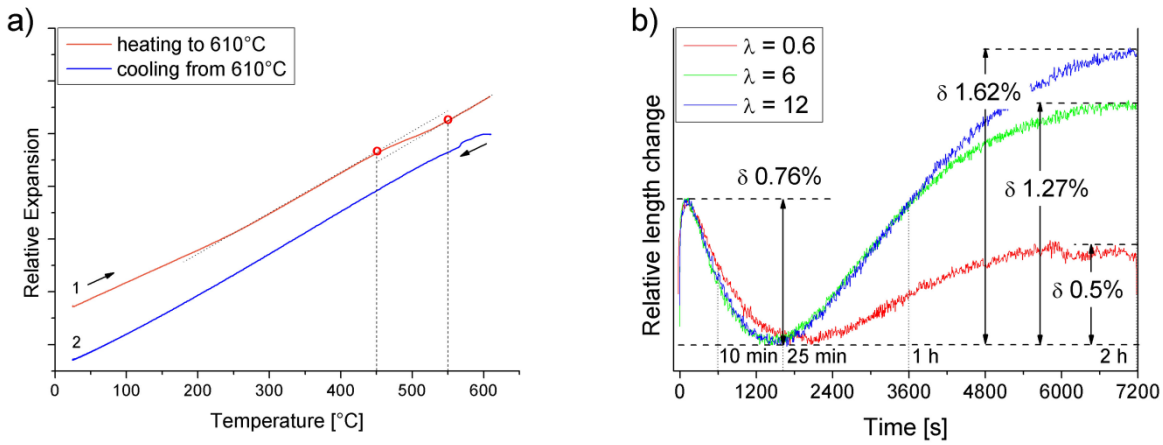

Figure 8: Dilatation during heating the hot-work tool steel X38CrMoV5-1 to 610°C and corresponding cooling curve. Taken from Publication III [68] **(a); Dilatation during subsequent 2 hours tempering at 610°C, providing 3 different cooling rates during hardening, hence, 3 different amounts of retained austenite. Taken from Publication IV** [69] **(b).**

3.2.2. Tempering of Nitrogen Alloyed Martensitic Stainless Steels

Nitrogen has been introduced as an additional alloying element in martensitic stainless steels two decades ago. Nitrogen increases interstitial solubility at hardening temperature, hence, hardenability, and the resistance to pitting corrosion, both key properties for those steels [70]. Metallurgical difficulties by introducing nitrogen are not discussed here.

The alloying with nitrogen allows for a chromium reduction of the alloy by providing same corrosion properties. The reduction of chromium on the one hand also reduces chromium segregations and the formation of undesired delta-ferrite within the microstructure [70].

The tempering behaviour is characterised by new types of precipitates compared to pure carbon martensites. Investigations have been performed on Fe-15Cr-1Mo martensites containing carbon or nitrogen or both [71–73]. The carbon martensite shows the same behaviour than pure Fe-C martensite, i.e. Ɛ-carbide precipitates at low temperatures, followed by cementite formation. At higher temperatures the chromium carbide Cr_7C_3 is formed. In the nitrogen alloyed high chromium alloy precipitation of α'' ($Fe_{16}N_2$) and γ' (Fe_4N) does not occur in contrast to pure Fe-N martensite. The tempering sequence starts with the precipitation of hexagonal Ɛ-nitride $(Fe,Cr)_2N$ followed by the orthorhombic ξ-nitride $(Fe,Cr)_2N$. At higher temperatures hexagonal Cr_2N is precipitated [71]. Tempering of C + N martensites is influenced by the competition of carbon and nitrogen in their interaction with chromium and iron. Carbides and nitrides are precipitated simultaneously and separately. On the one hand, cubic (fcc) chromium nitride (Cr,Fe)N precipitates, but on the other hand the $(Cr,Fe)_7C_3$ chromium carbide, which is typical for tempered chromium carbon martensites, does not occur [73]. No carbo-nitrides exist in this alloy, but, in a vanadium alloyed 12% chromium steel cubic (FeCrV)CN carbo-nitrides have been identified [74].

As a result of the stronger affinity of chromium to nitrogen it is preferentially bound in the chromium nitrides and is not available for the precipitation of high chromium Cr_7C_3 precipitates. However, the introduction of nitrogen into martensitic chromium steels leads to an increased short range atomic order of the chromium atoms in solid solution. As a consequence, the precipitation sequence is delayed and causes a finer dispersed structure of the tempered martensite compared to the pure carbon martensite. This results in improved mechanical and corrosion properties [73].

3.3. Toughness Related Phenomena within Martensitic Medium Carbon Steels

3.3.1. Pro-eutectoid Carbide Precipitation

Carbides which are formed during hardening within the temperature range from austenitisation temperature to the martensitic start temperature are called pro-eutectoid / pre-martensitic carbides. The occurrence of these carbides is reported in several studies on different tool steels [75,76] and also for the investigated hot-work tool steel X38CrMoV5-1. Bungardt et al. [9] proposed higher amounts of bainite and higher amounts of pro-eutectoid carbides at prior austenite grain boundaries for low quenching rates of the hot-work tool steel X38CrMoV5-1. It is meant that the pro-eutectoid carbides do not influence hot-toughness but toughness at room temperature. In their study pro-eutectoid carbides are already formed at relatively high quenching rates. Berns et al. [77] showed a carbide network along the prior austenite grain boundaries of a hot-work tool steel X40CrMoV5-1.

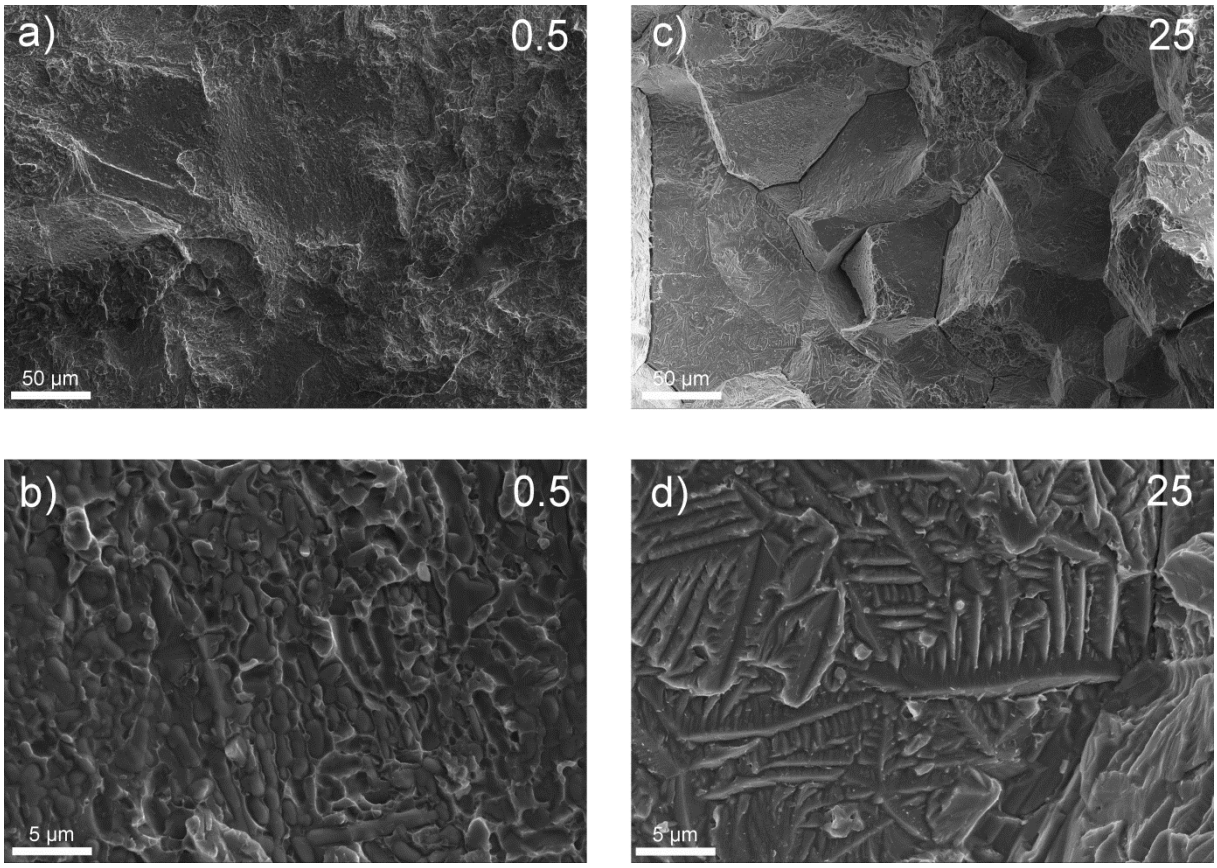

Figure 9: Fracture surfaces corresponding to impact bending tests of an as-quenched martensitic stainless chromium steel X38CrMo16. Overview of the sample quenched with λ = 0.5, showing trans-crystalline cleavage fracture (a); Corresponding detail showing globular carbides (b); Overview of the sample quenched with λ = 25, showing inter-crystalline cleavage fracture (c); Corresponding detail showing fernlike/dendritic pro-eutectoid grain boundary cementite (d). Taken from Publication V [79].

For these investigations a preceding high-temperature homogenisation treatment has been conducted, which naturally leads to a higher super-saturation of the austenite and promotes

the carbide formation. They also demonstrate the formation of pro-eutectoid carbides at former austenite grain boundaries surrounded by inter-granular martensite for the steel grade X20CrNiMo15-2. In the corresponding N-steel, N20CrNiMo15-2 the formation of pro-eutectoid precipitates, both inter-granular and martensitic, is almost completely suppressed [78]. The formation of pro-eutectoid carbides in tool steels is not extensively discussed in literature. Most investigations are conducted on hypereutectoid and austenitic model alloys. This is discussed in Publication V of the present thesis [79]. In case of the nitrogen alloyed plastic mould steel X38CrMo16, the cooling rate dependent toughness reduction could be correlated to the formation of pre-eutectoid carbides which are located at the former austenitic grain boundaries. Corresponding results have been published in Publication V of the present work. Figure 9 shows the fracture surfaces of two as-quenched samples which have been hardened with cooling rates $\lambda = 0.5$ and 25, respectively. It is clearly visible that the cleavage fracture is trans-crystalline in case of the fast quenched sample (Figure 9a) and inter-crystalline in case of the slowly quenched sample (Figure 9c). The trans-crystalline fracture surfaces contain globular alloy carbides (Figure 9b). On the grain surfaces of the slowly quenched sample fernlike/dendritic pro-eutectoid cementite structures can be seen (Figure 9d) which have been found to be responsible for the lowered impact toughness of the finalised material, as shown in Publication V [79]. Those dendritic cementite structures along austenite grain boundaries are well known from the investigations on hypereutectoid and austenitic steels [80]. The work of Andersson [81] demonstrates the formation of pre-martensitic F_3C particles not only at grain boundaries but also within the martensitic laths of a low-chromium hot-work tool steel. An increase of the martensitic start temperature towards lower cooling rates during hardening has been observed as an additive indication for pre-martensitic precipitates. However, the hot-work tool steel investigated in the present work has been found not to show such a pro-eutectoid carbide precipitation. SEM, TEM and fracture surface analysis results, which have not been published, confirm this. Additionally, bainite transformation does not occur until cooling rates are lower than 0.25°C/s [11]. However, cooling rate dependent toughness decrease is reported even in the “purely martensitic” condition [11,69]. Therefore, another mechanism during cooling must be responsible for the cooling rate dependent toughness behaviour of the investigated hot-work tool steel X38CrMoV5-1.

3.3.2. Temper Embrittlement / Tempered Martensite Embrittlement

So-called temper embrittlement deals with the segregation of impurity elements to prior austenite grain boundaries which most likely causes intergranular fracture [82]. This is not meant to play a significant role in the investigated steels firstly because of their high quality and, secondly, a dependence on the cooling rate during hardening seems not to make sense. A phenomenon called tempered martensite embrittlement spans and describes almost all imaginable toughness-lowering mechanisms during tempering of martensitic steels. All of them deal with the formation of carbides, i.e. interlath, intralath, elongated, coarse or resulting from the decomposition of retained austenite. This effect is characterized by a significant loss in Charpy impact toughness in a special range of tempering temperatures. Therefore, it is believed that one or a combination of some of these mechanisms depend on the cooling rate during hardening and explain the cooling rate dependent toughness behaviour. Investigations were performed for several times on commercial ultra-high strength steel AISI 4340 with respect to the occurrence of tempered martensite embrittlement (TME) [19,83,84]. Horn et al. [19] directly related the severity of the TME to the volume fraction of retained austenite which is predominantly present as thin films between martensitic laths. Thermal and mechanical instability of the retained austenite leads to the precipitation of interlath cementite particles and to the transformation of the remaining carbon-depleted retained austenite.

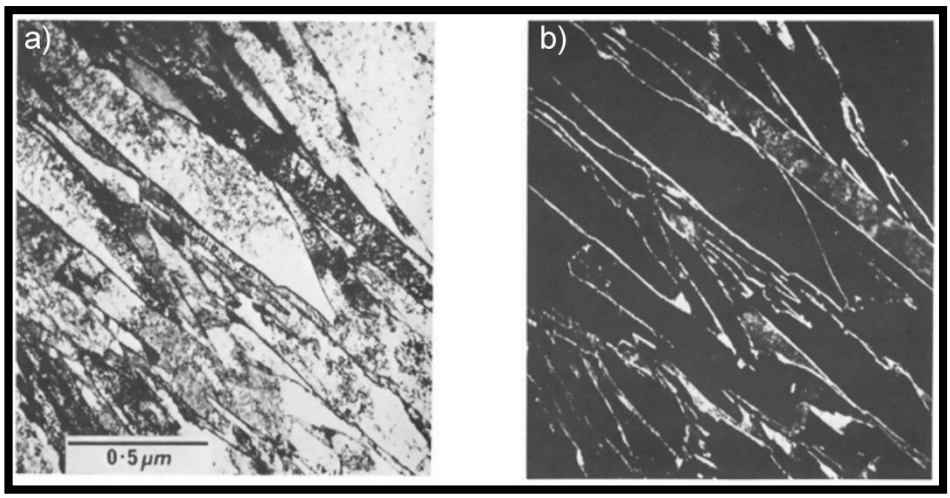

Figure 10: Electron micrograph of a Fe-10Cr-0.2C martensite quenched in iced brine from 1150°C. Bright field image (a); Dark field image using γ-diffraction beam. The austenite areas are bright (b). Taken from [85].

Thomas [39] proposed that retained austenite exists in most as-quenched dislocated martensitic medium carbon alloy steels except FeMoC as stabilized fine interlath films. Figure 10 demonstrates the occurrence of the retained austenite as thin films between martensitic laths in a Fe-10Cr-0.2C steel [85]. The fracture mechanisms corresponding to TME were found to be interlath and/or transgranular cleavage in most cases. Contrary to that, Bandyopadhyay et al. [83] observed that intergranular cleavage is the dominant TME fracture mechanism in these steels which is due to carbides formed at prior austenite grain boundaries

which are weakened by the segregation of impurity elements. Carbides formed from retained austenite and subsequent decomposition is not of primary significance. Ebrahimi et al. [86] showed for a medium carbon steel that phosphorus is not responsible for TME. Again, contrary to that, several other authors pick the correlation of retained austenite and tempered martensite embrittlement out as a central theme of their investigations and show that the formation of interlath carbide formation from the interlath retained austenite films negatively influences the toughness and fracture behaviour [39,40]. On the other hand, Peters et al. [87] do not correlate TME with the decomposition of interlath retained austenite, but with the coarsening of inter- and intralath carbides. However, all these findings illustrate that fracture mechanism interpretation and the correlation to the responsible microstructural features show differences although the investigated materials are nearly the same or at least very similar. Multiple microstructural contributors complicate a recent interpretation, but it is obvious that retained austenite which is located as interlath films after hardening plays an important role concerning the toughness behaviour of medium carbon martensitic steels. For the investigated hot-work tool steel it is shown in the present work that those retained austenite films are the dominant factor regarding the dependency of cooling rate and toughness. The thickening of the films at lower cooling rates, demonstrated in Publications I and II [42,43], and the resulting increased potential for interfacial carbides after decomposition, as shown in Publication III [68], negatively influence impact toughness of the finalised material.

3.3.3. Influence of Silicon on Toughness

A successful modification in order to improve toughness of hot-work tool steels is the reduction of the silicon content from the usual 1.0% to 0.3% silicon, introduced in the last years by several tool steel producers, e.g. [88]. Improvement of typical material properties like high temperature strength [89] and toughness [90] by reducing the silicon content was reported several times in literature for 5 % chromium hot-work tool steels. Recently, a lot of scientific work has been done on this topic in order to explain the microstructural mechanisms behind this Si influence. Delagnes et al. [67] correlated higher tensile and fatigue properties at 550°C with an observed higher volume fraction of small secondary carbides (mainly vanadium carbides) in a low silicon AISI H11 hot-work tool steel. Similar experiments, with the focus laid on the distribution of the secondary carbides, have been conducted on the same hot-work tool steel with silicon contents ranging from 2 % to 0.05 %. Again, higher toughness values have been found for the low silicon grade and the reason for that has been stated to be a finer and more homogeneous distribution of secondary carbides compared to the high silicon grade as demonstrated in Figure 11. The high silicon grade shows coarse intralath M_2C precipitates and coarse interfacial M_7C_3 precipitates which are located at lath and packet boundaries [91]. The occupation of the interfaces by M_7C_3 carbides is mentioned in several studies [53,92–94]. Mesquita and Kestenbach [95] performed a detailed fracture surface analysis where they could show ductile fracture for the low silicon variant and intergranular

fracture for the high silicon variant, being in agreement with the earlier mentioned difference of carbide distribution within the microstructure. Differences of the carbide distribution can be explained by an influence of silicon on the precipitation sequence during tempering after hardening. The low silicon grade forms cementite at relatively low temperatures, before alloy carbide elements become mobile, which leads to a homogeneous distribution of fine M_3C particles. The increase of the cementite volume fraction with low silicon contents is depicted in Figure 12.

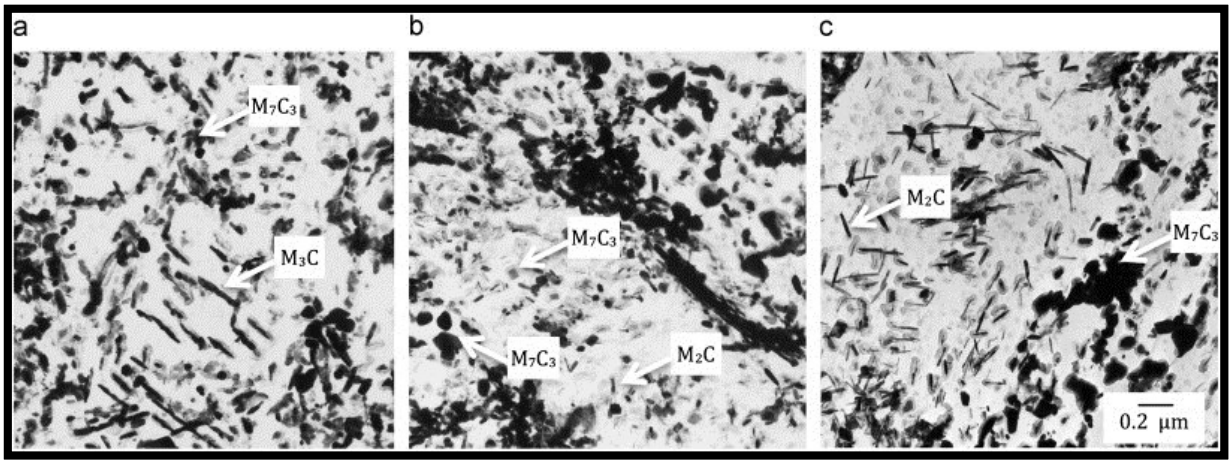

Figure 11: Example of the better distribution of secondary carbides in low silicon steels, after 2 x 2 h tempering at 625°C. (a) 0.05% Si, (b) 1.0% Si and (c) 2.0% Si [94].

Therefore, no carbon atoms in solution are available for direct alloy carbide formation. Instead of that, carbide forming elements such as chromium, molybdenum and vanadium begin to concentrate in the M_3C. The mechanism of alloy carbide formation, especially in the case of M_7C_3, is frequently discussed in literature, e.g. [96]. However, alloy carbide formation takes place at the former M_3C positions which leads to the preferred homogeneous distribution. In case of the high silicon grade the cementite formation is retarded and carbon is available in the whole microstructure. Due to the low diffusivity of the carbide forming elements, alloy carbide formation starts at preferential diffusion paths, hence, lath and inter-package boundaries. This inhomogeneous carbide distribution leads to low energy fracture paths and results in the observed brittle behaviour of the material [91]. The hot-work tool steel investigated in the present thesis has a relatively high silicon content of approximately 1 weight percent. This means that the inhomogeneous carbide distribution is on the one hand due to retained austenite decomposition at lath boundaries and on the other hand due to direct alloy carbide formation from the bulk, again preferred at interfaces, both provoked by the high silicon content.

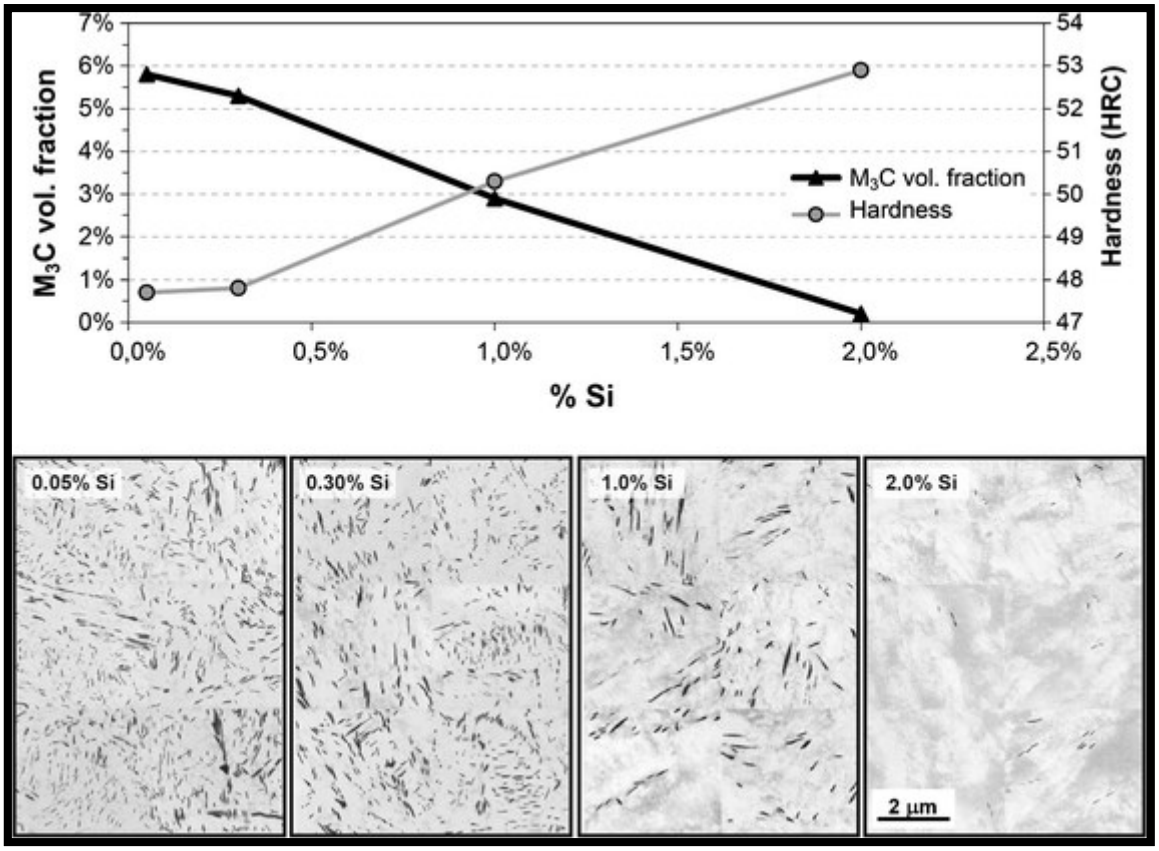

Figure 12: Quantification of the precipitated volume fraction of cementite particles and the resulting tempered hardness after the short 0 h/ 625°C tempering treatment as a function of silicon content. Graphs and images are taken from [53].

3.4. Summary of Publications

Publication I

Carbon Distribution And The Influence On The Tempering Behaviour In A Hot-Work Tool Steel Aisi H11

Christoph Lerchbacher, Silvia Zinner, Harald Leitner

Proceeding Thermec 2011

Advanced Materials Research Vol. 409 (2012) pp 702-706

The investigated hot-work tool steel AISI H11 shows a "pure" martensitic transformation down to quenching rates of $\lambda = 12$ (0.25 K/s) during hardening. However, from literature it is known that the carbon atoms are redistributed due to auto-tempering effects during cooling of the newly formed martensite. Therefore, the microstructure has been characterized by atom probe tomography with the focus laid on the carbon distribution after the hardening treatment and during the early stages of tempering. The carbon distribution shows significant differences within the probed volumes, regions differently affected by carbon segregation can be observed in some specimens. In all samples pronounced carbon segregation to dislocations and cluster formation is observed. Through all hardened samples no segregation of any substitutional elements has taken place. Heating to 500°C does not significantly change the elemental distribution which indicates that transition carbide formation has not taken place. Carbon enriched interlath retained austenite films with peak carbon levels of 6 to 9 at% show a thickness increase with increasing λ (lower cooling rates). These films and the pre-existing carbon clusters have been found to be nucleation sites for carbide formation during heating to 610°C, the standard tempering temperature of this hot-work tool steel.

Publication II

Atom probe study of the carbon distribution in a hardened martensitic hot-work tool steel X38CrMoV5-1

Christoph Lerchbacher, Silvia Zinner, Harald Leitner

Micron 43 (2012) 818-826

Cooling rate dependent mechanical properties of the common hot-work tool steel X38CrMoV5-1 lead to the assumption, that cooling rate influences the as-hardened microstructure. Therefore, the latter has been characterized by atom probe tomography with

the focus laid on the carbon distribution. Samples quenched with cooling parameters λ from 0.1 (30 K/s) to 12 (0.25 K/s), covering the complete martensitic region, have been investigated. This range of cooling rates has been chosen in order to avoid misinterpretations which might occur by the formation of bainite. In all samples pronounced carbon segregation to dislocations and cluster formation could be observed after quenching. Irregular carbon clusters with elemental concentrations of 8 to 15 at% are present. The evaluation of the segregation level of the single martensitic laths has been done by conducting statistical methods in order to confirm the visual impression. The level of segregation depends on the temperature where the corresponding laths have been formed during the martensitic transformation. Therefore, a correlation between cooling rate and carbon segregation level is not possible due to the small volumes analysed by atom probe tomography. Martensitic laths have been found to be surrounded by carbon enriched interlath films with peak carbon levels ranging from 6 to10 at%. The analysis of several samples showed an increase of the mean film thickness at lower cooling rates during quenching. The mean thickness ranges from 4 nm for λ = 0.1 to 14 nm for λ = 12. The thicker films have been identified to be retained austenite by TEM. The fraction of total carbon staying in the austenite is 10 at% and 60 at% for cooling rates λ = 0.1 and 12, respectively. Charpy impact tests showed lower impact energies for fast cooling rates, which is in agreement with the lower amount of carbon enriched retained austenite and the consequently higher carbon concentration in the martensitic matrix. Through all samples no segregation of any substitutional elements takes place.

Publication III

Retained Austenite Decomposition and Carbide Formation during Tempering a Hot-Work Tool Steel X38CrMoV5-1 Studied by Dilatometry and Atom Probe Tomography

Christoph Lerchbacher, Silvia Zinner, Harald Leitner

Metallurgical and Materials Transactions A 43A (2012) 4989-4998

Classical literature demonstrates the tempering behaviour of tool steels by providing classical tempering charts. This study characterizes the processes which occur during heating to tempering temperature and subsequent tempering, similar to the industrial process. Therefore, the microstructural development of a hot-work tool steel X38CrMoV5-1 during continuous heating to tempering temperature has been investigated with the focus laid on the decomposition of the retained austenite (Stage II) and carbide formation (Stage III and IV). Investigations have been carried out after heating to 400°C, 500°C, 610°C and after a dwell time of 10 minutes at 610°C. Dilatometry and atom probe tomography were used to identify tempering reactions. A distinctive reaction takes place between 450°C and 550°C during

heating which is determined to be the formation of M_3C. Stage II could be evidenced by means of atom probe results and indirectly with dilatometry, indicating the formation of new martensite during cooling. Retained austenite decomposition starts with the precipitation of alloy carbides formed from nanometric interlath retained austenite films. Consequently, these carbides are laminary arranged. This causes a reduction of the carbon content within the retained austenite. Higher carbon levels were observed within the carbides formed from retained austenite compared to carbides formed within the matrix which indicates that alloy carbide transformation progresses faster in the retained austenite. Additionally, preceding enrichment of substitutes at the matrix/carbide interface in the early stages of Cr_7C_3 alloy carbide formation could be visualized on the basis of coarse M_3C carbides within the matrix. Since the atom probe experiments have been performed in laser mode, carbon concentration evaluation within carbides has been discussed. Atom probe tomography has been found to be very useful to complement dilatational experiments in order to characterize and identify microstructural changes.

Publication IV

Direct or Indirect: Influence of type of retained austenite decomposition during tempering on the toughness of a hot-work tool steel

Christoph Lerchbacher, Silvia Zinner, Harald Leitner

Materials Science & Engineering A 564 (2013) 163-168

Dilatometric experiments have shown that during tempering the hot-work tool steel X38CrMoV5-1 at 610°C the decomposition of retained austenite starts, independently of the cooling rate during hardening, exactly after 25 minutes. From that, a heat treatment slightly differing from the classical 2 x 2 hours tempering treatment has been established in order to eliminate the direct retained austenite decomposition during tempering by reducing the first tempering step to 25 minutes. Instead of the direct decomposition into ferrite and cementite during the first tempering step, transformation into martensite during cooling after 25 min tempering has been forced. A quenching dilatometer has been used for the heat treatment and for the determination of transformation reactions. The two heat treatments have been compared with respect to toughness behaviour by conducting Charpy-impact tests. The investigations have been performed on samples hardened with quenching rates 5 K/s, 0.5 K/s and 0.25 K/s, providing different amounts of retained austenite within the as-quenched microstructure. The heat treatment modification does not show improvement regarding the toughness behaviour in case of low cooling rates where the specimen failure is dominated by interfaces, hence, the former interlath retained austenite films. Therefore, the indirect retained

austenite decomposition has no positive effect compared to the direct decomposition. In case of the highest cooling rate the failure is dominated by the matrix and the impact toughness could be improved by a factor of 12 % at the same hardness level and a dwell time reduction of 15 %. The reduction of the dwell time during the first tempering step causes a second significant nucleation and growth period during the second tempering sequence. This could positively influence the morphology and distribution of secondary carbides. For tools of small dimensions where these cooling rates during hardening can be achieved this heat treatment modification should be considered.

Publication V

Evidence of pro-eutectoid cementite formation and its influence on impact toughness of the plastic mould steel X38CrMo16

Christoph Lerchbacher, Silvia Zinner, Matthias Nöhrer, Harald Leitner

Submitted to Metallurgical and Materials Transactions A

The correlation between cooling rate during hardening and impact toughness is studied for a hardenable martensitic stainless steel X38CrMo16. For that, samples have been produced using cooling rates λ = 0.5 (6 K/s) and 25 (0.12 K/s) in a dilatometer. The slowly quenched sample shows a second martensite start temperature (Ms) at 320°C. Transmission electron microscopy revealed the existence of carbides along former austenite grain boundaries in case of the slowly quenched sample. Increased chromium contents and an orientation relationship with at least one of the adjacent matrix grains confirm that those carbides are formed from the austenite directly during cooling before reaching Ms. Corresponding inter-crystalline fracture surfaces of the as-quenched samples show fernlike, dendritic carbide structures on the grain boundaries which are attributed to pro-eutectoid cementite precipitates. Beneath the predominantly ductile fracture, small amounts of inter-crystalline cleavage occur after impact testing the hardened and tempered samples. The cleavage surfaces do also show these dendritic pro-eutectoid carbide structures. From that, a correlation between the occurrence of those grain boundary carbides and the decreased impact toughness of slowly quenched and tempered samples is given. Although the impact toughness dependency from the cooling rate is the same compared to the hot-work tool steel investigated in the earlier publications, the mechanism is completely different.

4. Resumé

As stated in the thesis title, the aim of the present work is to provide a detailed understanding of the microstructural mechanisms which are responsible for a toughness loss caused by reduced cooling rates during hardening of some tool steels. The influence of the additional formation of bainite has already been discussed, but also in the pure martensitic range this phenomenon is observed [11]. Therefore, two representative tool steel materials which show this phenomenon and which provide an extended martensitic range have been chosen for the investigations. Those are plastic mould steel X38CrMo16 and hot-work tool steel X38CrMoV5-1, known as Böhler trademarks M303 and W300, respectively.

The general assumption before starting the first investigations was that so-called pro-eutectoid carbides, which are formed at the former austenite grain boundaries during cooling from austenitisation temperature, reduce the toughness of the material. The amount of pro-eutectoid carbides might increase at lower cooling rates due to the longer diffusion time and therefore, might explain the cooling rate dependent toughness behaviour.

In Publication V this assumption could be verified in case of the plastic mould steel X38CrMo16. Pro-eutectoid cementite has been shown on the former austenite grain boundaries by TEM experiments in case of slowly quenched samples. The inter-crystalline fracture surfaces of slowly quenched samples gave an insight into the three dimensional appearance of these cementite particles. The pro-eutectoid cementite has a fernlike/dendritic structure with its growth direction only along the grain boundaries and not into the adjacent grains. The occurrence of small amounts of such inter-crystalline cleavage fracture surfaces within the corresponding tempered samples and their decoration with these fernlike cementite structures approves the correlation of cooling rate during hardening and the impact toughness of the tempered samples [79].

In case of hot-work tool steel X38CrMoV5-1 no pre-eutectoid carbides could be identified, hence, another mechanism has to be responsible for the cooling rate dependent toughness behaviour. Therefore, the focus of investigations was laid on the elemental distribution within the as-hardened microstructure. For this, atom probe tomography was conducted as the main characterization method, predestined for 3-dimensional elemental analysis on the nanoscale. From earlier studies on similar steels it is known that retained austenite occurs as interlath films between martensitic laths, e.g. [19], and is enriched in carbon, e.g. [30], which has also been found for the steel investigated in the present study. The decomposition of such films is known to contribute to so-called tempered martensite embrittlement [19,39,40]. In the present study it could be shown, representing the only cooling rate dependent significant change in

microstructure, that the mean thickness of those films depends on the cooling rate during quenching. Lower cooling rates lead to thicker films (Publications I and II) [42,43]. In Publication III the early stages of retained austenite decomposition are examined in detail and it is demonstrated that laminary arranged carbides are formed within the film plane of the interlath retained austenite films [68]. This finding combined with the increase in film thickness, hence, the increase of the potential for laminary arranged interlath carbides, explains the cooling rate dependent toughness properties.

The reduction of silicon is well established in order to increase the toughness level of the studied hot-work tool steel. Several studies on this topic state a more homogeneous and finer carbide distribution in the low silicon steel which increases toughness. Retained austenite is proposed not to play a significant role regarding toughness [53,90]. This is on the one hand related to the low amount of retained austenite within those studies and on the other hand because of the much higher influence of silicon on the carbide distribution. However, the retained austenite decomposition becomes the dominating factor which influences toughness with respect to the cooling rate during hardening in case of a given alloy composition. In Publication IV it could indirectly be shown that for low amounts of retained austenite, hence, high cooling rates, the matrix is the dominating microstructural component and for elevated amounts the retained austenite itself becomes dominant [69]. Mesquita et al. [53] propose that the important effects of silicon on the mechanical properties occur during tempering and not as a result of quenching. However, the results of the present study show that silicon affects mechanical properties of the finished tool also during hardening. The fine Fe_3C distribution is already created by auto-tempering effects during cooling the newly formed martensite in case of the low silicon steel. The higher consumption of carbon does also result in a lower amount of retained austenite [11]. Hence, the reduction of retained austenite counts in addition to the finer carbide distribution regarding toughness.

However, the results of the present study explain the cooling rate dependant toughness behaviour of these two representing tool steels, and, complement the insight into the influence of silicon on toughness.

During studying the tempering reactions of the hot-work tool steel it was noticeable that no transition carbide formation takes place before the cementite precipitation. This might be related to the overall carbon content of the matrix which is heavily reduced compared to the nominal composition because of not dissolved primary carbides and the carbon enriched retained austenite films. In Publication II it is found that 10 % and 60 % of the total carbon are trapped in the retained austenite for cooling rates $\lambda = 0.6$ and $\lambda = 12$, respectively [42]. Together with the primary carbides, this could lead to carbon contents below the minimum 0.2 mass% which are necessary for transition carbide formation in as-quenched carbon martensite [97].

Publication III provides an input to the long-termed discussion about the sequence of M_7C_3 formation. Cr_7C_3 particles have been shown to form in-situ at the α/Fe_3C interface by increasing the substitute content of the pre-existing Fe_3C particles. The atom probe tomography results definitely rebut the assumption of a separate nucleation and growth process [68].

The modified heat treatment discussed in Publication IV showed that a dwell time reduction of the first tempering step could improve toughness properties of small-sized parts. A second nucleation and growth process might lead to a finer distribution of secondary carbides. The experiments demonstrated an increase in impact toughness of 12% at a dwell time reduction of 15% for a cooling rate of $\lambda = 0.6$ during hardening. For tools of small dimensions where these cooling rates during hardening can be achieved this heat treatment modification should be considered [69].

5. Bibliography

[1] G.A. Roberts, G. Krauss, R. Kennedy, Tool Steels, 5th ed., ASM International, Materials Park, OH, 1998.

[2] A. Kulmburg, E. Kaiser, S. Wilmes, Härterei Technische Mitteilungen 42 (1987) 133–138.

[3] Produktdatenblatt, Böhler W300, Böhler Edelstahl GmbH & Co KG, Kapfenberg.

[4] N.S. Kalsi, R. Sehgal, V.S. Sharma, Materials and Manufacturing Processes 25 (2010) 1077–1100.

[5] A. Molinari, M. Pellizzari, S. Gialanella, G. Straffelini, K.H. Stiasny, Journal of Materials Processing Technology 118 (2001) 350–355.

[6] M. Koneshlou, K. Meshinchi Asl, F. Khomamizadeh, Cryogenics 51 (2011) 55–61.

[7] H. Jesperson, Metallurgia Italiana 98 (2006) 29–37.

[8] H. Jesperson, Metallurgia Italiana 101 (2009) 55–60.

[9] K. Bungardt, O. Mülders, R. Meyer-Rhotert, Archiv Für Das Eisenhüttenwesen 37 (1966) 381–389.

[10] S. Mayer, C. Scheu, H. Leitner, H. Clemens, I. Siller, BHM Berg- Und Hüttenmännische Monatshefte 152 (2007) 132–136.

[11] S. Mayer, Doctoral Thesis, Department of Physical Metallurgy and Materials Testing, Leoben, (2009).

[12] S. Zinner, H. Lenger, G. Jesner, I. Siller, J. Heat Treatm. Mat. 67 (2012) 95–99.

[13] V. Strobl, N. Dickinger, I. Siller, R. Schneider, J. Heat Treatm. Mat. 67 (2012) 91–94.

[14] D.A. Porter, K.E. Easterling, Phase Transformations in Metals and Alloys, 2nd ed., Chapman & Hall, London ; New York, 1992.

[15] R.W.K. Honeycombe, Steels - Microstructure and Properties, Third Edit, Edward Arnold, London, 1981.

[16] T. Inoue, S. Matsuda, Y. Okamura, K. Aoki, Transactions of the Japan Institute of Metals 11 (1970) 36–43.

[17] S. Morito, H. Tanaka, R. Konishi, T. Furuhara, T. Maki, Acta Materialia 51 (2003) 1789–1799.

[18] S. Morito, R. Igarashi, K. Kamiya, T. Ohba, T. Maki, Materials Science Forum 638-642 (2010) 1459–1463.

[19] R.M. Horn, R.O. Ritchie, Metallurgical Transactions A 9 (1978) 1039–1053.

[20] Produktdatenblatt, Premium 1.2343, Abrams Premium Stahl, Osnabrück.

[21] Produktdatenblatt, Thyrotherm 2343, Thyssenkrupp AG, Essen.

[22] Produktdatenblatt, Steel UTOPMO1, Metal Ravne, Ravne na Koroskem.

[23] Produktdatenblatt, Premium 1.2316, Abrams Premium Stahl, Osnabrück.

[24] Produktdatenblatt, Thyroplast 2316, Thyssenkrupp AG, Essen.

[25] Produktdatenblatt, Böhler M300, Böhler Edelstahl GmbH & Co KG, Kapfenberg.

[26] A. Kulmburg, F. Korntheuer, J. Heat Treatm. Mat. 31 (1976) 195–204.

[27] C.A. Siebert, D. V. Doane, D.H. Breen, The Hardenability of Steels: Concepts, Metallurgical Influences, And Industrial Applications, American Society for Metals, 1977.

[28] P. Payson, C.H. Savage, Transactions ASM 33 (1944) 261–275.

[29] G.R. Speich, W.C. Leslie, Metallurgical Transactions 3 (1972) 1043–1054.

[30] D.H. Sherman, S.M. Cross, S. Kim, F. Grandjean, G.J. Long, M.K. Miller, Metallurgical and Materials Transactions A 38 (2007) 1698–1711.

[31] C. Zhu, A. Cerezo, G.D.W. Smith, Ultramicroscopy 109 (2009) 545–552.

[32] M.K. Miller, P.A. Beaven, G.D.W. Smith, Metallurgical Transactions A 12 (1981) 1197–1204.

[33] K.A. Taylor, L. Chang, G.B. Olson, G.D.W. Smith, M. Cohen, J.B. Vander Sande, Metallurgical Transactions A 20 (1989) 2717–2737.

[34] E.V. Pereloma, M.K. Miller, I.B. Timokhina, Metallurgical and Materials Transactions A 39 (2008) 3210–3216.

[35] I.B. Timokhina, E. V Pereloma, S.P. Ringer, R.K. Zheng, P.D. Hodgson, ISIJ International 50 (2010) 574–582.

[36] R.C. Thomson, M.K. Miller, Acta Materialia 46 (1998) 2203–2213.

[37] J. Wilde, A. Cerezo, G.D.W. Smith, Scripta Materialia 43 (2000) 39–48.

[38] B. Hutchinson, J. Hagström, O. Karlsson, D. Lindell, M. Tornberg, F. Lindberg, M. Thuvander, Acta Materialia 59 (2011) 5845–5858.

[39] G. Thomas, Metallurgical Transactions A 9 (1978) 439–450.

[40] M. Sarikaya, a. K. Jhingan, G. Thomas, Metallurgical Transactions A 14 (1983) 1121–1133.

[41] R. Thomson, Scripta Metallurgica Et Materialia 32 (1995) 149–154.

[42] C. Lerchbacher, S. Zinner, H. Leitner, Micron 43 (2012) 818-826.

[43] C. Lerchbacher, S. Zinner, H. Leitner, Advanced Materials Research 409 (2012) 702–706.

[44] A.J. Clarke, J.G. Speer, M.K. Miller, R.E. Hackenberg, D. V Edmonds, D.K. Matlock, F.C. Rizzo, K.D. Clarke, E. De Moor, Acta Materialia 56 (2008) 16–22.

[45] C. Garcia-Mateo, F.G. Caballero, M.K. Miller, J. a. Jimenez, Journal of Materials Science 47 (2011) 1004–1010.

[46] F.G. Caballero, M.K. Miller, C. Garcia-Mateo, Acta Materialia 58 (2010) 2338–2343.

[47] F.G. Caballero, M.K. Miller, C. Garcia-Mateo, C. Capdevila, S.S. Babu, Acta Materialia 56 (2008) 188–199.

[48] F.G. Caballero, M.K. Miller, A.J. Clarke, C. Garcia-Mateo, Scripta Materialia 63 (2010) 442–445.

[49] F.G. Caballero, M.K. Miller, C. Garcia-Mateo, Metallurgical and Materials Transactions A 42 (2011) 3660–3668.

[50] W.S. Owen, Trans. ASM 46 (1954) 812–829.

[51] J.H. Jang, I.G. Kim, H.K.D.H. Bhadeshia, Computational Materials Science 44 (2009) 1319–1326.

[52] E. Kozeschnik, H.K.D.H. Bhadeshia, Materials Science and Technology 24 (2008) 343–347.

[53] R.A. Mesquita, C.A. Barbosa, E. V. Morales, H.-J. Kestenbach, Metallurgical and Materials Transactions A 42 (2011) 461–472.

[54] G.B. Olson, M. Cohen, Metallurgical Transactions A 14 (1983) 1057–1065.

[55] S. Primig, H. Leitner, Thermochimica Acta 526 (2011) 111–117.

[56] Y. Ohmori, I. Tamura, Metallurgical Transactions A 23 (1992) 2737–2751.

[57] Y. Hirotsu, S. Nagakura, Acta Metallurgica 20 (1972) 645–655.

[58] H.K.D.H. Bhadeshia, Bainite in Steels, The Institute of Materials, London, 1992.

[59] M.J. Van Genderen, M. Isac, A. Bottger, E.J. Mittemeijer, Metallurgical and Materials Transactions A 28A (1997) 545–561.

[60] K. Stiller, L.E. Svensson, P.R. Howell, W. Rong, H.O. Andrén, G.L. Dunlop, Acta Metallurgica 32 (1984) 1457–1467.

[61] W. Rong, G.L. Dunlop, Acta Metallurgica 32 (1984) 1591–1599.

[62] A.M. El-Rakayby, B. Mills, Journal of Materials Science 23 (1988) 4340–4344.

[63] S. Karagöz, H.-O. Andrén, Zeitschrift Für Metallkunde (1992).

[64] W. Rong, H.O. Andrén, H. Wisell, G.L. Dunlop, Acta Metallurgica Et Materialia 40 (1992) 1727–1738.

[65] S. Karagöz, H.F. Fischmeister, H.-O. Andrén, C. Guang-Jun, Metallurgical and Materials Transactions A 23 (1992) 1631–1640.

[66] H. Leitner, P. Staron, H. Clemens, S. Marsoner, P. Warbichler, Materials Science and Engineering A 398 (2005) 323–331.

[67] D. Delagnes, P. Lamesle, M.H. Mathon, N. Mebarki, C. Levaillant, Materials Science and Engineering A 394 (2005) 435–444.

[68] C. Lerchbacher, S. Zinner, H. Leitner, Metallurgical and Materials Transactions A 43 (2012) 4989–4998.

[69] C. Lerchbacher, S. Zinner, H. Leitner, Materials Science and Engineering A 564 (2013) 163–168.

[70] N. Krasokha, H. Berns, J. Heat Treatm. Mat. 66 (2011) 150–164.

[71] H. Berns, S.N. Bugajchuk, V.A. Duz, R. Ehrhardt, V.G. Gavriljuk, Y.N. Petrov, I.A. Yakubzov, Steel Research 65 (1994) 444–450.

[72] H. Berns, V.A. Duz, R. Ehrhardt, V.G. Gavriljuk, Y.N. Petrov, A.V. Tarasenko, Materials Research and Advanced Techniques 88 (1997) 109–116.

[73] H. Gavriljuk, V.G., Berns, Proceedings of the 5th International Conference on High Nitrogen Steels (HNS), Stockholm, 1998.

[74] F. Vanderschaeve, J.R. Taillard, Steel Research 64 (1993) 221–227.

[75] C. Ernst, E. Haberling, K. Rasche, Stahl Und Eisen 115 (1995) 71–76.

[76] T. Okuno, Transactions ISIJ 27 (1987) 51-59.

[77] H. Berns, P. Dyrda, F. Wendl, Steel Research 56 (1985) 167–170.

[78] R. Berns, H., Ehrhardt, Steel Research 67 (1996) 343–349.

[79] C. Lerchbacher, S. Zinner, M. Nöhrer, H. Leitner, Submitted.

[80] G. Spanos, M. V Kral, International Materials Reviews 54 (2009) 19–47.

[81] J. Andersson, Secondary Hardening in Some Low-chromium Hot-work Tool Steels, Chalmers University of Technology, Gothenburg, Sweden, 2011.

[82] I. Olefjord, International Materials Reviews 23 (1978) 149–163.

[83] N. Bandyopadhyay, C.J. McMahon, Metallurgical Transactions A 14 (1983) 1313–1325.

[84] W.-S. Lee, T.-T. Su, Journal of Materials Processing Technology 87 (1999) 198–206.

[85] P.R. Howell, J. V. Bee, R.W.K. Honeycombe, Metallurgical Transactions A 10 (1979) 1213–1222.

[86] F. Zia-Ebrahimi, G. Krauss, Acta Metallurgica 32 (1984) 1767–1778.

[87] J.A. Peters, J.V. Bee, B. Kolk, G.G. Garrett, Acta Metallurgica 37 (1989) 675–686.

[88] O. Sandberg, B. Klarenfjord, H. Lindow, Proceeding of the 5th International Conference on Tooling, Leoben, 1999, pp. 601–610.

[89] U. Masahide, S. Tomoaki, K. Kunio, O. Yasutaka, T. Harushige, Tetsu to Hagane 89 (2003) 673–679.

[90] W.M. Garrison, Materials Science and Technology 3 (1987) 4.

[91] R.A. Mesquita, C.A. Barbosa, E.V. Morales, H.J. Kestenbach, Materials Science Forum 636-637 (2010) 612–617.

[92] R.A. Mesquita, H.-J. Kestenbach, International Heat Treatment and Surface Engineering 4 (2010) 145–151.

[93] R.. Mesquita, H.-J. Kestenbach, Solid State Phenomena 172-174 (2011) 414–419.

[94] R.A. Mesquita, H.-J. Kestenbach, Materials Science and Engineering A 556 (2012) 970–973.

[95] R.A. Mesquita, H.-J. Kestenbach, Materials Science and Engineering A 528 (2011) 4856–4859.

[96] J. Nutting, J. Iron Steel Inst. 207 (1969) 872–893.

[97] D. Kalish, M. Cohen, Materials Science and Engineering 6 (1970) 156–166.

Section B

Publication I

Christoph Lerchbacher, Silvia Zinner, Harald Leitner

Carbon Distribution And The Influence On The Tempering Behaviour In A Hot-Work Tool Steel Aisi H11

Proceeding Thermec 2011

Advanced Materials Research Vol. 409 (2012) pp 702-706

Advanced Materials Research Vol. 409 (2012) pp 702-706
© (2012) Trans Tech Publications, Switzerland
doi:10.4028/www.scientific.net/AMR.409.702

Carbon Distribution And The Influence On The Tempering Behaviour In A Hot-Work Tool Steel Aisi H11

Christoph Lerchbacher[1,a], Silvia Zinner[2,b], Harald Leitner[1,3,c]

[1]Christian Doppler Laboratory of Early Stages of Precipitation, University of Leoben, Franz-Josef-Straße 18, A-8700 Leoben

[2]Böhler Edelstahl GmbH & Co AG, Mariazellerstraße 25, A-8605 Kapfenberg

[3]Department of physical metallurgy and materials testing, University of Leoben, Franz-Josef-Straße 18, A-8700 Leoben

[a]christoph.lerchbacher@unileoben.ac.at, [b]Silvia.Zinner@bohler-edelstahl.at, [c]harald.leitner@unileoben.ac.at

Keywords: hot-work tool steel, retained austenite, martensite, carbon segregation, atom probe

Abstract. The microstructure of the common hot-work tool steel AISI H11 has been characterized by atom probe tomography with the focus on the carbon distribution after the hardening treatment and in the early stages of tempering. The carbon distribution shows significant differences within the probed volumes, regions differently affected by carbon segregation can be observed in some specimens. In all samples pronounced carbon segregation to dislocations and cluster formation is observed. Through all hardened samples no segregation of any substitutional elements has taken place. Heating to 500°C does not significantly change the elemental distribution. Carbon enriched interlath austenite films with peak carbon levels of 6 to 9 at% show a thickness increase with increasing λ. These films and the pre-existing carbon clusters have been found to be nucleation sites for carbide formation during heating to 610°C.

Introduction

Chromium Hot-work tool steels are commonly used for hot-work applications as for example die-casting dies or forging dies for the production of light metals. The processing of light metals goes hand in hand with the requirement of the resistance to the exposure to higher temperatures without changing microstructure and mechanical properties [1]. These material properties can be achieved by a well-defined chemical composition, a high micro cleanness and a well-defined heat treatment. The heat treatment consists of an austenitization treatment with a subsequent hardening and a multiple tempering procedure. The hardened microstructure consists of a martensitic matrix with a few primary carbides and small amounts of retained austenite. Tempering causes the transformation of retained austenite into cubic martensite and cementite and the precipitation of a variety of secondary carbides, responsible for the high-temperature properties [2]. Quenching rate dependent mechanical properties after tempering lead to a need of the investigation of the hardened microstructure and its influence on the tempering behaviour. Retained austenite has been reported to be situated as thin films between martensitic laths, examined by transmission electron microscopy (TEM) [3] as well as by 3-dimensional atom probe tomography (3DAP) [4]. For instance, Horn et al. [5] found such retained austenite films to be jointly responsible for a loss in toughness correlated to the cementite precipitation during the tempering in an AISI 4340 low alloy steel. The severity of this "tempered martensite embrittlement" has been found to depend on the amount of retained austenite. Atom probe studies on similar steels depicted carbon segregation to dislocations, microtwins and interfaces and the formation of small carbon clusters [3, 4, 6-9]. A redistribution of the carbon from supersaturated martensite to the retained austenite during the martensitic transformation was reported too [10]. Tempering of 5% Cr martensitic steel leads to the precipitation of MC, M_3C, M_7C_3 and $M_{23}C_6$ [11, 12] through different precipitation sequences [2].

The aim of the present work is to depict the quenching rate induced microstructural distinctions in the martensitic matrix after hardening and the influence on the tempering behaviour. The main focus of attention is laid on the distribution of carbon and the carbide forming elements in the hardened microstructure and in the early stages of tempering. The main investigation method is atom probe tomography, predestined for compositional analysis on the nanoscale.

Experimental

The investigations have been carried out on a commercial hot-work tool steel AISI H11 with the nominal composition as given in Table 1. Cylindric samples 15 mm long and diameter of 5 mm have been heat treated in a quenching dilatometer Dil 805 A from Bähr Thermoanalyse GmBH. Heating to 1020°C was done with a heating rate of 0.55°C/min. After a 30 minutes austenitizing treatment the samples have been hardened with quenching rates λ = 0.6, 6 and 12, respectively. Additionally, samples have been heated up after hardening to 400°C, 500°C and 610°C (0.55°C/min) and immediately quenched, in order to simulate the very early temper stages for the sample quenched with λ = 12.
Bars of the dimension 0.3 x 0.3 x 12 mm^3 have been cut out from the heat-treated samples for the atom probe specimen preparation. The tips have been produced by a standard two step electrochemical polishing procedure [13]. The hardened samples have been measured in voltage mode on a LEAP 3000X HR from Cameca, former Imago Scientific Instruments, at a temperature of 60 K and with a pulse fraction of 20%. The heat treated samples were not measureable in voltage mode, therefore, the measurements have been carried out by using a 532 nm wavelength pulsed laser with a frequency of 250 kHz. The temperature has been set to 30 K and laser pulse energy of 0.6 nJ has been used. The reconstruction of the probed volumes and the analysis of the data sets have been carried out with the software package IVAS 3.4.3 from Cameca.

Table 1: Nominal composition and composition measured by atom probe.

	C	Si	Mn	Cr	Mo	V	Fe
wt%	0.37	1.11	0.41	4.90	1.23	0.33	bal.
at%	1.68	2.16	0.41	5.14	0.70	0.35	bal.
AP at%	1.77	2.52	0.44	5.36	0.82	0.39	bal.

Results and discussion

A number of atom probe measurements of the hardened samples have been carried out and the mean measured elemental contents satisfactorily agree with the nominal composition of the alloy as listed in Table 1. The general higher values for alloying elements obtained by atom probe tomography can be contributed to an error in the mass range determination.

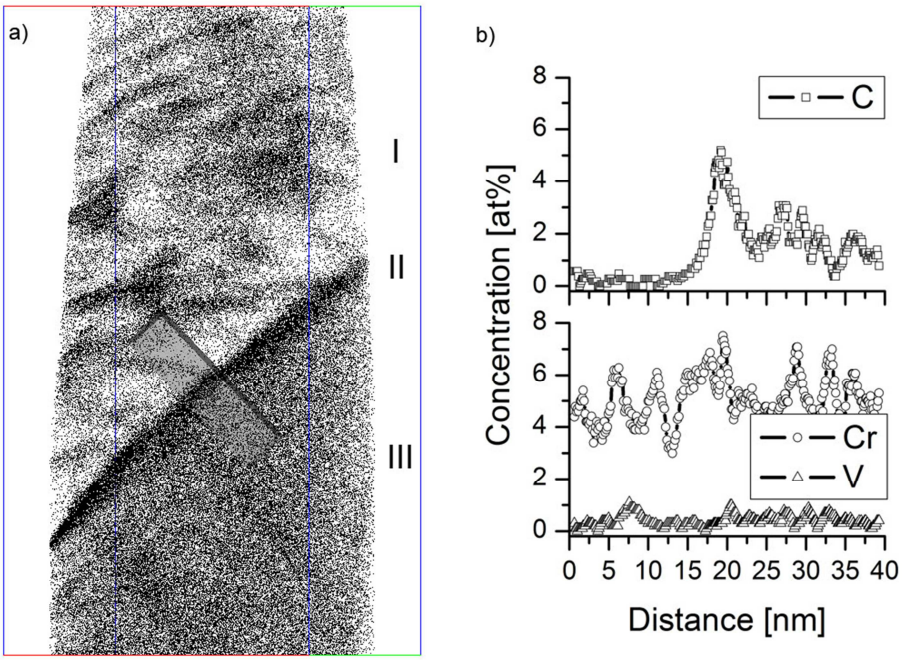

Figure 1: Carbon atom map of the sample quenched with λ = 0.6. Box size 75x75x150 nm^3 (a); Carbon, chromium and vanadium concentration profiles through a retained austenite film. Cube size 10x10x40 nm^3 (b).

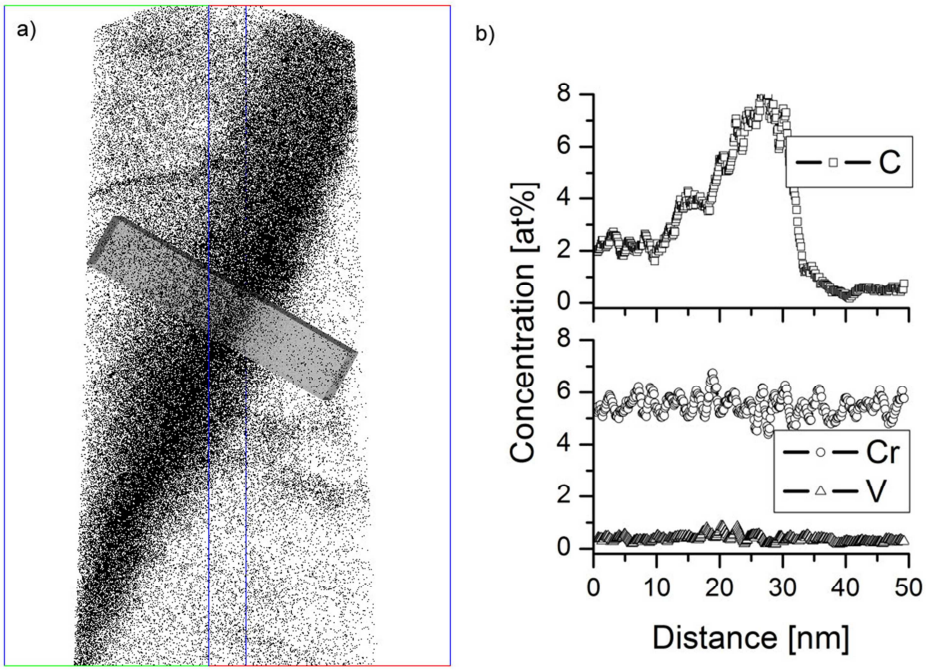

Figure 2: Carbon atom map of the sample quenched with λ = 12. Box size 60x60x120 nm^3 (a); Carbon, chromium and vanadium concentration profiles through a retained austenite film. Cube size 10x10x50 nm^3 (b).

The carbon atom map depicted in Figure 1a is a typical representative of very fast (λ = 0.6) quenched samples, showing three regions differently affected by carbon segregation. Region I shows heavy carbon segregations forming irregular shapes with peak carbon concentrations of ~8-10 at% whereas in region III the carbon seems to be homogeneously distributed. Parameter μ is a normalized χ^2 provided by distribution analysis and an indicator for the degree of segregation of an individual element [14]. The higher parameter μ (0-1) the more pronounced is the grade of

segregation. The μ value for the regions I and III is 0.64 and 0.05, respectively, which confirms the visual impression. The two described regions are separated by a high-carbon containing thin film (region II). The carbon concentration profile in Figure 1b through this film shows a peak carbon concentration of ~ 6 at% and a thickness of 4-6 nm. These characteristics evidence this feature to be retained austenite embedded between two martensitic laths [4]. Considering the carbon concentration of ~1.65 at% in the entire homogeneous lath leads to the assumption that carbon partitioning into the retained austenite film primarily originates from the inhomogeneous lath, which entirely contains ~1.15 at%. On the other hand, the chromium and vanadium concentrations as also depicted in Figure 1b keep constant. The carbon atom map in Figure 2a belongs to the sample quenched with λ = 12 and shows a film with a carbon concentration of ~8 at% as depicted in the corresponding carbon concentration profile in Figure 2b. Therefore, this film can also be related to retained austenite, but the thickness of the film is ~ 25 nm. This indicates that the amount of retained austenite increases with reduced cooling rate. Such a behaviour was also found by Mayer [15]. Figure 2b further reveals that the carbide forming elements chromium and vanadium also do not show variations through the interlath retained austenite film in this condition.

Applying frequency distribution analysis on the atom probe data of the differently heated samples evidences that almost no segregation of substitutional elements has taken place during heating to 400°C and 500°C (not shown here). The carbon atom map in Figure 4a belongs to the sample quenched with λ = 0.6 and heated up to 610°C representing a region consisting of several martensitic laths separated by four of the previously mentioned interlath retained austenite films. Inside the laths carbon clusters can be seen. The probed volumes of the samples heated up to 610°C indicate that a considerable rearrangement of the substitutional elements occurred. The segregation is exemplarily visualized by applying chromium-isosurfaces on a single measurement. Figure 4b depicts the corresponding 10 at% chromium isosurfaces, revealing the chromium segregation. It is illustrated that during heating to 610°C remarkable chromium segregation to high-carbon regions takes place. The former retained austenite films seem to transform to high chromium containing carbon clusters and the former inlath pure carbon clusters are chromium enriched. The proxigram in Figure 4c based on the isosurface in Figure 4b confirms that also the carbide forming elements vanadium and molybdenum are enriched in the carbon clusters.

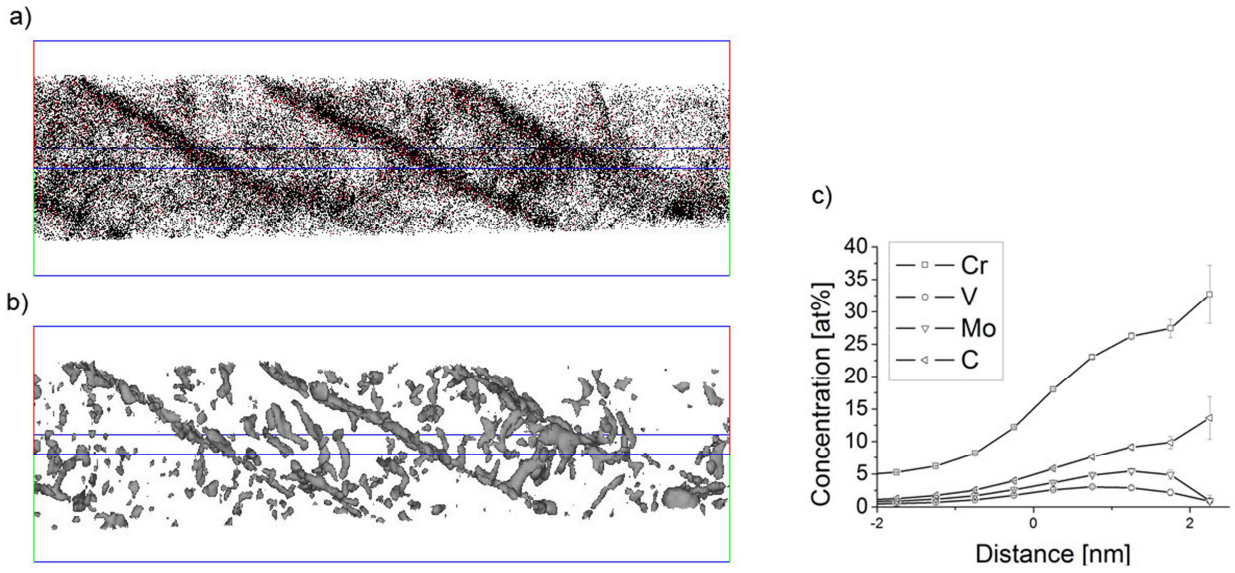

Figure 4: Carbon atom map of the sample quenched with l = 0.6 and heated up to 610°C. Box size 60x60x250 nm3 (a); Chromium isosurfaces (10 at%) of the same sample (b); Corresponding proxigram (c).

Significant differences between the samples differently quenched and heated up to 610°C are not visible. A reasonable distinction of the grade of segregation during heating between the differently quenched samples is not possible. This limitation is due to the existence of a variety of different regions in all of the probed volumes. The awareness of a thickness increase of the retained austenite films with lower quenching rates and the extensive carbide forming at these films as depicted in Figure 4b lead to the assumption that samples with in average thicker retained austenite films show a higher fraction of laminary arranged carbide phase.

Summary

The hardened microstructure of a common hot-work tool steel AISI H11 has been characterized by using 3-dimensional atom probe. On the one hand regions differently affected by carbon segregation could be observed in the hardened samples and on the other hand no segregation of any substitutional elements has taken place in any cases. Regions containing irregular shaped carbon clusters as well as almost homogeneously distributed regions could be found. The mean thickness of carbon enriched interlath retained austenite films increases with lower quenching rates. These films and the pre-existing inlath carbon clusters act as nucleation sites of alloy carbide formation. Heating of the quenched samples to 400°C, 500°C and 610°C revealed that the enrichment of chromium, vanadium and molybdenum at high-carbon regions does not occur till heating to 610°C.

References

[1] Roberts GA, Krauss G, Kennedy R. Tool steels. ASM International (1998).

[2] Porter DA, Easterling KE. Phase transformations in metals and alloys. Chapman & Hall (1992).

[3] Caballero FG, Miller MK, Babu SS, Garcia-Mateo C. Acta Materialia 55 (2007) 381.

[4] Sherman DH, Cross SM, Kim S, Grandjean F, Long GJ, Miller MK. Metallurgical and Materials Transactions A 38 (2007) 1698.

[5] Horn RM, Ritchie RO. Metallurgical Transactions A 9 (1978) 1039.

[6] Caballero FG, Miller MK, Garcia-Mateo C. Acta Materialia 58 2338.

[7] Thomson RC, Miller MK. Acta Materialia 46 (1998) 2203.

[8] Wilde J, Cerezo A, Smith GDW. Scripta Materialia 43 (2000) 39.

[9] Zhu C, Cerezo A, Smith GDW. Ultramicroscopy 109 (2009) 545.

[10] Clarke AJ, Speer JG, Miller MK, Hackenberg RE, Edmonds DV, Matlock DK, Rizzo FC, Clarke KD, De Moor E. Acta Materialia 56 (2008) 16.

[11] Delagnes D, Lamesle P, Mathon MH, Mebarki N, Levaillant C. Materials Science and Engineering A 394 (2005) 435.

[12] Mebarki N, Delagnes D, Lamesle P, Delmas F, Levaillant C. Materials Science and Engineering A 387-389 (2004) 171.

[13] Miller MK. Atom probe field ion microscopy. Clarendon Press ;

Oxford University Press (1996).

[14] Moody MP, Stephenson LT, Ceguerra AV, Ringer SP. Microscopy Research and Technique 71 (2008) 542.

[15] Mayer S. Einfluss einer bainitischen/martensitischen Mikrostruktur auf die mechanischen Eigenschaften von Warmarbeitsstählen. Department of physical metallurgy and materials testing. Leoben: University of Leoben (2009).

Publication II

Christoph Lerchbacher, Silvia Zinner, Harald Leitner

Atom probe study of the carbon distribution in a hardened martensitic hot-work tool steel X38CrMoV5-1

Micron 43 (2012) 818-826

Micron 43 (2012) 818–826

Contents lists available at SciVerse ScienceDirect

Micron

journal homepage: www.elsevier.com/locate/micron

Atom probe study of the carbon distribution in a hardened martensitic hot-work tool steel X38CrMoV5-1

Christoph Lerchbacher[a,*], Silvia Zinner[b], Harald Leitner[c]

[a] Christian Doppler Laboratory of Early Stages of Precipitation, University of Leoben, Franz-Josef-Straße 18, A-8700 Leoben, Austria
[b] Böhler Edelstahl GmbH & Co AG, Mariazellerstraße 25, A-8605 Kapfenberg, Austria
[c] Department of Physical Metallurgy and Materials Testing, University of Leoben, Franz-Josef-Straße 18, A-8700 Leoben, Austria

ARTICLE INFO

Article history:
Received 4 November 2011
Received in revised form 6 February 2012
Accepted 9 February 2012

Keywords:
Hot-work tool steel
Martensite
Carbon distribution
Retained austenite
Atom probe tomography

ABSTRACT

The microstructure of the hardened common hot-work tool steel X38CrMoV5-1 has been characterized by atom probe tomography with the focus on the carbon distribution. Samples quenched with technically relevant cooling parameters λ from 0.1 (30 K/s) to 12 (0.25 K/s) have been investigated. The parameter λ is an industrially commonly used exponential cooling parameter, representing the cooling time from 800 to 500 °C in seconds divided with hundred. In all samples pronounced carbon segregation to dislocations and cluster formation could be observed after quenching. Carbon enriched interlath films with peak carbon levels of 6–10 at.%, which have been identified to be retained austenite by TEM, show a thickness increase with increasing λ. Therefore, the fraction of total carbon staying in the austenite grows. This carbon is not available for the tempering induced precipitation of secondary carbides in the bulk. Through all samples no segregation of any substitutional elements takes place. Charpy impact testing and fracture surface analysis of the hardened samples reveal the cooling rate induced microstructural distinctions.

1. Introduction

Hot-work tool steels are mainly used as die-casting dies, forging dies and as various tools for different hot-work applications. The main application field is the processing of light metals. Therefore, these materials have to resist the exposure to higher temperatures without changing microstructure and mechanical properties (Roberts et al., 1998). These properties are generated by the chemical composition, a high micro-cleanness and a well-defined heat treatment of the virgin blocks. The latter consists of an austenitization treatment with a subsequent hardening and a multiple tempering procedure. The microstructure after hardening contains a martensitic matrix with few primary carbides and small amounts of retained austenite. Tempering leads to the precipitation of a variety of secondary carbides embedded in the relaxed matrix and the transformation of retained austenite into ferrite and cementite. The retained austenite is mainly situated between the martensitic laths in form of thin films. The existence of these austenite films with varying thicknesses was reported in several papers, examined by transmission electron microscopy (TEM) (Horn and Ritchie, 1978; Sarikaya et al., 1983) as well as by 3-dimensional atom probe tomography (3DAPT) (Sherman et al., 2007). Also redistribution of carbon from supersaturated martensite to retained austenite films takes place during the martensitic transformation. This carbon enrichment has also been shown for different steels and processing routes in several atom probe studies (Caballero et al., 2010a; Clarke et al., 2008; Thomson and Miller, 1995, 1998). Beside the redistribution of carbon from the martensitic matrix to the austenite films, other auto-tempering effects like carbon segregation to dislocations, microtwins and cluster formation have been reported in martensitic steels (Miller et al., 1981, 1983; Pereloma et al., 2008; Sherman et al., 2007; Taylor et al., 1989; Thomson and Miller, 1998; Timokhina et al., 2010; Wilde et al., 2000; Zhu et al., 2009) as well as in bainitic steels (Caballero et al., 2007, 2010b).

The toughness of the finished tool and therefore its performance in use strongly depends on the cooling rate during hardening (Bungardt et al., 1966; Jesperson, 2009). As already mentioned, tempering causes the transformation of the retained austenite to ferrite and Fe_3C particles. Consequently, the lath boundaries are occupied by carbides, which leads to a loss in toughness. Horn and Ritchie (1978) correlated the severity of this "tempered martensite embrittlement" with the amount of retained austenite in an AISI 4340 low alloy steel.

However, the cooling rate dependence of the microstructure in the hardened martensitic region produced with technically relevant cooling parameters has not been questioned in a detailed way. Thus, the aim of the present work is to depict the quenching rate induced microstructural distinctions in the martensitic matrix

* Corresponding author.
E-mail address: christoph.lerchbacher@unileoben.ac.at (C. Lerchbacher).

0968-4328/$ – see front matter © 2012 Elsevier Ltd. All rights reserved.
doi:10.1016/j.micron.2012.02.005

Table 1
Details of the cooling paths.

	λ						
	0.1	0.3	0.6	1	3	6	12
Cooling rate [K/s]	30	10	5	3	1	0.5	0.25
Time from Ms to RT [s]	80	240	480	800	2400	4800	9600
RT-aging [h]	24	24	24	24	–	–	–

after hardening with technically relevant cooling conditions. Exponential T8/5 quenching rates simulate the real conditions in an industrial block in an appropriate way, therefore, technically relevant process parameters from λ = 0.1 (30 K/s) to 12 (0.25 K/s) have been chosen. The main focus of attention is held on the carbon distribution in the martensitic microstructure using atom probe tomography as the main investigation method, predestined for compositional analysis on the nanoscale.

2. Experimental

The commercial hot-work tool steel X38CrMoV5-1 with the nominal composition as shown in Table 1 has been used for the experiments. The heat treatment has been performed on cylindrical samples with a length of 15 mm and a diameter of 5 mm using a quenching dilatometer Dil 805 A from Bähr Thermoanalyse GmbH. Heating to the austenitization temperature of 1020 °C has been done with a heating rate of 0.5 °C/s. The dwell time was set to 30 min under vacuum. Afterwards, the material has been quenched with cooling parameter λ = 0.1, 0.3, 0.6, 1, 3, 6, and 12 (corresponding cooling rates 30, 10, 5, 3, 1, 0.5 and 0.25 K/s), covering the complete martensitic region of the steel investigated.

Bars of the dimension 0.3 mm × 0.3 mm × 12 mm have been cut out from the heat-treated samples for the atom probe specimen preparation. The tips have been produced by a standard two step electrochemical polishing procedure (Miller et al., 1996). The measurements have been carried out in voltage mode on a LEAP 3000X HR from Cameca, former Imago Scientific Instruments, at a temperature of 60 K and with a pulse fraction of 20%. The reconstruction of the probed volumes and the analysis of the data sets have been carried out with the software package IVAS 3.4.3. from Cameca. Carbon peaks in the mass spectrum have been defined on m/n positions 6, 6.5, 12, 13, 18, 18.5, 24 and 36 with the corresponding isotopes and ionization states C^{12++}, C^{13++}, C^{12+}, C^{13+}, C_3^{2+}, C_3^{2+}($2 \times C^{12}$ and $1 \times C^{13}$), C_2^{+} and C_3^{+}, respectively.

Transmission electron microscopy (TEM) has been done on a Philips CM12.

XRD-measurements have been performed on a Siemens D500 using CuKα radiation with a wave length of 1.542 Angstrom. Details of the technique can be found in the work of Mayer (2009).

Instrumented impact tests conducted on a 300 J impact pendulum from Zwick were performed to evaluate the impact toughness of the samples hardened with λ = 0.6, 6 and 12. The mean absorbed energy was measured using 3 Charpy U-notched specimens of the dimension 55 mm × 10 mm × 7 mm per sample state. Fracture surface analysis was carried out by scanning electron microscopy using a Zeiss EVO50.

3. Results and discussion

The transformation of the austenite into martensite starts at a temperature of approximately 280 °C. Fig. 1 shows the cooling paths of the differently quenched samples in the region from Ms to room temperature (RT). It is obvious that the cooling time significantly increases with increasing λ-value. This implies that solute atoms in the newly built martensitic laths have much more time to segregate and to relax the matrix at higher λ-values. The cooling

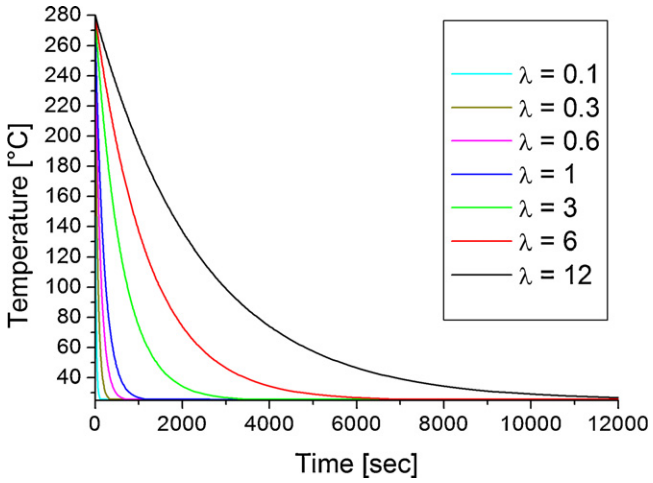

Fig. 1. Time–temperature curves of the differently quenched samples in the range from Ms to RT.

time from Ms to RT ranges from 80 s for λ = 0.1 up to 160 min for λ = 12. Details of the cooling paths can be found in Table 1. However, the martensitic transformation is incomplete as the martensite finish temperature is not reached and therefore retained austenite is present. Thus, the hardened microstructure consists of martensite, retained austenite and a very small amount of primary carbides which have not been dissolved during austenitization.

3.1. Atom probe tomography

Atom probe measurements depict the microstructural features and their arrangement with corresponding elemental concentrations in a detailed way. It should be noted that the steel used in the present work does not show any carbide formation during hardening (Mayer, 2009), which can be related to the high silicon content of the alloy. Silicon is known to retard the cementite precipitation due to the low solubility of silicon in Fe_3C associated with the limited atom mobility at low temperatures (Kozeschnik and Bhadeshia, 2008). The mean measured composition over all analysed volumes is in good agreement with the nominal composition as depicted in Table 2. The substitutional elements generally show slightly higher contents which might suggest a minor loss of Fe during field evaporation. All measurements show equal concentration values, and therefore, an effect of segregation can be excluded. The mean standard deviation has been calculated using compositional atom probe data of all evaluated volumes.

Table 2
Nominal composition of the investigated steel X38CrMoV5-1 compared with the mean composition measured by atom probe.

	C	Si	Mn	Cr	Mo	V	Fe
wt%	0.37	1.11	0.41	4.90	1.23	0.33	bal.
at.%	1.68	2.16	0.41	5.14	0.70	0.35	bal.
AP at.%	1.80	2.55	0.44	5.41	0.85	0.39	bal.
σ at.%	0.24	0.06	0.02	0.21	0.07	0.02	

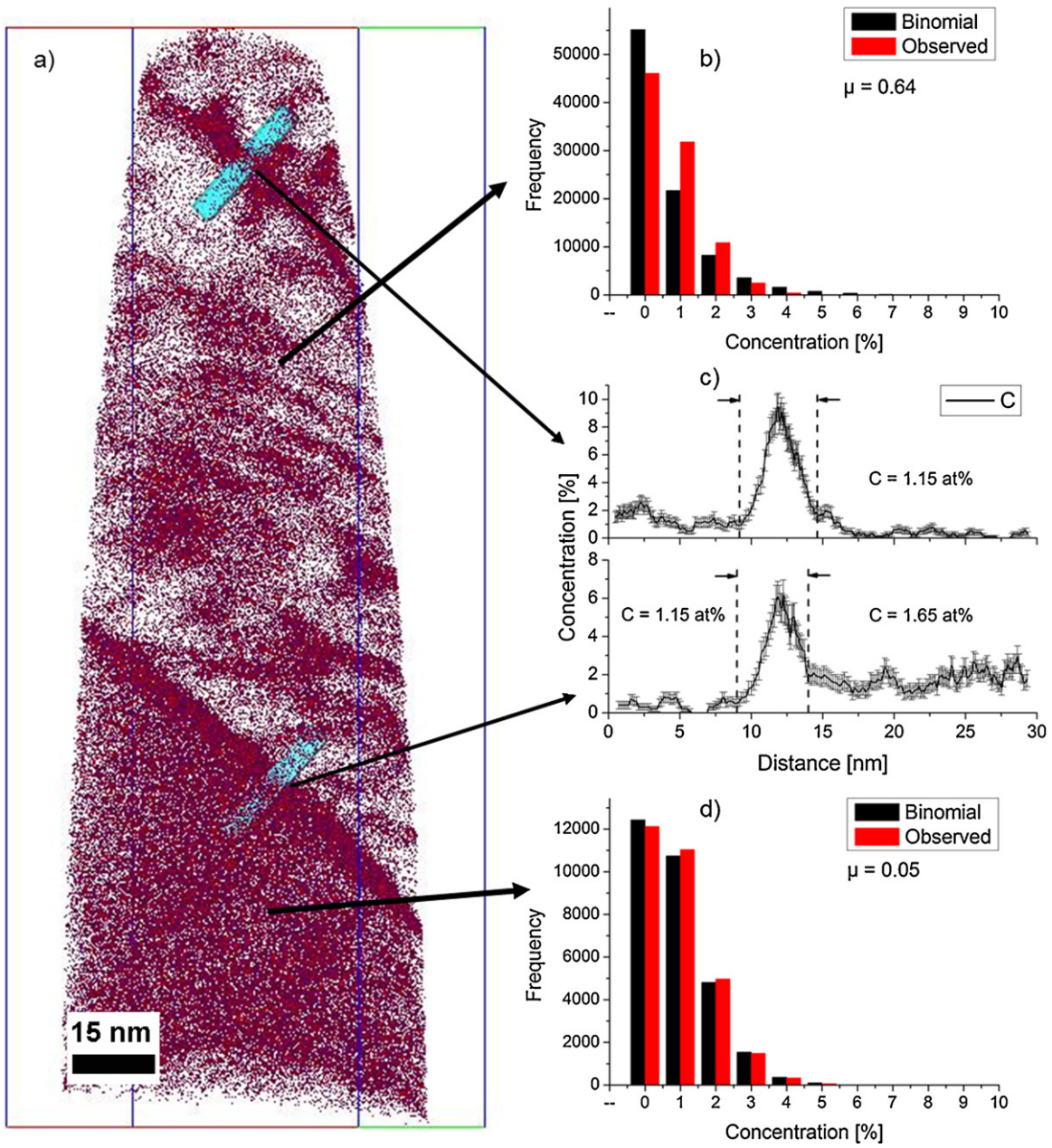

Fig. 2. Carbon atom map (box size 81 nm × 82 nm × 240 nm) of the sample quenched with λ = 0.3 (a); frequency distribution of carbon atoms in the heavily segregated region inside the probed volume (b); carbon concentration profiles in the cubes' *z*-directions (5 nm × 5 nm × 30 nm) through the two interlath austenite films (c); and frequency distribution of carbon atoms in the homogeneous region inside the probed volume (d).

However, the exact measurement of substitutional elements is beyond the scope of this study. Single carbon concentrations must be questioned because of the fact that significant carbon segregation takes place and regions differently affected by carbon segregation occur. The mean carbon content conforms to the nominal composition which leads to the assumption that no carbon is lost during the atom probe measurements. That might be an indicator that no carbides are formed at this stage of heat treatment since no multiple event related carbon loss is obvious, which preferably occurs with the presence of carbides (Yao et al., 2010). In all 3D reconstructions only carbon is depicted because segregation of the other alloying elements could not be observed in any case. Fig. 2(a) shows the carbon atom map of the sample quenched with λ = 0.3. This measurement is a typical representative for the samples quenched in the λ range 0.1–0.6. The map reveals three different regions: two interfaces, regions of a nearly homogenous carbon distribution and regions where significant carbon segregation can be seen. The concentration profiles through the interfaces, illustrated in Fig. 2(c), indicate a thickness of ~4–5 nm and a carbon peak concentration in the range of ~6–10 at.% which is significantly higher than the nominal composition of the alloy. These characteristic values suggest the interfaces to be retained austenite occurring as thin films between martensitic laths (Sherman et al., 2007). The carbon in the region between the two austenite films in Fig. 2(a) is heavily segregated, forming irregular shapes with peak concentrations of approximately 8–15 at.%. Such features inside martensitic laths were reported to be Cottrell atmospheres in the vicinity of dislocations and carbon precursor clusters (Wilde et al., 2000; Zhu et al., 2009). The region in the lower third of the atom map shows a nearly homogenous carbon distribution with a carbon level of about 1.65 at.% which is in the same order of magnitude as the nominal composition of the alloy. This leads to the assumption that this

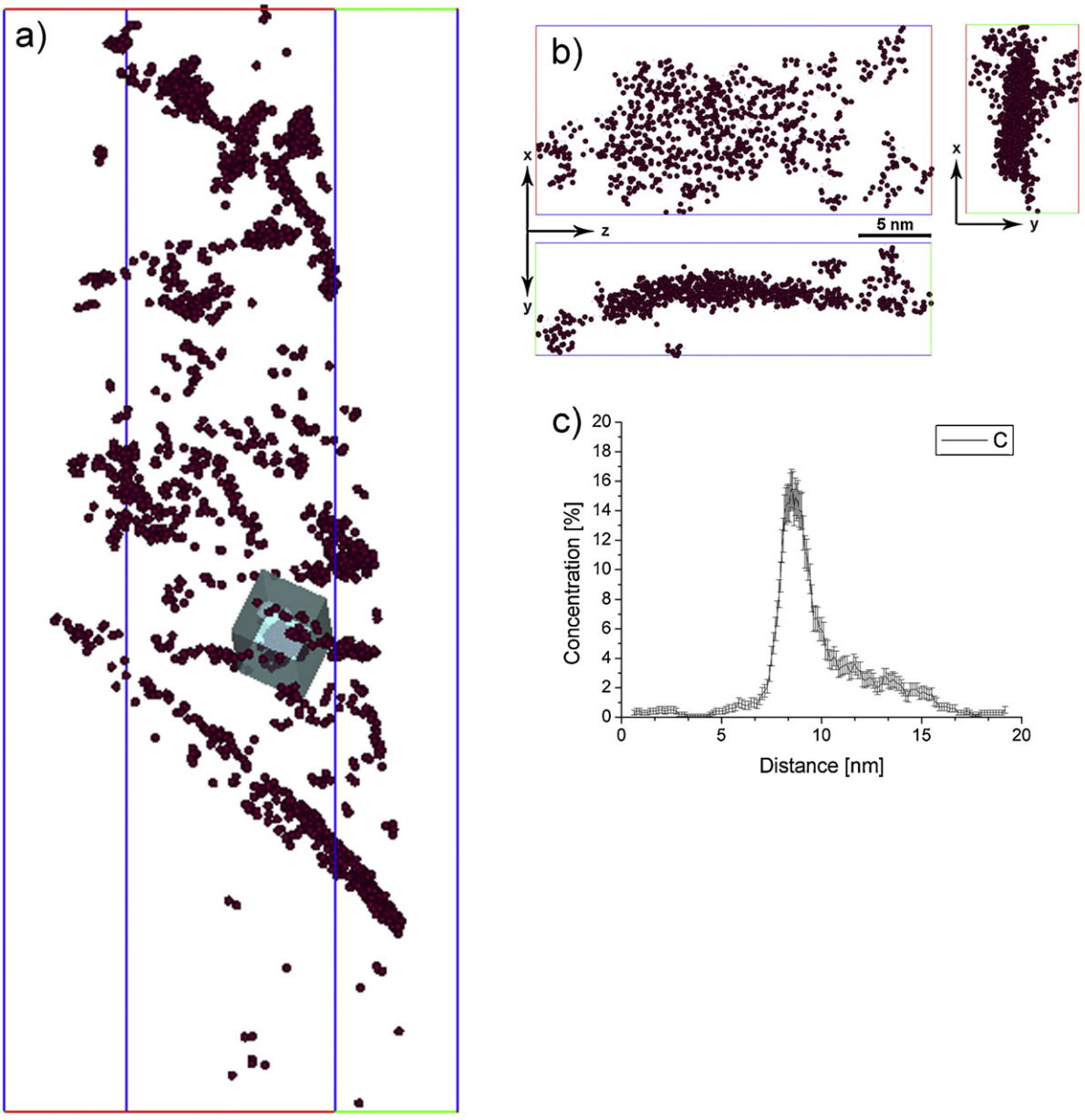

Fig. 3. Carbon clusters in the volume of Fig. 2 found by a maximum distance separation method, d_{max} 0.60 nm (a); representative carbon cluster from 3 perpendicular directions showing the shape of the cluster (b); and corresponding carbon concentration profile (c).

region belongs to a martensitic lath which has formed at lower temperature. Carbon clustering is suppressed because of the low temperature and the high alloying content in this material, which reduce diffusion. Frequency distributions (Fig. 2(b) and (d)) have been plotted in order to quantitatively provide the level of segregation in the two martensitic regions differently affected by carbon segregation. The parameter μ, which is gained from the frequency distributions, is presented for further evaluations of the carbon segregation. The parameter is a normalized χ^2 (Moody et al., 2008) ranging from 0 to 1, representing the degree of segregation. These values, 0.05 for the lath in the lower region and 0.64 for the lath in the upper region in Fig. 2, confirm the visual impression. The carbon in the upper lath shows extensive auto-tempering effects, whereas the lower lath shows a homogeneous carbon distribution. Considering the carbon concentration of 1.65 at.% in the homogeneous lath leads to the assumption that carbon migrating into the retained austenite film primarily originates from the inhomogeneous lath, which only contains 1.15 at.% carbon.

The thickness and the carbon content of the two interlath austenite films in Fig. 2(a) are similar with ~5 nm and 6–10 at.%, respectively. However, the two films differentiate considering the characteristics of the martensitic regions they separate. The upper austenitic film lies between two heavily segregated martensite laths, whereas the lower film separates a homogeneous and an inhomogeneous martensitic lath. Assuming that the homogeneous lath has been formed at lower temperatures, as mentioned above, suggests that the film thickness is independent of the temperature at which the adjacent laths are formed.

A maximum distance separation algorithm has been applied on the same volume in order to confirm the presence of clusters in the matrix as depicted in Fig. 3(a). Fig. 3(b) shows a selected cluster from 3 perpendicular directions visualising its plate-like shape with the largest extent in z-axis. The shape might indicate that the cluster has formed in the core of a dislocation. The corresponding carbon concentration profile given in Fig. 3(c) reveals a peak carbon concentration of 15 at.% in the cluster's core.

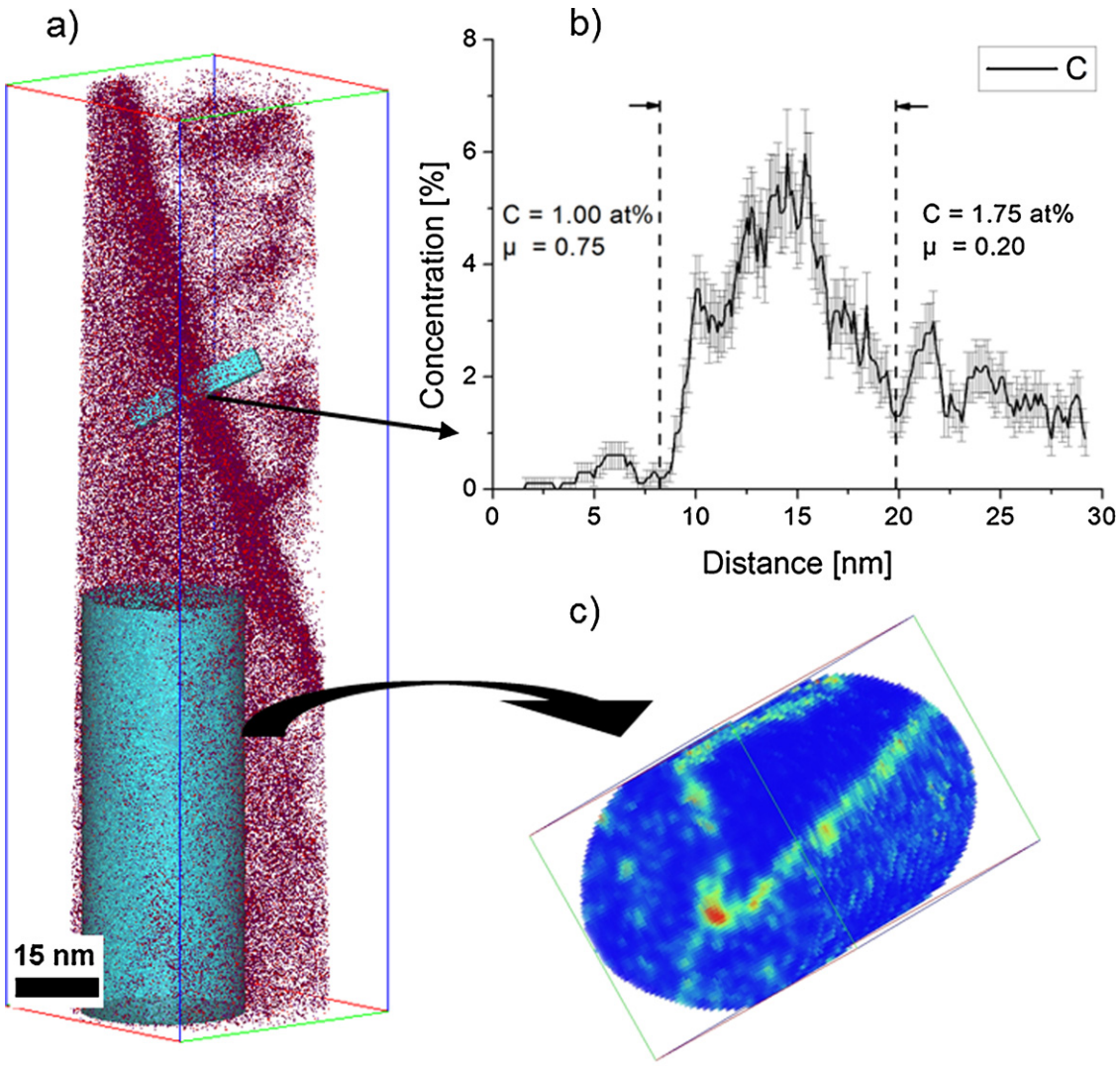

Fig. 4. Carbon atom map (box size 58 nm × 58 nm × 200 nm) of the sample quenched with λ = 3 (a); carbon concentration profile in the cube's *z*-direction (5 nm × 5 nm × 30 nm) through an interlath austenite film (b); and intersecting edge of a martensitic lath bordered by interlath austenite films (c).

Fig. 4(a) shows the probed volume of the sample quenched with λ = 3. Again, a carbon enriched interface can be seen. The linear concentration profile (Fig. 4(b)) through the interface reveals a carbon peak concentration of ~6 at.% and a thickness of this carbon segregation of about 10 nm. Based on the carbon concentration, this region again is attributed to austenite. Beside this thin film, also two regions differently affected by carbon segregation, and separated by this interlath austenite film, are obvious. The carbon concentration in the upper lath is 1.00 at.% and the corresponding μ-value is 0.75, revealing the obviously high degree of segration. The lath in the lower region shows a carbon level of 1.75 at.% and a μ-value of 0.20. The carbon concentration of this lath is slightly overestimated due to a feature within the lath which is not clearly visible on the carbon atom map. Therefore, a cylindrical area of interest has been extracted in the lower part of the analysed volume. Fig. 4(c) represents a partly transparent 3-dimensional carbon map of the tilted cylinder. The image reveals the intersection of the edge of a martensitic lath into the probed volume. The green regions in the cylinder correspond to carbon levels of ~6 at.%, indicating interlath austenite films. Inside of this martensitic lath no carbon segregation can be observed, whereas in the surrounding volume several carbon clusters, indicated by the green spots, can be seen.

Fig. 5(a) and (c) shows interlath austenite films found in the probed volumes of the samples quenched with λ = 6 and 12, respectively. The carbon concentration profiles through such regions reveal in both cases peak carbon levels of 8–10 at.%, but their thicknesses differ. The profile through the layer in the sample quenched with λ = 6 (Fig. 5(b)) reveals a thickness of ~12 nm, whereas in the sample quenched with λ = 12 (Fig. 5(d)) a thickness of ~25 nm is obtained. The films in both samples separate different types of martensitic laths. Fig. 5(a) depicts laths showing carbon concentration levels of 0.80 at.% and 1.76 at.% with corresponding μ-values of 0.33 and 0.24, respectively. The laths in Fig. 5(b) show carbon concentrations of 1.72 at.% and 0.52 at.% with corresponding μ-values of 0.19 and 0.50, respectively. The observed laths show a broad distribution of carbon concentrations and μ-values, which is assumed to be related to the temperature at which the laths were formed during the transformation. This issue and the extremely small probed volumes make it impossible to quantitatively determine the degree of carbon segregation of the differently quenched samples. However, the carbon concentrations and the corresponding μ-values of the observed martensitic laths show a clear trend. Higher carbon levels lead to lower μ-values, hence, higher randomness of the carbon atoms within the lath. In fact, this confirms the assumption that low-carbon laths are formed at higher temperatures

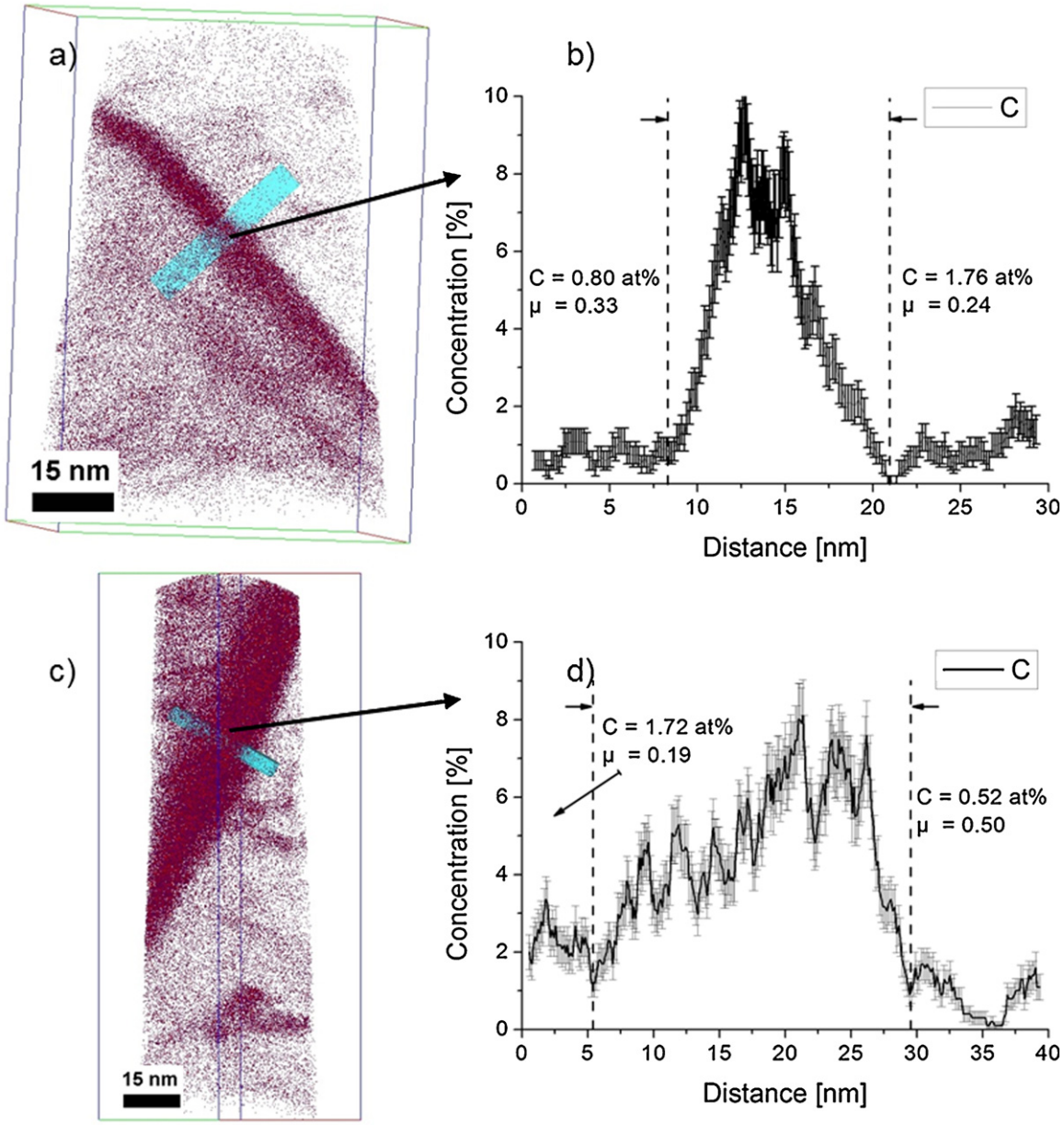

Fig. 5. Carbon atom map (box size 61 nm × 62 nm × 88 nm) of the sample quenched with λ = 6 (a) and the corresponding carbon concentration profile in the cube's *z*-direction (5 nm × 5 nm × 30 nm) (b); carbon atom map (box size 62 nm × 62 nm × 181 nm) of the sample quenched with λ = 12 (c) and the corresponding concentration profile in the cube's *z*-direction (5 nm × 5 nm × 40 nm).

enhanced by dislocations and provide the majority of carbon for the retained austenite enrichment. Additionally, the shape of the carbon concentration profile through the martensite/retained austenite interface affirms this assumption. The interfaces between inhomogeneous laths and the retained austenite films are relatively sharp compared to that of homogeneous laths. The concentration profile through the retained austenite film according to the sample quenched with λ = 12 as shown in Fig. 5(d) gives a representative example. The interface to the homogeneous lath shows a relatively long and irregular shaped gradient in the carbon concentration. It seems that the carbon diffusion process to the retained austenite has not been finished during quenching. Again, this leads to the assumption that such a lath has been formed at lower temperatures where diffusion is slower. Such gradients in the concentration profiles can also be found in Figs. 2(c) and 4(b). These gradients and irregularities make the evaluation of the film thickness somewhat difficult. Although the determination is uncertain, a clear trend can be seen.

3.2. TEM

In order to confirm the observed thin films to be retained austenite, TEM investigations have been performed. The thicker films could be clearly identified as retained austenite by TEM-diffraction experiments. Fig. 6 depicts the bright-field (Fig. 6(a)) and the corresponding dark-field (Fig. 6(b)) TEM images of the observed films in the sample quenched with λ = 12. The dark field image was obtained using the circled diffraction spot in Fig. 6(c), which corresponds to the austenitic lattice.

Even when the films depicted in Figs. 5(c) and 6 show equal thicknesses, this does not necessarily say that all films within a sample obtain the same thickness. At least three atom probe

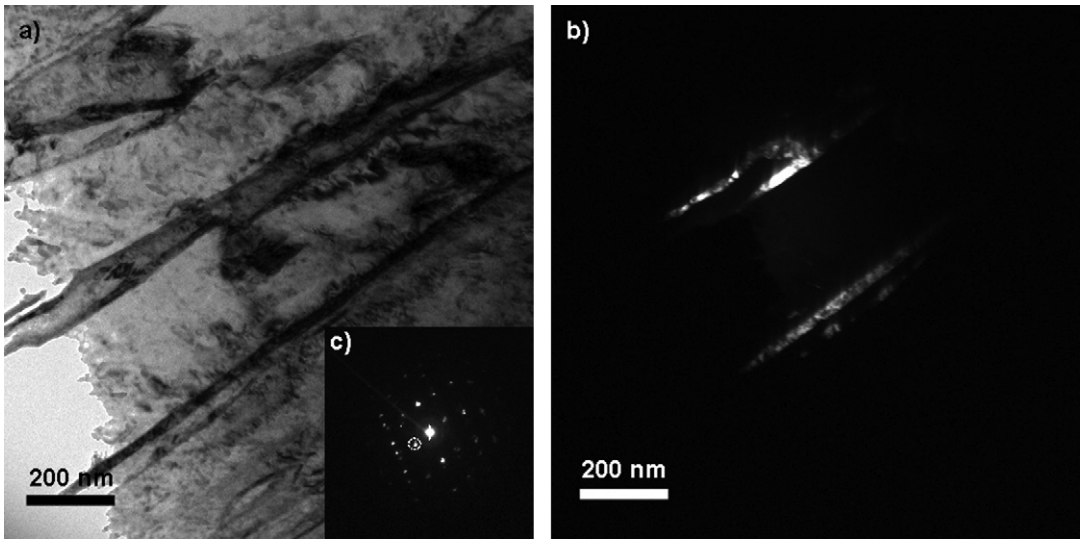

Fig. 6. Bright field TEM-image of the sample quenched with λ = 12 (a); corresponding dark field TEM-image (b); and diffraction pattern with the encircled diffraction spot used for dark-field TEM-imaging (c).

measurements containing a retained austenite film for each sample have been performed and representative images have been presented. The probability to probe a thicker film increases in samples cooled with lower cooling rates, therefore, the mean film thickness within the sample reaches higher values with increasing λ.

3.3. Retained austenite – cooling rate

Fig. 7 summarizes the measured film thicknesses as a function of the quenching parameter. Additionally, the volume fraction of retained austenite determined by Mayer (2009) using X-ray diffraction is illustrated. No retained austenite has been detected up to a quenching rate of λ = 1, therefore, the volume fraction is arbitrary set to 3%, the lower limit of the X-ray technique. This issue is also marked in the diagram. Though the statistical spread of the retained austenite volume data, it is clearly visible that the increase of the amount of austenite in the material comes along with a growth in mean thickness of the observed retained austenite films. This is in agreement with the investigations of Sherman et al. (2007), who found a film thickness increase from the sample cooled with 560 K/s to a sample cooled with 25 K/s and tempered at 215 °C. The film thickness of the sample cooled with 560 K/s is similar to the

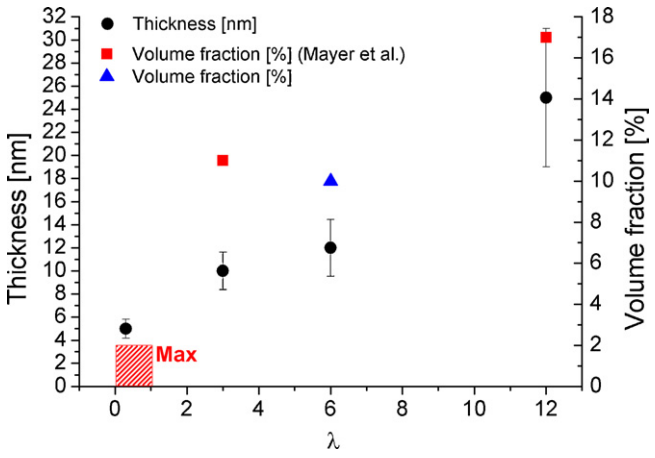

Fig. 7. Development of the interlath austenite film thickness and the volume fraction of retained austenite (Mayer, 2009) in dependence of the quenching parameter λ.

film thicknesses of the samples cooled in the λ range of 0.1–0.6 in the present study, which could be explained by the equal amount of retained austenite. The thickness increase is linked with the cooling paths in the following way: on the one hand the samples with lower cooling rates are longer exposed in the austenite phase region during quenching, which leads to a reduction of dislocations, hence, nucleation sites for the martensitic transformation (Porter and Easterling, 1992). Following the investigations of Morito et al. (2010), slightly larger martensitic packets and blocks are formed with lower quenching rates, which means that a decreased effective area for interlath austenite films exists. On the other hand the samples have longer time for the martensitic transformation which leads to higher fractions of retained austenite due to longer times for diffusion controlled carbon enrichment and stabilization of the austenite. Consequently, the increase of the volume fraction of retained austenite according to Fig. 7 paired with a decrease of the effective interface area causes the thickening of the interlath austenite films.

A rough estimation of the mean carbon diffusion path using diffusion parameters from Landolt-Börnstein (1990) during the quenching process leads to a few hundred nm for λ = 0.1 and a few microns for λ = 12 in the temperature range from Ms to room temperature. For the calculation of the diffusion paths the diffusion coefficient at Ms has been used, which is an overestimation of the real diffusion path. Nevertheless, considering the distance between the two parallel interlath austenitic films (~80 nm) in Fig. 2(a) paired with the estimation of the diffusion length reveals the carbon to reach an austenitic film from all positions inside the lath for all quenching rates. This affirms the assumptions of a diffusion controlled, or at least diffusion assisted process.

3.4. Charpy impact testing

Horn and Ritchie (1978) proposed such interlath retained austenite films to be the dominant factor for so-called tempered martensite embrittlement in an AISI 4340 low alloy steel. This is related to the destabilization of the austenite during tempering, hence, the formation of interlath cementite precipitates causes a loss in toughness. This would imply that the potential for interlath cementite precipitation increases with increasing λ. Such a dependence of the toughness on the cooling rates of double-tempered hot-work tool steel X38CrMoV5-1 has been proposed by Mayer

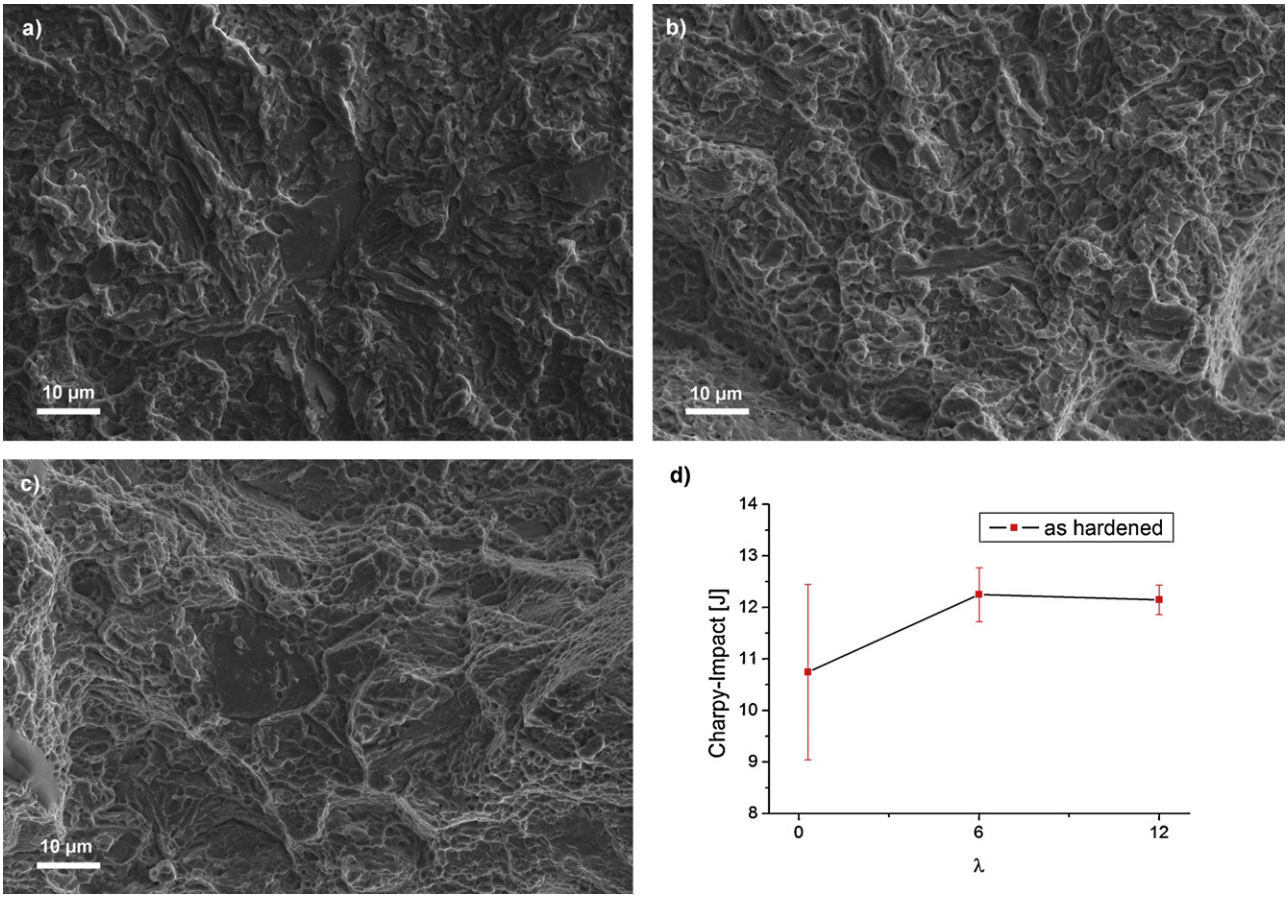

Fig. 8. Fracture surfaces of the Charpy impact specimen cooled with λ = 0.6 (a); λ = 6 (b); and λ = 12 (c); Charpy impact energy of the hardened samples in dependence of the cooling parameter λ.

et al. (2007). The cooling rate dependent microstructure evolution during hardening would suggest converse toughness behaviour for the hardened sample state. To test this, the toughness properties of the initially hardened sample state have to be investigated. In the present study Charpy impact testing has been performed on the hardened material in order to correlate the cooling rate induced microstructural distinctions, hence, the carbon distribution with mechanical properties. Fig. 8 shows the measured impact values and the corresponding fracture surfaces of the differently quenched specimens. The fracture surfaces of the investigated samples reveal the fracture to be quasi-cleavage for all samples. The crack initiation occurs at a single defect within the sample for all cases. Fig. 8(a) shows the fracture surface of the sample quenched with λ = 0.6 and reveals the lowest ductile fraction compared to the samples quenched with λ = 6 (Fig. 8(b)) and 12 (Fig. 8(c)). This fracture behaviour is in agreement with the measured impact values as depicted in the graph in Fig. 8(d). A toughness increase with increasing λ is obvious, though the error-bar enlarges at low cooling rates, which is due to the higher sensitivity to single defects within the material. This toughness increase can be explained by the presence of a higher amount of retained austenite, hence, the martensitic regions are less strained due to the carbon enrichment of the retained austenite.

Considering the amount of retained austenite and its peak carbon concentrations it is obvious that a high amount of the total carbon content is incorporated in the retained austenite films. When identical densities for martensite and austenite are assumed, carbon contents of 10% and 60% of the total carbon for the cooling parameters λ = 0.6 and 12, respectively, are obtained for the austenite. The enriched interlath austenite films transform into carbides and untempered martensite during the first tempering step, which leads to an occupancy of the lath boundaries with carbides. The majority of the carbon in the retained austenite forms planar arranged carbides during tempering. This carbon content is not available for the subsequent tempering induced precipitation of secondary carbides within the martensite laths, which are responsible for the typical high-temperature strength of hot-work tool steels. A recent assessment of this issue is subject for a future work. Even when the second tempering step relaxes the newly formed martensite regions, the toughness lowering interface-carbides might persist. Therefore, it is of great interest to follow in future studies the development of these austenite films and, hence, the carbides which form during the tempering process.

4. Summary

The common hot-work tool steel X38CrMoV5-1 experiences pronounced carbon redistribution during hardening. The degree of carbon segregation within a martensitic lath depends on the temperature of formation, hence, a higher temperature enhances the segregation. No segregation of the substitutional elements takes place during hardening. The most noticeable microstructural change with the cooling rate is a thickness increase of the interlath austenite films with increasing λ. The peak carbon concentrations in the interlath austenite films range from 6 to 10 at.% in the X38CrMoV5-1 samples quenched with λ from 0.1 to 12. A large amount, from 10 to 60%, of the total carbon atoms are located in the interlath retained austenite films.

References

Bungardt, R., Mülders, K., Meyer-Rhotert, O., 1966. Einfluss der Abkühlgeschwindigkeit beim Härten auf die Zähigkeit von Warmarbeitsstählen. Archiv Für Das Eisenhüttenwesen 37, 381–389.

Caballero, F.G., Miller, M.K., Babu, S.S., Garcia-Mateo, C., 2007. Atomic scale observations of bainite transformation in a high carbon high silicon steel. Acta Materialia 55, 381–390.

Caballero, F.G., Miller, M.K., Clarke, A.J., Garcia-Mateo, C., 2010a. Examination of carbon partitioning into austenite during tempering of bainite. Scripta Materialia 63, 442–445.

Caballero, F.G., Miller, M.K., Garcia-Mateo, C., 2010b. Carbon supersaturation of ferrite in a nanocrystalline bainitic steel. Acta Materialia 58, 2338–2343.

Clarke, A.J., Speer, J.G., Miller, M.K., Hackenberg, R.E., Edmonds, D.V., Matlock, D.K., Rizzo, F.C., Clarke, K.D., De Moor, E., 2008. Carbon partitioning to austenite from martensite or bainite during the quench and partition (Q&P) process: a critical assessment. Acta Materialia 56, 16–22.

Horn, R.M., Ritchie, R.O., 1978. Mechanisms of tempered martensite embrittlement in low alloy steels. Metallurgical Transactions A 9, 1039–1053.

Jesperson, H., 2009. Influence of the cooling rate during quenching on the toughness at typical working temperatures of die-casting dies. Metallurgia Italiana 101, 55–60.

Kozeschnik, E., Bhadeshia, H.K.D.H., 2008. Influence of silicon on cementite precipitation in steels. Materials Science and Technology 24, 343–347.

Landolt-Börnstein, 1990. Diffusion in Solid Metals and Alloys. Springer-Verlag, Berlin, Heidelberg.

Mayer, S., 2009 Einfluss einer bainitischen/martensitischen Mikrostruktur auf die mechanischen Eigenschaften von Warmarbeitsstählen. Doctoral Thesis. Department of Physical Metallurgy and Materials Testing, University of Leoben, Leoben.

Mayer, S., Scheu, C., Leitner, H., Clemens, H., Siller, I., 2007. Influence of the cooling rate on the mechanical properties of a hot-work tool steel. BHM Berg- Und Hüttenmännische Monatshefte 152, 132–136.

Miller, M.K., Beaven, P.A., Smith, G.D.W., 1981. A study of the early stages of tempering of iron–carbon martensites by atom probe field ion microscopy. Metallurgical Transactions A 12, 1197–1204.

Miller, M.K., Beaven, P.A., Brenner, S.S., Smith, G.D.W., 1983. An atom probe study of the aging of iron–nickel–carbon martensite. Metallurgical Transactions A 14, 1021–1024.

Miller, M.K., Cerezo, A., Hetherington, M.G., Smith, G.D.W., 1996. Atom Probe Field Ion Microscopy. Clarendon Press/Oxford University Press, Oxford, New York.

Moody, M.P., Stephenson, L.T., Ceguerra, A.V., Ringer, S.P., 2008. Quantitative binomial distribution analyses of nanoscale like-solute atom clustering and segregation in atom probe tomography data. Microscopy Research and Technique 71, 542–550.

Morito, S., Igarashi, R., Kamiya, K., Ohba, T., Maki, T., 2010. Effect of cooling rate on morphology and crystallography of lath martensite in Fe–Ni alloys. Materials Science Forum 638–642, 1459–1463.

Pereloma, E.V., Miller, M.K., Timokhina, I.B., 2008. On the decomposition of martensite during bake hardening of thermomechanically processed transformation-induced plasticity steels. Metallurgical and Materials Transactions A 39, 3210–3216.

Porter, D.A., Easterling, K.E., 1992. Phase Transformations in Metals and Alloys, 2nd ed. Chapman & Hall, London, New York.

Roberts, G.A., Krauss, G., Kennedy, R., 1998. Tool Steels, 5th ed. ASM International, Materials Park, OH.

Sarikaya, M., Jhingan, A.K., Thomas, G., 1983. Retained austenite and tempered martensite embrittlement in medium carbon steels. Metallurgical Transactions A 14, 1121–1133.

Sherman, D.H., Cross, S.M., Kim, S., Grandjean, F., Long, G.J., Miller, M.K., 2007. Characterization of the carbon and retained austenite distributions in martensitic medium carbon, high silicon steel. Metallurgical and Materials Transactions A 38, 1698–1711.

Taylor, K.A., Chang, L., Olson, G.B., Smith, G.D.W., Cohen, M., Sande, J.B.V., 1989. Spinodal decomposition during aging of Fe–Ni–C martensites. Metallurgical Transactions A 20, 2717–2737.

Thomson, R.C., Miller, M.K., 1995. An atom probe study of carbon distribution in martensite in 2.25Cr1Mo steel. Scripta Metallurgica et Materialia 32, 149–154.

Thomson, R.C., Miller, M.K., 1998. Carbide precipitation in martensite during the early stages of tempering Cr- and Mo-containing low alloy steels. Acta Materialia 46, 2203–2213.

Timokhina, I.B., Pereloma, E.V., Ringer, S.P., Zheng, R.K., Hodgson, P.D., 2010. Characterization of the Bake-hardening Behavior of Transformation Induced Plasticity and Dual-phase Steels Using, 50, pp. 574–582.

Wilde, J., Cerezo, A., Smith, G.D.W., 2000. Three-dimensional atomic-scale mapping of a cottrell atmosphere around a dislocation in iron. Scripta Materialia 43, 39–48.

Yao, L., Gault, B., Cairney, J.M., Ringer, S.P., 2010. On the multiplicity of field evaporation events in atom probe: a new dimension to the analysis of mass spectra. Philosophical Magazine Letters 90, 121–129.

Zhu, C., Cerezo, A., Smith, G.D.W., 2009. Carbide characterization in low-temperature tempered steels. Ultramicroscopy 109, 545–552.

Publication III

Christoph Lerchbacher, Silvia Zinner, Harald Leitner

Retained Austenite Decomposition and Carbide Formation During Tempering a Hot-Work Tool Steel X38CrMoV5-1 Studied by Dilatometry and Atom Probe Tomography

Metallurgical and Materials Transactions A 43A (2012) 4989-4998

Retained Austenite Decomposition and Carbide Formation During Tempering a Hot-Work Tool Steel X38CrMoV5-1 Studied by Dilatometry and Atom Probe Tomography

CHRISTOPH LERCHBACHER, SILVIA ZINNER, and HARALD LEITNER

The microstructural development of a hot-work tool steel X38CrMoV5-1 during continuous heating to tempering temperature has been investigated with the focus on the decomposition of retained austenite (Stage II) and carbide formation (Stages III and IV). Investigations have been carried out after heating to 673.15 K, 773.15 K, 883.15 K (400 °C, 500 °C, 610 °C) and after a dwell time of 600 seconds at 883.15 K (610 °C). Dilatometry and atom probe tomography were used to identify tempering reactions. A distinctive reaction takes place between 723.15 K and 823.15 K (450 °C and 550 °C) which is determined to be the formation of M_3C from transition carbides. Stage II could be evidenced with the atom probe results and indirectly with dilatometry, indicating the formation of new martensite during cooling. Retained austenite decomposition starts with the precipitation of alloy carbides formed from nanometric interlath retained austenite films which are laminary arranged and cause a reduction of the carbon content within the retained austenite. Preceding enrichment of substitutes at the matrix/carbide interface in the early stages of Cr_7C_3 alloy carbide formation could be visualised on the basis of coarse M_3C carbides within the matrix. Atom probe tomography has been found to be very useful to complement dilatational experiments in order to characterise and identify microstructural changes.

DOI: 10.1007/s11661-012-1358-3

I. INTRODUCTION

CHROMIUM hot-work tool steels gain their microstructure and mechanical properties from a well-defined composition and heat treatment. The latter commonly consists of a hardening treatment followed by a subsequent multi-step tempering procedure in the case of X38CrMoV5-1. The microstructure after hardening would be a fully martensitic microstructure which could, in principle, be produced by extremely rapid quenching but technically this is very difficult to achieve. The real microstructure additionally consists of cooling-rate dependent amounts of carbon enriched retained austenite and a few primary carbides which are not dissolved during austenitisation.[1] The retained austenite is primarily located as thin films between martensitic laths[2] and has been found to negatively influence the materials properties during tempering.[3] Therefore, the development of these retained austenite films during tempering is investigated, especially during heating to the final temperature.

CHRISTOPH LERCHBACHER, Ph.D. Student, is with Christian Doppler Laboratory of Early Stages of Precipitation, University of Leoben, Franz-Josef-Straße 18, 8700 Leoben, Austria. Contact e-mail: christoph.lerchbacher@unileoben.ac.at SILVIA ZINNER, Product Engineer, is with Böhler Edelstahl GmbH & Co. AG, Mariazellerstraße 25, 8605 Kapfenberg, Austria. HARALD LEITNER, Scientist, is with Department of Physical Metallurgy and Materials Testing, University of Leoben, Franz-Josef-Straße 18, 8700 Leoben, Austria.

Manuscript submitted May 10, 2012.
Article published online August 8, 2012

Tempering of iron-carbon martensites including the decomposition of retained austenite has been subject of scientific and technical interest for a long time[4] and has been intensively investigated employing different experimental methods. However, the tempering process is generally classified into the following stages[5]: Stage 0 indicates the carbon redistribution to dislocations and carbon cluster formation. Stage I follows with the precipitation of transition carbides. Retained austenite decomposition into ferrite and cementite occurs with Stage II. Stage III describes the formation of cementite from the transition carbides and from carbon clusters. At elevated temperatures Stage IV occurs with the formation of alloy carbides. Details on temperature ranges of the different stages can be found elsewhere.[6] Dilatometric experiments on several model alloys[7–9] as well as on technical materials[10,11] have been widely used to identify tempering reactions. Caballero *et al.*[12] proposed that the relative length change caused by the retained austenite decomposition depends on the carbon content of the austenite. High carbon content leads to a volume decrease whereas a low carbon content in the retained austenite leads to an expansion. The decomposition of retained austenite is generally proposed to be a transformation into ferrite and cementite[13] or the formation of bainite.[5] Van Genderen *et al.*[14] divided the retained austenite decomposition into two successive ways. A preceding ferrite formation occurs before the final transformation into ferrite and cementite takes place. Saha Podder *et al.*[9] showed that during heating at 723.15 K (450 °C) of a bainitic steel containing

retained austenite leads to a cementite precipitation but ferrite formation does not occur within 1 hour of tempering. The microstructural evolution in steels during tempering has been recently investigated by means of atom probe tomography in several studies.[15–17]

Tempering of martensite is also a major objective of alloy design and processing of tool steels, which cover a wide range of alloys.[1] The temperature ranges of the different tempering stages depend on the chemical composition of the treated alloy and on the heating rate in case of non-isothermal experiments. Kulmburg *et al.*[11] found that during heating to tempering temperature no transformations take place in a high speed steel S 6-5-2. Martensite start temperatures, after the first tempering step, were taken as an indication for the amount of cementite precipitated from retained austenite. Alloy X38CrMoV5-1 is in the sub-group chromium hot-work tool steels which should show similar tempering behaviour. However, tempering reactions and the microstructural evolution during heating to tempering temperature have not been discussed in detail. For the heat treatment of hot-work tool steel X38CrMoV5-1 it is essential to know if ferrite has already formed during tempering or if the retained austenite has just lower carbon content due to former cementite precipitation. Knowledge of this could lead to an optimised heat treatment strategy. The multi-step tempering treatment is based on the fact that after the first tempering step new martensite is formed from the carbon depleted retained austenite.

The volume fraction of retained austenite of the investigated steel in the present study is below the common X-ray detection limit. However, it was possible to study the retained austenite decomposition and carbide formation by using dilatometry and atom probe tomography.

II. EXPERIMENTAL

The commercial hot-work tool steel X38CrMoV5-1 with the nominal composition given in Table I has been used for the experiments. The heat treatment has been performed on cylindrical samples with a length of 15 mm and a diameter of 5 mm using a quenching dilatometer Dil 805 A from Bähr Thermoanalyse GmbH. Heating to the austenitisation temperature of 1293.15 K (1020 °C) has been done with a heating rate of 0.55 K/seconds. The dwell time was set to 1800 seconds (30 minutes) under vacuum. Afterwards, the material has been quenched with cooling parameter $\lambda = 0.6$ (cooling rate 5 K/seconds). Samples of the material were then given three different heat treatments: heating to (a) 673.15 K (400 °C), (b) 773.15 K (500 °C) and (c) 883.15 K (610 °C) (the standard tempering temperature for X38CrMoV5-1) and subsequently quenched with $\lambda = 0.6$ (cooling rate 5 K/seconds). The heating rate has been set to 0.5 K/seconds which is similar to that in the industrial process. Additionally, one sample has been held at 883.15 K (610 °C) for 600 seconds (10 minutes). The linear length changes during heating and subsequent quenching were recorded.

The same sample conditions have been chosen to perform atom probe investigations. For that, bars of the dimension 0.3 mm × 0.3 mm × 12 mm have been cut out from the heat treated samples. Subsequently, tips have been produced by a standard two step electrochemical polishing procedure. The measurements have been carried out using laser mode on a LEAP 3000× HR from Cameca, former Imago Scientific Instruments, at a temperature of 60 K and with laser pulse energy of 0.6 nJ. As measurements in voltage mode were not successful reconstruction artefacts arising during laser mode measuring were accepted. The reconstruction of the probed volumes and the analysis of the data sets have been carried out with the software package IVAS 3.4.3. from Cameca. The detection efficiency has been assumed to be 37 pct.

A. *Material*

The nominal composition of the alloy is given in Table I. The initial microstructure after hardening with $\lambda = 0.6$ (5 K/seconds) consists of a martensitic matrix with carbon enriched interlath retained austenite films which have a thickness of 3 to 5 nm and a carbon concentration of 6 to 10 at. pct as described in the work of Lerchbacher *et al.*[2] Additionally, irregular shaped carbon clusters with elemental concentrations of 8 to 15 at. pct carbon are present. No segregation of any substitutional elements takes place.[2] The amount of retained austenite is below 3 vol. pct.[3]

III. RESULTS

A. *Dilatometry*

Figure 1(a) shows the relative length change (relative to the origin length of the sample) during heating to 883.15 K (610 °C) and subsequent cooling. The cooling curve has been translated to lower values compared to the heating curve in order to illustrate the characteristics in a better way. The heating curve shows a positive change in slope at a temperature of 523.15 K (250 °C) indicating a volume increase. Further temperature increase causes linear expansion until 723.15 K (450 °C) where a reaction starts which shows a volume decrease. This reaction seems to be finished at 823.15 K (550 °C). Start and end points

Table I. Nominal Composition of the Investigated Alloy X38CrMoV5-1

	C	Si	Mn	Cr	Mo	V	Fe
wt pct	0.37	1.11	0.41	4.90	1.23	0.33	bal.
at. pct	1.68	2.16	0.41	5.14	0.70	0.35	bal.

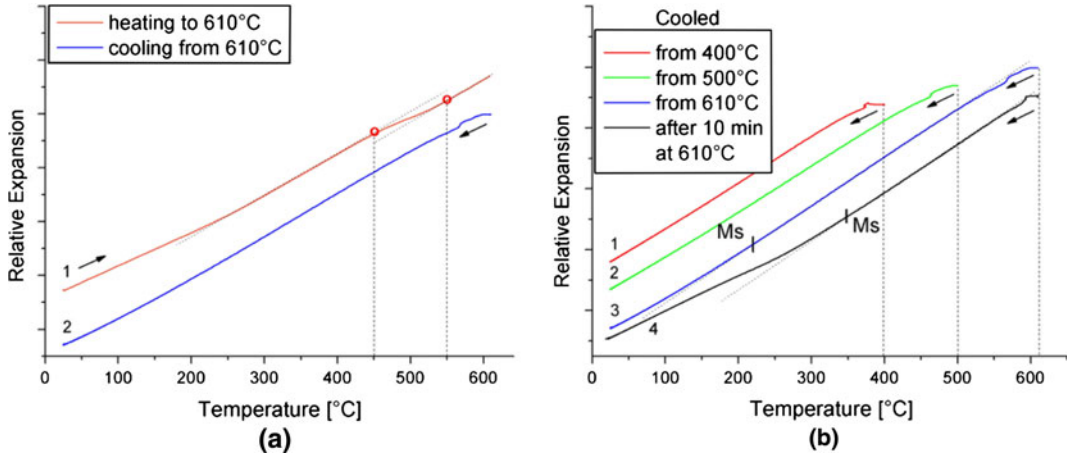

Fig. 1—Relative length change with temperature during heating to 883.15 K (610 °C) with 0.55 °C/seconds and subsequent cooling (*a*); relative length changes during cooling from 673.15 K (400 °C); from 773.15 K (500 °C); from 883.15 K (610 °C) with quenching parameter $\lambda = 0.6$; cooling after holding at 883.15 K (610 °C) for 600 s (10 min) with $\lambda = 0.6$ (*b*).

corresponding to this reaction are marked with red circles in the dilatation during heating. In order to reveal microstructure before, during and after this reaction further experiments have been chosen based on this curve: heating to 673.15 K (400 °C), a temperature between the two observed reactions with subsequent quenching; heating to 773 K (500 °C), a temperature where the second reaction is still going on, with subsequent quenching; heating to 883.15 K (610 °C), the standard tempering temperature of this alloy and subsequent quenching; tempering for 600 seconds at 883.15 K (610 °C) and subsequent quenching.

Figure 1(b) shows the relative length changes during cooling of the different samples. Curves 1 and 2 show that no reactions are evident during cooling from 673.15 K and 773.15 K (400 °C and 500 °C), respectively. The cooling curve of the sample heated to 883.15 K (610 °C) (3) shows a positive change in slope at a temperature of approximately 493.15 K (220 °C). Although the determination of the transformation temperature is difficult, a change in slope is noticeable. However, the change in slope is attributed to the martensite start temperature (Ms) of retained austenite. The relative length change during cooling of the sample tempered for 600 seconds (10 minutes) at 883.15 K (610 °C) shows a remarkable reaction at approximately 623.15 K (350 °C) which again is indicated by a volume increase and can be attributed to martensite formation.

B. *Atom Probe Tomography*

Atom probe tomography has been carried out in order to evidence compositional and structural development of the microstructure corresponding to the observed reactions during heat treatment. For a satisfactory visualisation of the carbon enriched features within the probed volumes 5 at. pct carbon iso-surfaces are shown in all cases in addition to the carbon atom maps. Cluster core concentrations and the behaviour of solute and substitutes at the interface have been estimated from maximum values given by the proximity histograms (proxigram). Details on this evaluation method can be found elsewhere.[18]

In Figure 2 the carbon atom map (a) and the corresponding 5 at. pct carbon iso-surfaces (b) of the sample heated to 673.15 K (400 °C) and subsequently quenched are presented. Plate shaped carbon enriched features with a length of 60 nm and width of 10 nm at the edge of a diffuse network of carbon enriched clusters can be seen. The corresponding proxigram given in Figure 2(c) shows a carbon core concentration of 14 to 15 at. pct and slight increases of chromium and molybdenum compared to the matrix composition. The silicon content shows a continuous decrease approaching the core.

Figure 3(a) shows the carbon atom map of the probed volume of the sample heated to 773.15 K (500 °C) and subsequently quenched. The 5 at. pct carbon iso-surfaces given in Figure 3(b) visualise a plate like carbon enriched region on the top of the measured volume and a large planar feature in the lower part. The corresponding proxigrams (Figures 3(c) and (d)) show carbon concentrations of 13 at. pct for the carbon enrichment on the top and 10 at. pct for the carbon enriched film in the lower part. The nature of this planar feature combined with a carbon concentration of 10 at. pct are typical characteristics for interlath retained austenite films within the microstructure.[2] Again, slight irregularities of substitutes can be seen through the interface in both cases.

Figure 4(a) shows the carbon atom map of the probed volume of the sample heated to 883.15 K (610 °C) which consists of several former retained austenite films and carbon enriched features within the matrix. In order to investigate a single retained austenite film a region of interest has been extracted by means of a thin box as depicted in Figure 4(b). The 5 at. pct carbon iso-surfaces are presented in a top view on this region of interest, hence, onto the film (Figure 4(c)). The corresponding proxigram of the carbon features within that film is presented in Figure 4(d). Significantly increased concentrations of the substitutional elements are obvious.

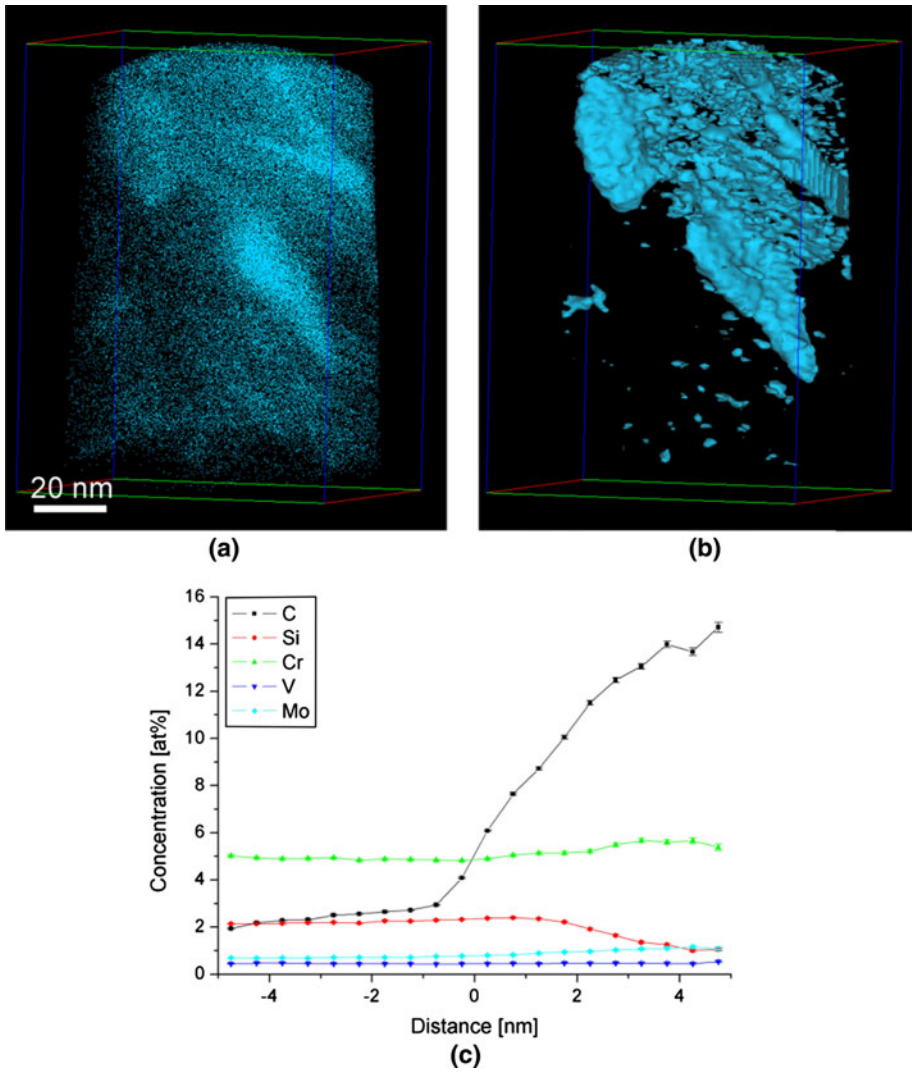

Fig. 2—Carbon atom map of the probed sample quenched from 673.15 K (400 °C) (*a*) and the corresponding 5 at. pct carbon iso-surfaces (*b*); proximity histogram corresponding to the large carbon feature (*c*); box size 94 × 97 × 131 nm^3.

Contents of 35 at. pct chromium, 8 at. pct molybdenum and 5.5 at. pct vanadium can be estimated from the diagram. The carbon content is approximately 19 at. pct.

The carbon atom map of the sample tempered at 883.15 K (610 °C) for 600 seconds (10 minutes) is displayed in Figure 5(a). The probed volume predominantly consists of film-like carbon enriched regions, which again contribute to former retained austenite films. Again, a single former film has been extracted by means of a thin volume box as depicted in Figure 5(b). The top view on the 5 at. pct carbon iso-surfaces within that box is presented in Figure 5(c). The corresponding proxigram as given in Figure 5(d) shows elemental concentrations of 24 at. pct carbon, 30 at. pct chromium, 10 at. pct molybdenum and 9 at. pct vanadium.

Figure 6(a) shows the carbon atom map of another probed volume of the sample tempered for 600 seconds (10 minutes) at 883.15 K (610 °C). A different type of carbon enriched regions could be examined compared to the previous volume, large disc shaped carbides with sizes more than 50 nm can be seen. The 5 at. pct carbon iso-surfaces as given in Figure 6(b) reveal the presence of two large carbides and surrounding carbides of smaller size. The proxigram corresponding to the two large carbides (Figure 6(c)) shows elemental concentrations of 15 at. pct carbon, 32 at. pct chromium, 2.6 at. pct molybdenum and 1.5 at. pct vanadium. A linear concentration profile through the carbide in the lower half of the analysed volume has been generated in order to evidence the uncommon characteristic of the chromium concentration as shown in the proxigram. The linear concentration profile as given in Figure 6(d) confirms this characteristic showing heavily increased chromium concentration in the edge of the particle compared to the core concentration.

The silicon content seems to decrease approaching the core of the particles in all observed features and can be clearest seen in the proxigram corresponding to the large particles of the sample tempered for 600 seconds (10 minutes) at 883.15 K (610 °C) (Figure 6(c)).

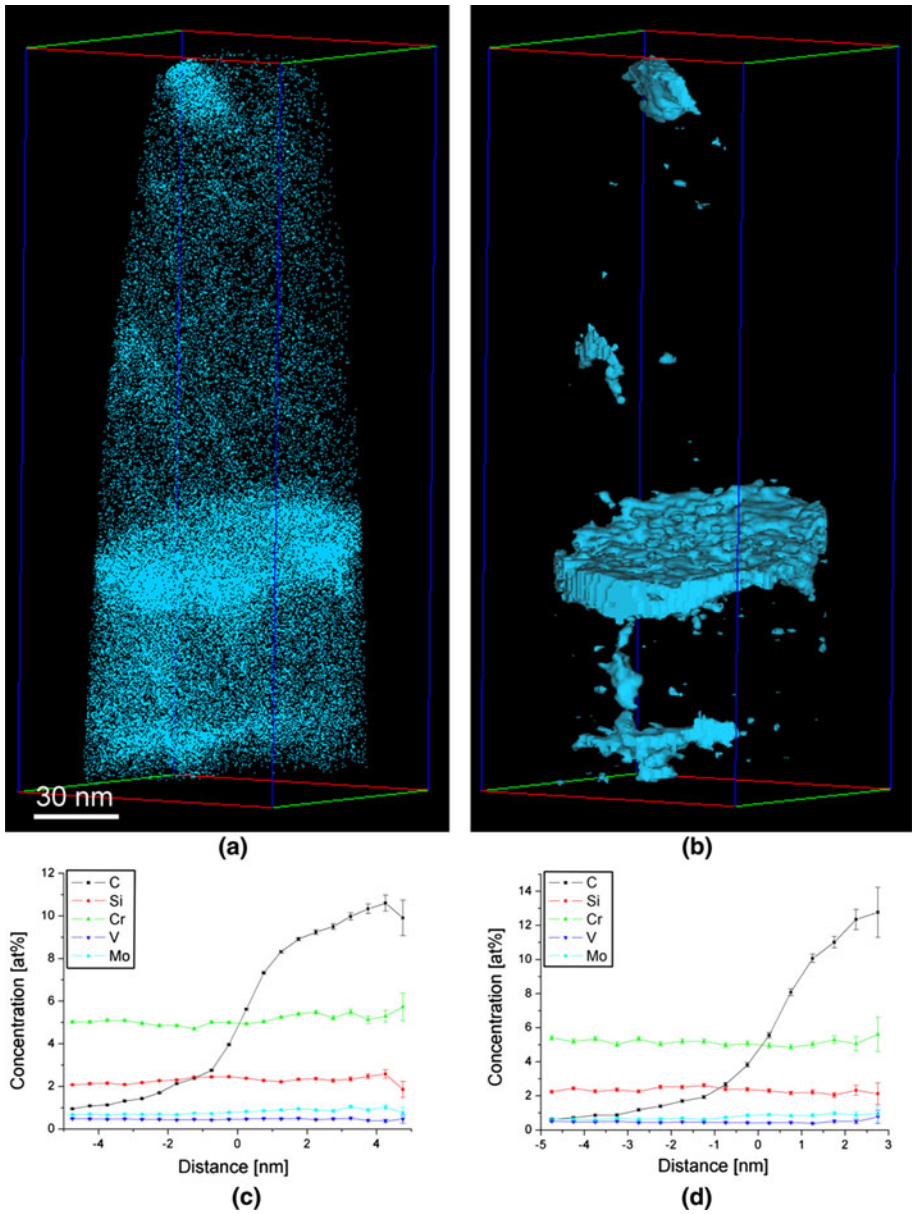

Fig. 3—Carbon atom map of the sample quenched from 773.15 K (500 °C) (*a*) and the corresponding 5 at. pct carbon iso-surfaces (*b*); proximity histogram of the carbon enriched film (*c*); proximity histogram of the carbon enriched region within the top of the probed volume (*d*); box size 79 × 82 × 204 nm^3.

IV. DISCUSSION

Hot-work tool steel X38CrMoV5-1 is a martensitic medium carbon steel which gains its outstanding properties for hot-work applications *via* a finalising tempering procedure. The reactions and microstructural changes during the early stages of tempering have been characterised.

The dilatation during heating to 883.15 K (610 °C) depicted in Figure 1(a) does not show the typical characteristics as given in the relevant literature about tempering of carbon martensite. The reactions of stage 0 most likely have already taken place during hardening.[2] The only distinctive feature in the lower temperature regime is a positive change in slope at 523.15 K (250 °C). Thus, this kink cannot be correlated to any of the extensively studied tempering reactions (*e.g.*, Reference 5), since stages I and III come along with a volume decrease.[8] On the other hand, the volume change due to stage II strongly depends on the carbon content in the retained austenite. Caballero *et al.*[12] showed that the decomposition of high carbon retained austenite causes a volume decrease during the transformation whereas low carbon austenite causes a volume increase. The plate shaped precipitate within the probed volume of the sample heated to 673.15 K (400 °C) (Figure 2(b)) leads to the assumption that transition carbide formation has already taken place even when no corresponding reaction in the dilatation is visible. Since

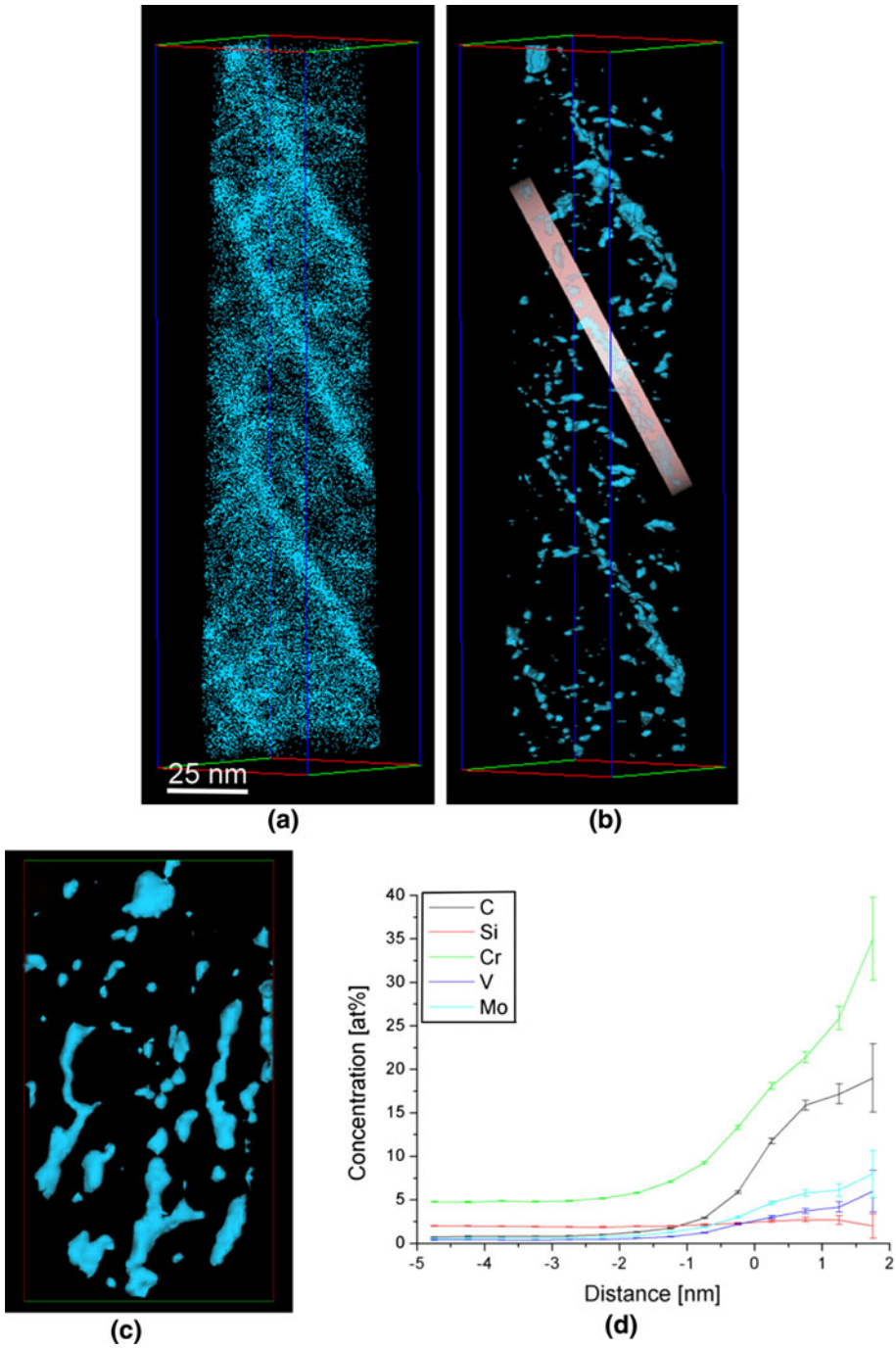

Fig. 4—Carbon atom map of the sample quenched from 883.15 K (610 °C) (*a*) and corresponding 5 at. pct carbon iso-surfaces (*b*); box size 64 × 65 × 250 nm^3; top view on the separated region of interest, box size 57 × 100 × 8 nm^3 (*c*); proximity histogram corresponding to the separated region of interest (*d*).

the carbon content of the retained austenite after hardening with 6 to 10 at. pct[2] is relatively high, the kink at 523.15 K (250 °C) is not believed to be caused by the retained austenite decomposition, because a volume decrease would be expected. A second indication that the transformation has not taken place at that temperature is the probed retained austenite film in the sample quenched from 773.15 K (500 °C) in Figure 3(b). The film shows a maximum carbon concentration of 10 at. pct and nearly no enrichment or depletion of substitutional elements, similar to the situation of the as-quenched condition.[2] The significant reaction between 723.15 K and 823.15 K (450 °C and 550 °C) comes along with a volume decrease. Retained austenite decomposition (Stage II) and the transformation of transition carbides and carbon clusters into cementite (Stage III) could be responsible for this length change. The virgin retained austenite film shown in Figure 3(b) does not necessarily exclude stage II to be contribution because the reaction is not completed at

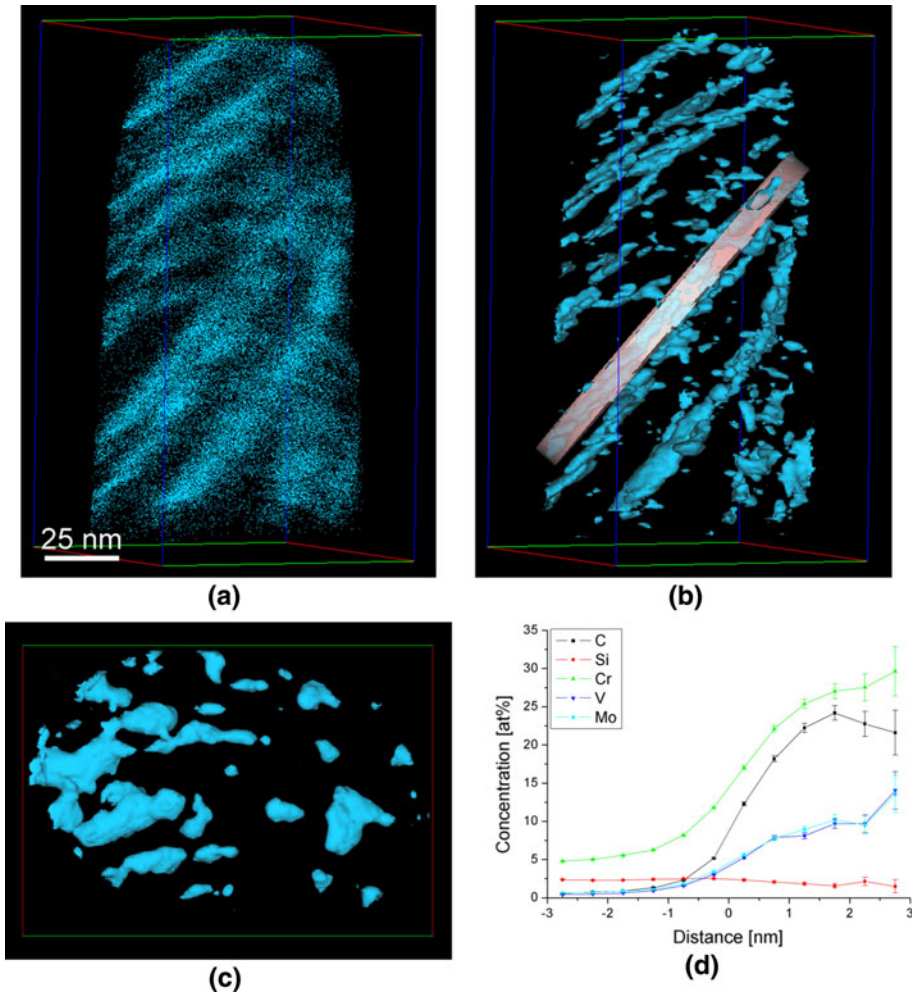

Fig. 5—Carbon atom map of the sample hold for 600 s (10 min) at 883.15 K (610 °C) and quenched (*a*) and corresponding 5 at. pct carbon iso-surfaces (*b*); box size 86 × 88 × 161 nm^3; top view on the separated region of interest, box size 85 × 120 × 8 nm^3 (*c*); proximity histogram corresponding to the separated region of interest (*d*).

773.15 K (500 °C). However, if retained austenite decomposition has already taken place after heating to 773.15 K (500 °C), the carbon depleted austenite would transform into martensite during quenching. Stage II can be excluded due to the fact that the dilatation in the cooling curve of the sample quenched after heating to 773.15 K (500 °C) does not show a feature which could be correlated to a martensitic start temperature, similar to the behaviour of the 673.15 K (400 °C) sample. Therefore, the reaction between 723.15 K and 823.15 K (450 °C and 550 °C) most likely corresponds to tempering Stage III. Retained austenite decomposition (Stage II) could not be found by means of the dilatation during heating to 883.15 K (610 °C). However, carbide formation in the retained austenite films revealed by atom probe tomography and the martensitic transformation found in the dilatation during cooling indicate that the decomposition of the retained austenite has already begun though no further reaction can be drawn from the dilatation. This could most likely be explained with the low amount of retained austenite and with the carbon content of the retained austenite which might be in a range where nearly no volume change takes place during decomposition. The significant martensitic transformation at 623.15 K (350 °C) drawn from the dilatation during quenching of the sample held for 600 seconds (10 minutes) at 883.15 K (610 °C) evidences the progression of the retained austenite decomposition. In summary, it can be said that the volume change at 523.15 K (250 °C) could not be identified. The reaction between 723.15 K and 823.15 K (450 °C and 550 °C) corresponds to Stage III. Stage II takes place during heating to 883.15 K (610 °C).

The observed carbides and corresponding elemental concentrations have been summarized in Table II in order to give an overview. The carbides are categorized into matrix-carbides and into carbides which have formed from retained austenite films. The elemental concentrations have been estimated from the maximum concentrations observed in the proxigrams calculated from the atom probe data. The observed carbon enriched regions are listed chronologically corresponding to the temperature when they were observed during continuous heating.

Additionally, it must be noted that the evaluation of the carbon concentration within steels from atom probe data

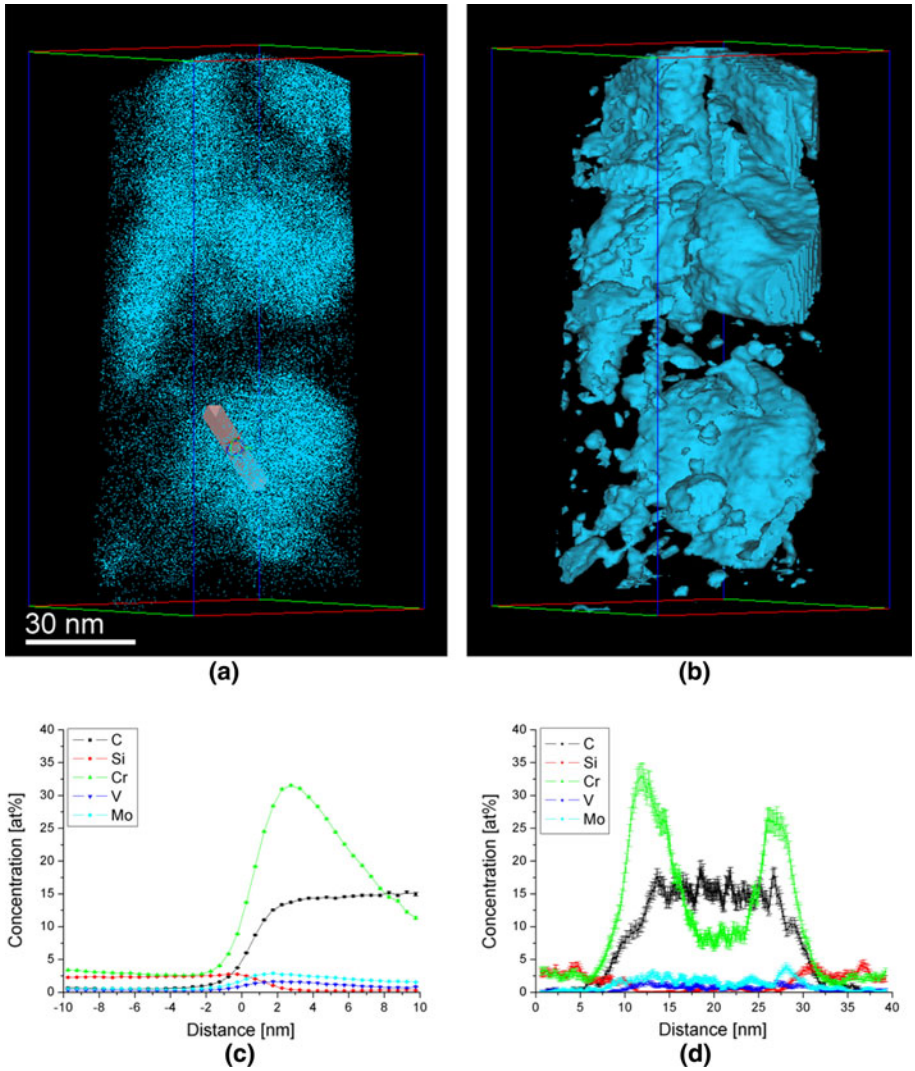

Fig. 6—Carbon atom map of the sample hold for 600 s (10 min) at 883.15 K (610 °C) and subsequently quenched (*a*) and the corresponding 5 at. pct carbon iso-surfaces (*b*); proximity histogram of the two big carbon features (*c*); 1-dimensional concentration profile through the big carbon feature in the lower half of the probed volume (*d*); box size 92 × 94 × 183 nm^3.

Table II. Elemental Concentrations According to the Observed Features Within the Probed Samples

Sample	Carbides/Clusters	C (at. pct)	Cr (at. pct)	Mo (at. pct)	V (at. pct)
As-quenched[2]	films*	6 to 10	nom.	nom.	nom.
	matrix	8 to 15	nom.	nom.	nom.
673.15 K (400 °C)	matrix	14	5.5	1.2	nom.
773.15 K (500 °C)	film*	10	5.3	1.2	nom.
	matrix	13	5	1	nom.
883.15 K (610 °C)	film	19	35	8	6
883.15 K (610 °C) 600 s (10 min)	film	24	29	10.5	9.5
	M_3C edge	14	32	2.9	1.6
	M_3C core	15	6	1.2	nom.

*No carbides or carbon clusters.

is affected by inherent difficulties. Carbon peaks in the recorded mass spectrum have been defined on m/n positions 6, 6.5, 12, 13, 18, 18.5, 24, 24.5 and 36 with the corresponding isotopes and ionization states C^{12++}, C^{13++}, C^{12+}, C^{13+}, C_3^{++}, C_3^{++} ($2 \times C^{12}$ and $1 \times C^{13}$), C_2^{+}, C_4^{++} ($3 \times C^{12}$ and $1 \times C^{13}$) and C_3^{+},

respectively. The latter mentioned peak definition on m/n positions 12 and 24 combined with the inability to separate C^+ from C_2^{++} and C_2^+ from C_4^{++} leads to an under-estimation of the real carbon concentrations. Laser mode increases the potential for molecule formation during the evaporation process which leads to an increased under-estimation of the carbon concentration compared to voltage mode. Under-estimation is further increased by so-called multiple events, which consist of two or more ions originating from adjacent sites within the sample. Details to the carbon loss caused by increased number of multiple events during measuring carbides can be found in the work of Thuvander *et al.*[19] However, the estimated maximum carbon concentrations from the calculated proxigrams are taken for a comparative study of the formed carbon enriched features.

The carbides which form within the matrix (Figures 2(c), 3(d), and 6(c)) show similar carbon levels for all sample conditions with approximately 13 to 15 at. pct as demonstrated in Table II. As the dilatometric experiments suggest that the pronounced transformation before reaching 883.15 K (610 °C) belongs to stage III, these carbides are determined to be Fe_3C, more precisely, M_3C considering the amounts of substitutional elements. A second indication for this is the fact that silicon seems to be pressed out from these particles as depicted in all proxigrams. The low silicon solubility in cementite has been proposed in several papers (*e.g.*, Reference 20). The relatively high deviation of the measured carbon content from the nominal Fe_3C composition can be explained by a carbon loss due to the C_2^+/C_4^{++} and the C^+/C_2^{++} determination within the measured spectrum at mass-to-charge state ratios 12 and 24, respectively,[19] and to an increased number of multiple events during measuring carbides.[21] Multiple events are not considered in the reconstruction algorithm which affects the accuracy of the reconstruction. Artefacts within the reconstructed volume can also occur due to surface migration slightly before the evaporation process caused by the laser-induced temperature increase. Especially silicon and carbon are affected by this phenomenon, which, again, complicates accurate reconstruction and composition evaluation. However, choice of laser energy is a compromise of previously mentioned artefacts, sample life-time, mass resolution and background reduction.

The high chromium concentration and the increased vanadium and molybdenum contents within the carbides after heating to 883.15 K (610 °C) lead to the assumption that the formation of alloy carbides starts at a temperature between 773.15 K and 883.15 K (500 °C and 610 °C). On the other hand, carbides formed within the film of the sample heated to 883.15 K (610 °C) show higher carbon contents in comparison to those formed within the matrix. This is not surprising because the carbon enriched retained austenite offers more carbon than the matrix. Holding for 600 seconds (10 minutes) at 883.15 K (610 °C) causes a further increase in carbon to 24 at. pct within the carbides which form from retained austenite films.

For the investigated chromium hot-work tool steel alloy carbide formation predominantly takes place on the Fe_3C/α interface.[22] Baker *et al.*[23] proposed that the transformation of Fe_3C to Cr_7C_3 takes place after chromium enrichment within the Fe_3C at matrix/particle interface. Since no corresponding reaction is obvious in the dilatation during heating it is believed that at this stage just a preceding enrichment of substitutes within the cementite has taken place. This enrichment has taken place over the full extent in case of the small carbides. The large Fe_3C particles, as illustrated in Figure 6(b) and in the corresponding 1-dimensional concentration profile in Figure 6(d), show high enrichment only in the outer shell. The concentration of carbon and substitutional atoms within the core of the carbide is the same as that observed for the other non-enriched particles found after heating to 673.15 K (400 °C) (Figure 2(c)) and 773.15 K (500 °C) (Figure 3(d)). The fact that the carbon concentration in the enriched shell is the same than that in the Fe_3C core confirms the assumption of a preceding enrichment and that the Fe_3C-Cr_7C_3 transformation has not taken place at that moment of tempering. The higher carbon content in the film-carbides might suggest that the Fe_3C-Cr_7C_3 transformation has progressed compared to the matrix-carbides.

V. CONCLUSIONS

The microstructural development during the early stages of tempering of hot-work tool steel X38CrMoV5-1 has been analysed using dilatometer and atom probe tomography. Following conclusions can be drawn from the experiments:

- The microstructural development of nm thin retained austenite films during the early stages of tempering could be visualised by using atom probe tomography. Laminary arranged alloy carbides precipitate within the film-plane.
- Carbon reduction within the retained austenite induced by the alloy carbide precipitation precedes the decomposition of retained austenite into ferrite and cementite.
- Cr_7C_3 alloy carbide formation at the Fe_3C/α interface could be visualised by atom probe tomography. The preceding chromium enrichment within the Fe_3C particles takes place over the full extent of small particles, whereas large particles experience this enrichment only in the shell regions.
- Higher carbon levels were observed within the carbides formed from retained austenite compared to carbides formed within the matrix which indicates that alloy carbide transformation progresses faster in the retained austenite.

REFERENCES

1. G. Roberts, G. Krauss, and R. Kennedy: *Tool Steels*, 5th ed., ASM International, Materials Park, OH, 1998.
2. C. Lerchbacher, S. Zinner, and H. Leitner: *Micron*, 2012, vol. 43, pp. 818–26.

3. S. Mayer: Doctoral Thesis, Department of Physical Metallurgy and Materials Testing, University of Leoben, 2009.
4. G.B. Olson and M. Cohen: *Metall. Trans. A*, 1983, vol. 14A, pp. 1057–65.
5. G.R. Speich and W.C. Leslie: *Metall. Trans. A*, 1972, vol. 3A, pp. 1043–54.
6. S. Primig and H. Leitner: *Thermochim. Acta*, 2011, vol. 526, pp. 111–17.
7. P.V. Morra, A.J. Böttger, and E.J. Mittemeijer: *J. Therm. Anal. Calorim.*, 2001, vol. 64, pp. 905–14.
8. L. Cheng, C.M. Brakman, B.M. Korevaar, and E.J. Mittemeijer: *Metall. Trans. A*, 1988, vol. 19A, pp. 2415–26.
9. A. Saha Podder and H.K.D.H. Bhadeshia: *Mater. Sci. Eng. A*, 2010, vol. 527, pp. 2121–28.
10. M. Jung, S.-J. Lee, and Y.-K. Lee: *Metall. Mater. Trans. A*, 2009, vol. 40A, pp. 551–59.
11. A. Kulmburg, E. Kaiser, and S. Wilmes: *Härterei Technische Mitteilungen*, 1987, vol. 42, pp. 133–38.
12. F.G. Caballero, C. Garcia-Mateo, and C. Garcia-de Andres: *Mater. Trans.*, 2005, vol. 46, pp. 581–86.
13. H.K.D.H. Bhadeshia: *Bainite in Steels*, 2nd ed., IOM Communications, London, 2001.
14. M.J. Van Genderen, M. Isac, A. Böttger, and E.J. Mittemeijer: *Metall. Mater. Trans. A*, 1997, vol. 28A, pp. 545–61.
15. D.H. Sherman, S.M. Cross, S. Kim, F. Grandjean, G.J. Long, and M.K. Miller: *Metall. Mater. Trans. A*, 2007, vol. 38A, pp. 1698–11.
16. F.G. Caballero, M.K. Miller, C. Garcia-Mateo, C. Capdevila, and S.S. Babu: *Acta Mater.*, 2008, vol. 56, pp. 188–99.
17. F.G. Caballero, M.K. Miller, and C. Garcia-Mateo: *Metall. Mater. Trans. A*, 2011, vol. 42, pp. 3660–68.
18. O.C. Hellman, J.A. Vandenbroucke, J. Rüsing, D. Isheim, and D.N. Seidman: *Microsc. Microanal.*, 2000, vol. 6, pp. 437–44.
19. M. Thuvander, J. Weidow, J. Angseryd, L.K.L. Falk, F. Liu, M. Sonestedt, K. Stiller, and H.-O. Andrén: *Ultramicroscopy*, 2011, vol. 111, pp. 604–08.
20. E. Kozeschnik and H.K.D.H. Bhadeshia: *Mater. Sci. Technol.*, 2008, vol. 24, pp. 343–47.
21. L. Yao, B. Gault, J.M. Cairney, and S.P. Ringer: *Philos. Mag. Lett.*, 2010, vol. 90, pp. 121–29.
22. R.W.K. Honeycombe: *Steels Microstructure and Properties*, Metallurgy and Materials Science Series, Arnold, London, 1981.
23. R.G. Baker and J. Nutting: *J. Iron Steel Inst.*, 1959, vol. 192, pp. 257–68.

Publication IV

Christoph Lerchbacher, Silvia Zinner, Harald Leitner

Direct or Indirect: Influence of type of retained austenite decomposition during tempering on the toughness of a hot-work tool steel

Materials Science & Engineering A 564 (2013) 163-168

Materials Science & Engineering A 564 (2013) 163–168

Contents lists available at SciVerse ScienceDirect

Materials Science & Engineering A

journal homepage: www.elsevier.com/locate/msea

Direct or indirect: Influence of type of retained austenite decomposition during tempering on the toughness of a hot-work tool steel

Christoph Lerchbacher [a,*], Silvia Zinner [b], Harald Leitner [c]

[a] Christian Doppler Laboratory of Early Stages of Precipitation, University of Leoben, Franz-Josef-Straße 18, A-8700 Leoben, Austria
[b] Böhler Edelstahl GmbH & Co AG, Mariazellerstraße 25, A-8605 Kapfenberg, Austria
[c] Department of Physical Metallurgy and Materials Testing, University of Leoben, Franz-Josef-Straße 18, A-8700 Leoben, Austria

ARTICLE INFO

Article history:
Received 2 October 2012
Received in revised form
26 November 2012
Accepted 27 November 2012
Available online 2 December 2012

Keywords:
Hot-work tool steel
Retained austenite
Decomposition
Tempering
Dilatometry
X38CrMoV5-1

ABSTRACT

A heat treatment slightly differing from the classical 2 × 2 h tempering treatment has been established in order to eliminate the direct retained austenite decomposition during tempering of the common hot-work tool steel X38CrMoV5-1 . Instead of the direct decomposition into ferrite and cementite during the first tempering step, transformation into martensite has been forced. A quenching dilatometer has been used for heat treatment and for the determination of transformation reactions. The two heat treatments have been compared with respect to toughness behaviour by conducting Charpy-impact tests. The investigations have been performed on samples hardened with quenching rates 5 K/s, 0.5 K/s, and 0.25 K/s, providing different amounts of retained austenite within the as-quenched microstructure. The heat treatment modification does not show improvement regarding the toughness behaviour in case of low cooling rates where the specimen failure is dominated by interfaces, hence, the former interlath retained austenite films. Therefore, the indirect retained austenite decomposition has no positive effect compared to the direct decomposition. In case of the highest cooling rate the failure is dominated by the matrix and the impact toughness could be improved by a factor of 12% at the same hardness level and a dwell time reduction of 15%. For tools of small dimensions where these cooling rates during hardening can be achieved this heat treatment modification should be considered.

1. Introduction

The classical heat treatment of tool steels consists of two procedures called hardening and tempering. Hardening means austenitisation for a specific time followed by rapid quenching, which leads to a martensitic microstructure. Subsequent multi-step tempering leads to the relaxation of the stressed martensite, the formation of secondary carbides and the decomposition of retained austenite [1]. The more-step strategy enables the relaxation of untempered martensite newly formed from untransformed retained austenite during cooling after the first tempering step [2]. In order to gain required material properties, predominantly hardness and toughness, hardening as well as tempering parameters have to be chosen from a narrow range. This is hardly achievable when tool dimensions become large and results in insufficient toughness behaviour.

When no grain-boundary carbides are formed during quenching from austenitisation temperature, as it is the case for the investigated hot-work tool steel, austenite retained after quenching has been found to be responsible for undesired toughness behaviour [3]. Ultra-thin carbon enriched retained austenite films between martensitic laths lead to carbide formation at lath boundaries during tempering [4] which reduces toughness. The amount of retained austenite after quenching strongly depends on the quenching rate and goes hand in hand with a thickness increase of the interlath films [5], hence, the potential for interfacial carbides increases. Regarding large tool dimensions, the amount of retained austenite after quenching is not adjustable in any order by the manufacturer for a given alloy composition. Therefore, to manipulate toughness properties, retained austenite decomposition during tempering could be manipulated.

Decomposition of retained austenite in steels is generally proposed to be a transformation into ferrite and cementite [6] or the formation of bainite [7]. Van Genderen et al. [8] divided the retained austenite decomposition of a FeC model alloy into two successive ways. A preceding ferrite formation occurs before the final transformation into ferrite and cementite takes place. Saha Podder and Bhadeshia [9] showed by means of dilatometer tests that during heating at 450 °C of a bainitic steel ferrite formation does not occur within 1 h of tempering. Previously published work on the investigated hot-work tool steel X38CrMoV5-1 shows that heating to 610 °C already leads to alloy carbide formation from

* Corresponding author. Fax: +43 3842 402 4202.
E-mail address: christoph.lerchbacher@unileoben.ac.at (C. Lerchbacher).

0921-5093/$ - see front matter © 2012 Elsevier B.V. All rights reserved.
http://dx.doi.org/10.1016/j.msea.2012.11.105

the retained austenite though no reaction is visible from the dilatometer curves [4]. This carbide formation progresses during tempering. Similar to that, Kulmburg et al. [2] proposed for a high speed steel that carbides form during tempering from the retained austenite which transforms into martensite during cooling. No transformations take place during heating to tempering temperature. All these findings demonstrate that the behaviour of retained austenite during tempering significantly varies for different steel grades and lead to the assumption that individual heat treatments for individual steel grades might improve material properties.

However, traditional multi-step tempering is somehow manifested in steel industry. The intention of the present work is the evaluation of different heat treatment strategies with special regard laid on the retained austenite decomposition. Therefore, the standard tempering treatment has been compared with respect to toughness to a treatment where the retained austenite has been transformed into martensite instead of a direct decomposition into ferrite and cementite. Additionally, the effect of retained austenite decomposition manipulation has been determined with respect to different cooling rates during hardening.

2. Experimental

Dilatometric experiments have been performed in a dilatometer Dil 805A from Bähr Thermoanalyse GmbH. Therefore, samples of 15 mm in length and 5 mm in diameter have been produced. The material has been austenitised at 1020 °C with a dwell time of 30 min. Subsequent quenching has been conducted with quenching rates $\lambda=0.6$, 6 and 12, which correspond to linear quenching rates of 5 K/s, 0.5 K/s and 0.25 K/s, respectively. Then, the samples have been tempered at 610 °C two times for 2 h simulating the standard heat treatment. The relative length change (relative to the origin length of the sample) of the samples during tempering has been recorded. From these results, modified tempering parameters have been chosen.

Instrumented impact tests conducted on a 300 J impact pendulum from Zwick were performed in order to evaluate the impact toughness of the samples. The mean absorbed energy was measured using 3 specimens per sample state. For the impact tests Charpy U-notched specimens with dimensions of $55\times10\times7.5$ mm^3 were used. The samples have been heat treated using similar parameters as mentioned above conducting a special instrumentation in the quenching dilatometer in order to simulate real quenching conditions and to provide comparability with the samples heat treated for the length change measurements. The impact tests have been performed at sample temperatures of 200 °C, a common preheating temperature for tools of this material in use. Fracture surface analysis was carried out by scanning electron microscopy using a Zeiss EVO50.

3. Material

The nominal composition of the alloy investigated is given in Table 1. The initial microstructure after hardening consists of a martensitic matrix with nanometric interlath retained austenite films [5]. The volume fraction of retained austenite is $<3\%$ [3], 10% [5] and 17% [3] corresponding to the quenching rates $\lambda=0.6$, 6 and 12, respectively.

Table 1
Nominal composition of the investigated alloy X38CrMoV5-1.

	C	Si	Mn	Cr	Mo	V	Fe
wt%	0.37	1.11	0.41	4.90	1.23	0.33	Bal.

4. Results

4.1. Dilatometer

Tempering at 610 °C of the differently quenched samples leads to a dilatation as given in Fig. 1a. The diagram shows the dilatation corresponding to the section from reaching 610 °C to the end of 2 h dwell time. The relative expansion during tempering qualitatively shows similar behaviour for the samples with quenching rates $\lambda=0.6$, 6 and 12. In order to compare the behaviour of the different samples, the corresponding curves have been translated in a way that at tempering start point the curves have the same level, therefore, no numerical scaling on the vertical axis is given. First, a volume decrease occurs until a minimum is reached after approximately 1600 s of tempering. This volume decrease corresponds to alloy carbide formation within the matrix and within the retained austenite as stated in earlier studies [4,9], hence, carbon enriched retained austenite and matrix become depleted in carbon. Further tempering leads to a volume increase approaching a maximum in volume, corresponding to retained austenite decomposition [9]. The minimum corresponding to each curve has been chosen as base for the calculation of relative changes during tempering. The curves behave quite similar for the range from tempering start to the volume minimum, showing a volume decrease of 0.76%. The extent of the following volume increase beyond the minimum depends on the quenching rate during hardening. The relative volume change with respect to the minimum is 0.5%, 1.27% and 1.62% after tempering for 2 h corresponding to the samples quenched with $\lambda=0.6$, 6 and 12, respectively. This cooling rate dependent extent of volume increase is most likely related to the amount of retained austenite within the microstructure. In order to prove this, cooling curves after selected times of tempering corresponding to the sample with the most pronounced volume change ($\lambda=12$) have been recorded. Fig. 1b shows the corresponding cooling curves after tempering for 600 s (10 min), 1600 s (25 min), 3600 s (1 h) and 7200 s (2 h). Again, the curves have been vertically translated in a way to provide an optimum in comparability. The curve corresponding to the sample cooled after 10 min tempering at 610 °C depicts a pronounced reaction showing a volume increase with a start point at approximately 350 °C, indicating the martensitic transformation of the retained austenite. The sample cooled from the minimum (after 25 min) again shows this reaction, but more pronounced and shifted to approximately 370 °C. Cooling after 1 h tempering shifts the reaction to approximately 390 °C and the reaction is not well distinctive. During cooling after 2 h of tempering at 610 °C no reaction occurs. The continuous increase of the martensite start temperature indicates that carbon depletion within the retained austenite develops at least up to 1 h of tempering. The well distinctive reaction during cooling after tempering for 25 min shows that the majority of the retained austenite has a carbon level which allows for a martensitic transformation.

From these results a modified tempering treatment has been chosen. The dwell time of the first tempering step is set to 1600 s (25 min) which corresponds to the volume minimum in the dilatation curve, in order to avoid the direct decomposition of the retained austenite into ferrite and cementite. The dwell time for the second tempering step is set to 3 h, a value which provides similar hardness after heat treatment as in the case for traditional 2×2 h treatment. The different treatments are depicted schematically in Fig. 2. After the first tempering step, the samples are oil-

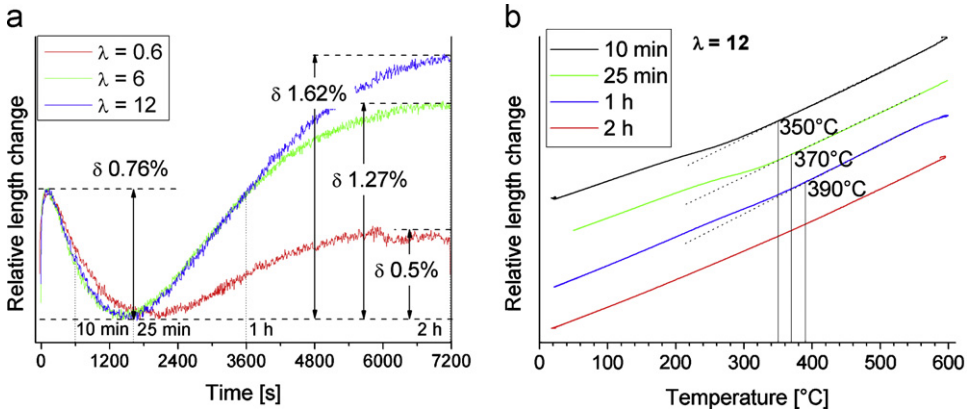

Fig. 1. (a) Dilatation during 2 h tempering at 610 °C corresponding to the samples quenched with λ=0.6, 6 and 12; and (b) dilatation during cooling the λ=12 sample after tempering at 610 °C for different times.

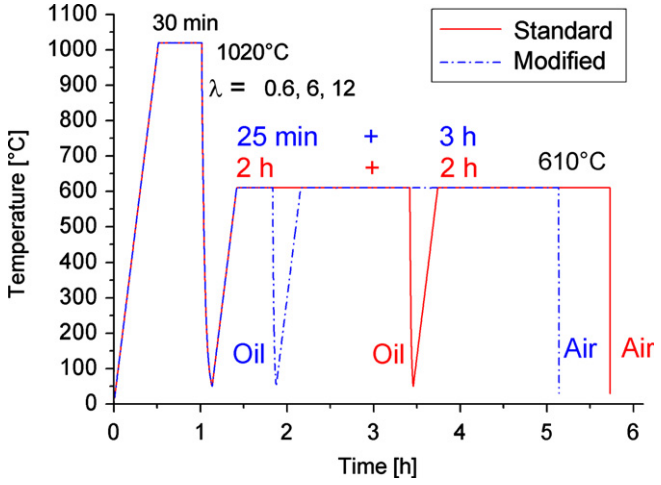

Fig. 2. Time–temperature programs corresponding to the standard and modified heat treatment.

quenched and after the second sequence the samples are air-cooled .

Fig. 3a compares the dilatation during the first and the second tempering step corresponding to the standard treatment of the sample quenched with λ=12. During the first 2 h of tempering the dilatation behaves like previously mentioned, indicating alloy carbide formation by a volume decrease and decomposition of retained austenite by the following volume increase. During the second 2 h of tempering the sample just shows a continuous volume decrease which indicates that no new reaction corresponding to retained austenite decomposition occurs. Fig. 3b shows the dilatation of the λ=12 sample during the two tempering steps corresponding to the modified heat treatment. Continuous volume decreases can be seen in both cases. The retained austenite decomposition which comes along with a volume increase as observed in the first tempering step of the standard treatment (Fig. 3a) has been eliminated. The second 3 h of tempering also just show a continuous volume decrease.

As the dwell time of the first tempering step of the modified heat treatment is less than a fourth compared to the standard treatment it is essential to know if the processes during heating to the second tempering step are comparable. Fig. 4 demonstrates the dilatation of the samples during the heating sequence corresponding to the second tempering step. Again, the lines have been vertically translated in order to provide satisfactory comparability. The dashed lines correspond to the standard heat treatment with λ=0.6 and 12. The curves show a continuous increase of the relative length during heating which indicates that no reaction except to the thermal expansion takes place during heating to tempering temperature. The modified heat treatment shows a different behaviour. All three samples (λ=0.6, 6, and 12) show a more or less well distinctive reaction, i.e. a volume decrease at 450 °C ranging up to approximately 600 °C as marked by the grey region within the diagram. The characteristic of this reaction is most pronounced in the case of the λ=0.6 sample.

4.2. Charpy impact testing

Fig. 5 shows the results of the Charpy impact tests. Additionally, hardness values are depicted. The hardness of the samples corresponding to the modified heat treatment shows similar or at least slightly higher values for all three sample conditions than the standard heat treated samples. Hence, comparability of toughness behaviour is given. In case of the standard heat treatment the Charpy-Impact values drop linearly from 20.5 to 15.5 with decreasing cooling rate from λ=0.6 to λ=12. The modified heat treatment shows a similar trend, decreasing impact toughness at lowered quenching rates. But, it causes an obvious increase from 20.5 J to 22.9 J in case of the sample quenched with λ=0.6. In case of the samples quenched with λ=6 and 12 the Charpy impact toughness slightly decreases, from 17.4 to 17.0 and from 15.5 to 14.4, respectively. Fracture surface observation should confirm this behaviour.

Fig. 6 shows SEM micrographs of the fracture surfaces of the tested samples. Standard and modified heat treated samples show similar fracture surfaces; an almost ductile behaviour can be seen. The λ=0.6 samples, hence, those corresponding to the highest cooling rate during hardening, show an almost 100% ductile behaviour. On the other hand, the fracture surfaces corresponding to the slower quenched samples (λ=6, 12) show small amounts of quasi-cleavage and grain boundary structures between the ductile regions. This indicates an influence of the fracture mechanism, most likely by phases which are located at grain boundaries. Again, standard and modified heat treatment samples do not show significant differences.

5. Discussion

The demand for larger tools and enhanced material properties by the tool manufacturing industry forces the tool steel producers to improve their materials and processes. The heat treatment of large blocks does not allow for desired cooling rates during hardening, therefore, modified heat treatments can be the key for improved material properties. As the decomposition of retained austenite during tempering might negatively influence the toughness behaviour of this hot-work tool steel, a tempering treatment has been

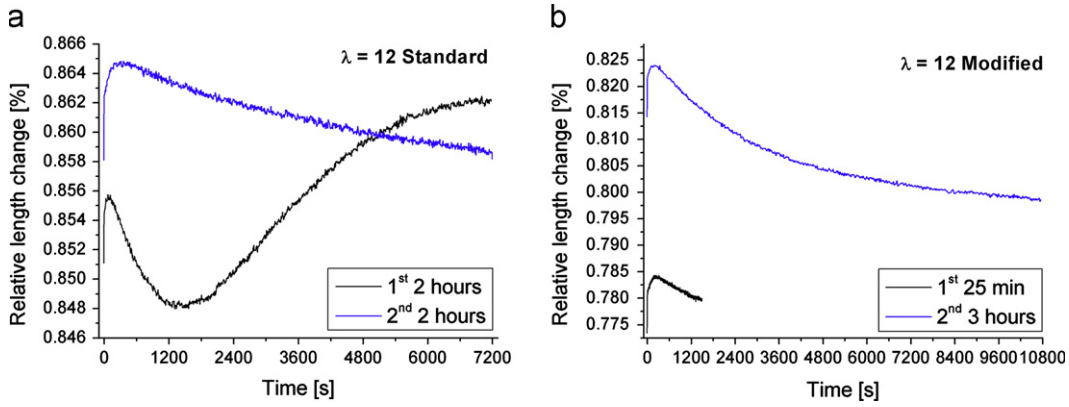

Fig. 3. Dilatation during first and second tempering step of the $\lambda=12$ samples corresponding to (a) the standard treatment and (b) the modified treatment.

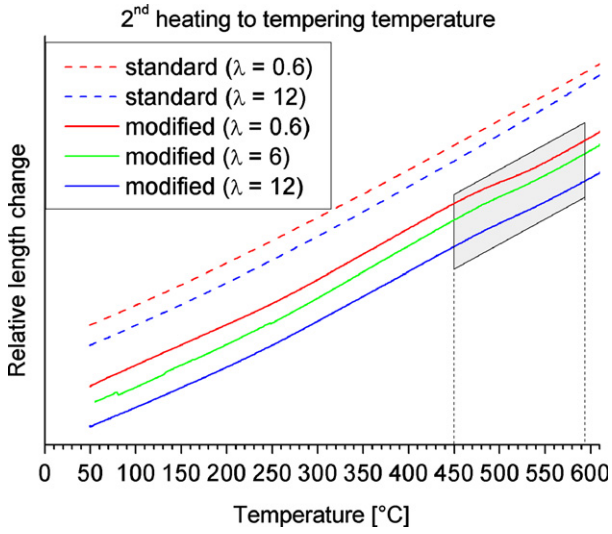

Fig. 4. Dilatation curves corresponding to the heating process of the second tempering sequence.

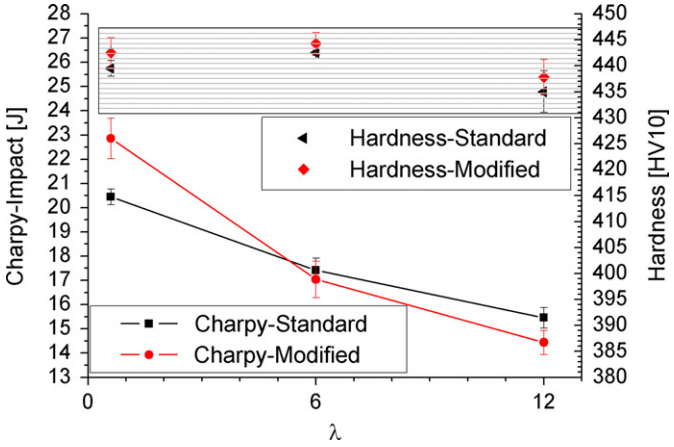

Fig. 5. Charpy-Impact toughness and hardness values in dependence of the cooling parameter λ corresponding to the standard and modified tempering treatment.

established in order to eliminate this direct decomposition. Similar to the investigations of Saha Podder and Bhadeshia [9] the retained austenite decomposition starts after a special dwell time at tempering temperature. Dilatometric experiments have shown that it is possible to avoid the direct retained austenite decomposition by means of a modified heat treatment. Instead of the direct decomposition the retained austenite transforms into martensite after the first tempering step, similar to the high speed steel investigated by Kulmburg et al. [2]. During the second tempering sequence this newly formed martensite is tempered. The corresponding Charpy-impact tests showed that the toughness significantly increases compared to the standard heat treatment in case of high cooling rates during hardening, whereas in case of low cooling rates the toughness is at the same level or even lower. The parameters for Charpy impact testing, U-notch and 200 °C test temperature, have been chosen in order to better distinguish between the fracture mechanisms. Room temperature tested V-notch samples mainly show quasi-cleavage dominated fracture surfaces [3] which are very hard to compare even qualitatively. As preheating of the tools during operation is recommended by the steel producers, the test conditions at elevated temperature seem to be reasonable. As could be seen from the fracture surfaces, the failure of the samples corresponding to the low cooling rates during hardening is partly controlled by interfaces and grain boundaries, hence, the former retained austenite films which are situated between martensitic laths. This indicates that the indirect decomposition occurring during the modified treatment has no positive or even a negative effect on toughness. This might be correlated to a different morphology of the interfacial carbides which have been formed from the newly formed interfacial martensite compared to those directly formed from retained austenite. To prove this, high resolution characterization methods like transmission electron microscopy have to be conducted. At very high cooling rates during hardening the fracture surface is completely ductile which indicates that the failure mechanism is dominated by the matrix. The low volume fraction of retained austenite within this sample leads to a higher carbon supersaturation of the matrix after hardening compared to the samples cooled with low quenching rates. 90% of the total carbon is incorporated in the martensitic matrix [5]. The dilatations during heating to tempering temperature of the second tempering sequence show that in case of the standard heat treatment the total matrix carbon is consumed during the first tempering step. The reaction during heating to the second tempering sequence corresponding to the modified heat treatment shows that new carbides are formed, most likely M_3C as previously reported for this temperature range and material [4]. This reaction corresponding to the formation of new carbides is most pronounced in case of the fast quenched sample which goes hand in hand with the previously mentioned higher supersaturation of the martensitic matrix. This indicates that increased nucleation and growth takes place during the second tempering sequence giving rise for the assumption that the matrix contains finer carbides with a higher number density. This might also explain the same or even slightly increased hardness level after shorter total tempering dwell time. In order to prove this, as a first attempt X-ray peak profile analysis has been performed for the fast quenched sample. Peak profile analysis has been performed corresponding to the method described by

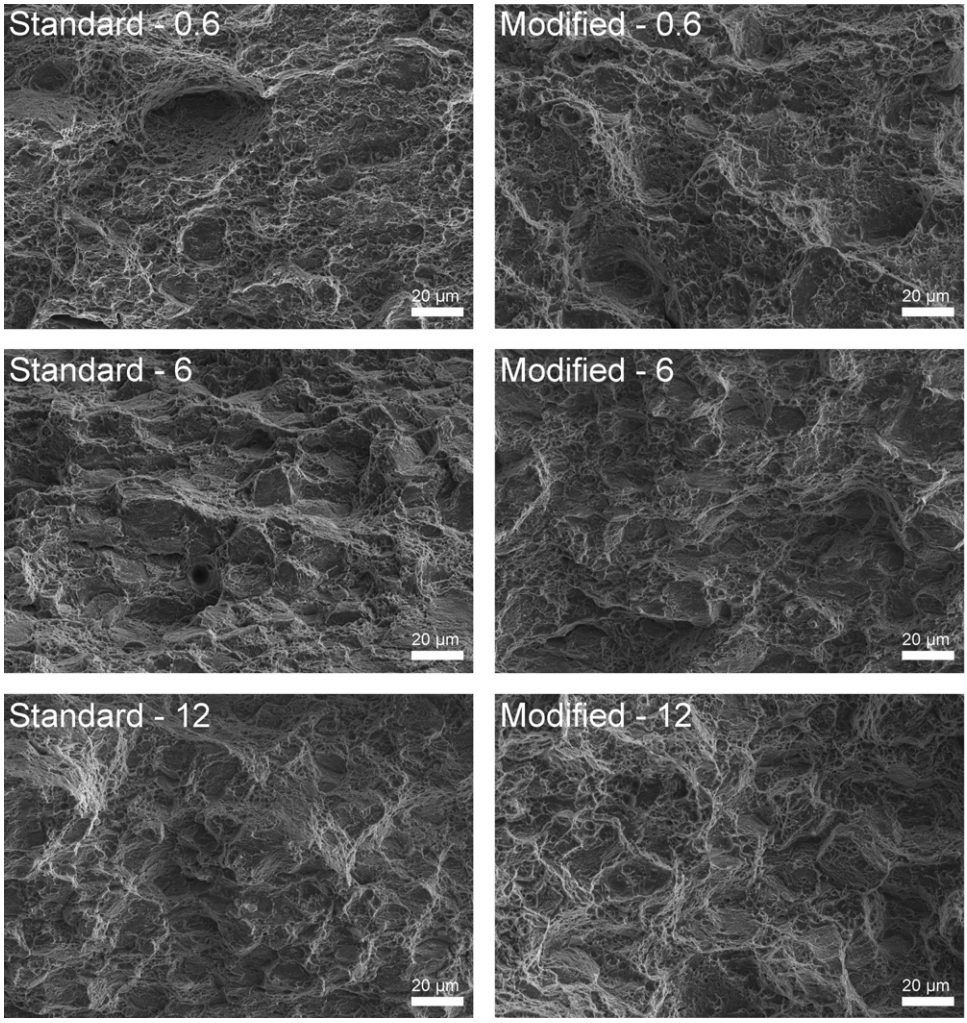

Fig. 6. SEM-micrographs corresponding to the fracture surfaces of the charpy-impact tested samples.

Langford [10]. Leitner et al. proposed that this method is sufficiently sensitive to characterize the matrix of high-speed steels during tempering [11]. This method has been chosen because of the similar matrix characteristics of high-speed steels and the present hot-work tool steel. The results show that the integral breadth of the Gaussian component of the 110_{α} peak corresponding to the modified heat treatment increases 8% compared to that of the standard heat treatment. This indicates a higher lattice distortion after the modified heat treatment, most likely caused by a higher fraction of incoherent interfaces, hence more and smaller embedded particles. This finer distribution of carbides could also be an explanation for the increased impact toughness behaviour of the sample corresponding to the modified heat treatment. Again, for a detailed characterization and description of the carbide distribution high resolution techniques have to be conducted. However, for small tools where high cooling rates during hardening can be realised, this modified heat treatment might improve tool lifetime.

6. Conclusions

Two different tempering treatments have been applied on the common hot-work tool steel X38CrMoV5-1 in order to investigate the influence of the type of retained austenite decomposition with respect to the toughness behaviour. Following conclusions can be drawn:

1. The direct retained austenite decomposition into ferrite and cementite could be eliminated by reducing the dwell time during the first tempering step. Instead of that, the majority of the retained austenite has been transformed into martensite and subsequently tempered.
2. At low quenching rates during hardening, where toughness is limited by interfacial features, the new indirect decomposition leads to a slight degradation of the toughness behaviour. Therefore, at low quenching rates the direct decomposition is recommended.
3. The reduction of the dwell time during the first tempering step causes a second significant nucleation and growth period during the second tempering sequence. This could positively influence the morphology and distribution of secondary carbides.
4. At high quenching rates during hardening the modified tempering treatment increases impact toughness for 12% at a dwell time reduction of 15%. These improvements make the new heat treatment interesting for the production of small-sized tools.

References

[1] G.A. Roberts, G. Krauss, R. Kennedy, Tool Steels, 5th ed., ASM International, Materials Park, OH, 1998.
[2] A. Kulmburg, E. Kaiser, S. Wilmes, Härterei Technische Mitteilungen 42 (1987) 133–138.
[3] S. Mayer, Doctoral Thesis, Department of Physical Metallurgy and Materials Testing, University of Leoben, 2009.

[4] C. Lerchbacher, S. Zinner, H. Leitner, Metall. Mater. Trans. A, http://dx.doi.org/10.1007/s11661-012-1358-3, in press.
[5] C. Lerchbacher, S. Zinner, H. Leitner, Micron 43 (2012) 818–826.
[6] H.K.D.H. Bhadeshia, Bainite in Steels, 2nd ed., IOM Community, London, 2001.
[7] G.R. Speich, W.C. Leslie, Metall. Trans. 3 (1972) 1043–1054.
[8] M.J. Van Genderen, M. Isac, A. Böttger, E.J. Mittermeijer, Metall. Mater. Trans. A 28A (1997) 545–561.
[9] A. Saha Podder, H.K.D.H. Bhadeshia, Mater. Sci. Eng. A 527 (2010) 2121–2128.
[10] J.I. Langford, J. Appl. Crystallogr. 11 (1978) 10–14.
[11] H. Leitner, H. Clemens, Int. J. Mater. Res. (formerly Z. Metallkd.) 100 (2009) 1109–1113.

Publication V

Christoph Lerchbacher, Silvia Zinner, Matthias Nöhrer, Harald Leitner

Evidence of pro-eutectoid cementite formation and its influence on impact toughness of the plastic mould steel X38CrMo16

Submitted to Metallurgical and Materials Transactions A

Evidence of pro-eutectoid cementite formation and its influence on impact toughness of the plastic mould steel X38CrMo16

Christoph Lerchbacher[a], Silvia Zinner[b], Matthias Nöhrer[a], Harald Leitner[c]
[a]Christian Doppler Laboratory of Early Stages of Precipitation, University of Leoben, Franz-Josef-Straße 18, A-8700 Leoben
[b]Böhler Edelstahl GmbH & Co AG, Mariazellerstraße 25, A-8605 Kapfenberg
[c]Department of physical metallurgy and materials testing, University of Leoben, Franz-Josef-Straße 18, A-8700 Leoben

Corresponding author: christoph.lerchbacher@unileoben.ac.at

Submitted to Metallurgical and Materials Transactions A

Abstract

The correlation between cooling rate during hardening and impact toughness is studied for a hardenable martensitic stainless steel X38CrMo16. For that, samples have been produced using cooling rates 6 K/s and 0.12 K/s (λ = 0.5 and 25) in a dilatometer. The slowly quenched sample shows a second martensite start temperature (Ms) at 593.15 K (320°C). Transmission electron microscopy revealed the existence of carbides along former austenite grain boundaries in case of the slowly quenched sample. Increased chromium contents and an orientation relationship with at least one of the adjacent matrix grains confirm that those carbides are formed in the austenite directly during cooling before reaching Ms. Corresponding inter-crystalline fracture surfaces of the as-quenched samples show fernlike, dendritic carbide structures on the grain boundaries which are attributed to pro-eutectoid cementite. Beneath the predominantly ductile fracture, small amounts of intercrystalline cleavage occur after impact testing the hardened and tempered samples. The cleavage surfaces do also show these dendritic pro-eutectoid carbide structures. From that, a correlation between the occurrence of those grain boundary carbides and the decreased impact toughness of slowly quenched and tempered samples is given.

Introduction

The investigated tool steel X38CrMo16 is a nitrogen alloyed hardenable martensitic stainless chromium steel and is mainly used for plastic mould applications or for die casting applications. The processing of chemically aggressive plastics demands special properties such as high corrosion resistance, well-balanced toughness and hardness, wear resistance as well as good machinability and polishability. These properties are gained by a well-defined composition, high micro-cleanness and a well-defined heat treatment. The latter consists of an austenitisation treatment with subsequent hardening followed by a multi-step tempering procedure [1]. Final mechanical properties are controlled by the tempering parameters. The tempering behaviour and its influence on mechanical properties of martensitic stainless steels containing carbon, nitrogen or both have been extensively studied [2–5]. However, toughness properties are also influenced by the cooling rate during hardening. Low impact toughness is observed for low cooling rates during hardening, although no bainite or perlite is formed, as it

has been reported for similar tool steels [6–8]. This behaviour becomes prominent for large tools where the cooling rate during hardening cannot be set high enough.

So-called pro-eutectoid carbides which are formed within the austenitic phase field during cooling have been found at former austenite grain boundaries for the steel grade X20CrNiMo15-2 after slow cooling. Decreasing cooling rates lead to a higher intensity of the formation of such carbides. Those carbides are meant to play a major role regarding toughness because they build a film-like network around former austenite grain boundaries which enhances crack growth. Contrary to that, pro-eutectoid carbide formation is almost suppressed in the corresponding nitrogen steel N20CrNiMo15-2 [5]. The pro-eutectoid carbide transformation has been studied for a long time ago. $Cr_{23}C_6$ carbides have been found at grain boundaries in a heat treated commercial grade AISI304 stainless steel [9]. Those precipitates have a flat dendritic form. Later it was shown that these precipitates lie within the plane of the grain boundaries [10] and that they can also obtain triangular, trapezium, cubic and rectangular shapes on coherent twin boundaries [11,12]. Spanos and Kral give an extensive review on the pro-eutectoid cementite transformation in steels, summing up morphologies, orientation relationships and formation mechanisms [13]. Newer studies using deep etching methods on hypereutectoid model alloys proof the dendritic morphology of this grain boundary cementite [14–16].

Another cooling rate dependent mechanism which influences toughness has been recently proposed for a hot-work tool steel. The increase of retained austenite content and its decomposition during tempering have been found to be responsible for a toughness loss at low quenching rates [17,18]. Laminary arranged carbides form from the interlath retained austenite films and enhance crack propagation [19].

Thus, the aim of the present work is the identification of the origin of the cooling rate dependent toughness behaviour for nitrogen alloyed plastic mould steel X38CrMo16. Therefore, the microstructure of the as-hardened material has been studied with the focus laid on the influence of the cooling rate. Impact bending tests and corresponding fracture surface analysis have been performed on the as-hardened as well as on the tempered material in order to provide a correlation to the toughness properties.

Experimental

The nominal composition of the investigated plastic mould steel X38CrMo16 is given in Table 1. The samples for the microstructural investigations have been heat treated in a dilatometer DIL 805A from Bähr Thermoanalyse GmbH and the corresponding relative length changes have been recorded. For that, samples of 15 mm in length and 5 mm in diameter have been used. The material has been austenitised at 1020°C with a dwell time of 30 minutes. Subsequent quenching has been conducted with quenching rates 6 K/s and 0.12 K/s (λ = 0.5 and 25). Tempering has been done at 883.15 K (610°C) two times for 2 hours.

For the microstructural investigations electron microscopy has been conducted using a Zeiss EVO50 scanning electron microscope (SEM) and a Philips CM12 transmission electron microscope (TEM). TEM sample preparation has been conducted using standard electrochemical etching with electrolyte A2 provided by Struers.

Impact testing has been performed with a 300 J impact pendulum from Zwick. The mean absorbed energy was measured using 3 specimens per sample state. For the impact tests un-

notched specimens with dimensions of 55 x 10 x 7 mm^3 according to SEP (Stahl und Eisen Prüfblatt) 1314 were used. The samples have been heat treated conducting a special instrumentation in the quenching dilatometer in order to simulate real quenching conditions and to provide comparability with the samples heat treated for the length change measurements. Fracture surface analysis was carried out by scanning electron microscopy using a Zeiss EVO50.

Table 1: Nominal composition of the investigated plastic mould steel X38CrMo16

	C	Si	Mn	Cr	Mo	Ni	V	N	Fe
wt%	0.28	0.26	0.63	14.45	0.92	0.84	0.06	0.10	bal.

Results

Figure 1a depicts the temperature program which has been applied to the samples in order to demonstrate the difference of cooling paths during the exponential cooling with 6 K/s and 0.12 K/s (λ = 0.5 and 25). In Figure 1b the corresponding dilatometer curves are shown. It is obvious that during cooling from austenitisation temperature no reaction occurs at high temperatures. For both cooling rates, significant positive volume changes occur at 493.15 K (220°C), indicating the start of the martensitic transformation (Ms). In case of the slowly quenched sample (0.12 K/s) an additional more or less distinct change in slope occurs at approximately 593.15 K (320°C). The change in slope is highlighted in the zoomed insert given in Figure 1b. This point is termed Ms', indicating a preceding martensitic transformation of regions most likely being depleted in carbon at that time [20]. This kink in the dilatometer curve of the slowly quenched sample is a sign that a reaction might have happened within the austenite during cooling.

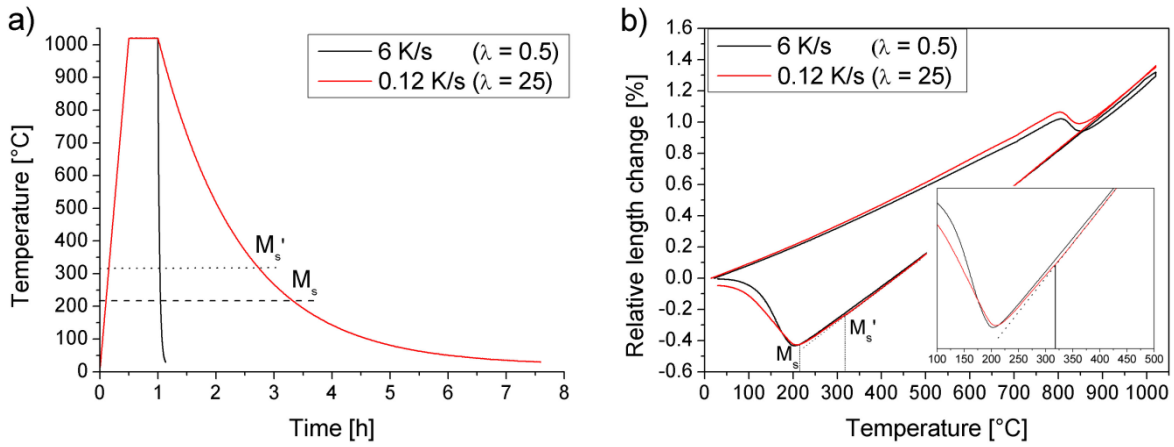

Figure 1: Heat treatment characteristics including cooling paths after the austenitisation treatment corresponding to the samples quenched with 6 K/s and 0.12 K/s (λ = 0.5 and 25), respectively (a); Corresponding relative length changes recorded by dilatometry (b).

Microstructure

The reaction found by the dilatometer experiments most likely goes hand in hand with a change in the microstructure. This has to be proven by microstructural investigations. In order to give an insight into the overall microstructure, corresponding SEM micrographs are shown in Figure 2. The contrast gained by the back-scattered electrons is not very well because of the

high chromium content within the matrix. However, a martensitic microstructure with embedded globular carbides with sizes up to one micron can be seen in both cases. The martensitic structure, size and volume fraction of the carbide phase do not differ between the differently quenched samples. The globular carbides are chromium rich particles which have not been dissolved during the austenitisation treatment. No carbides are visible on interfaces or on grain boundaries from those micrographs.

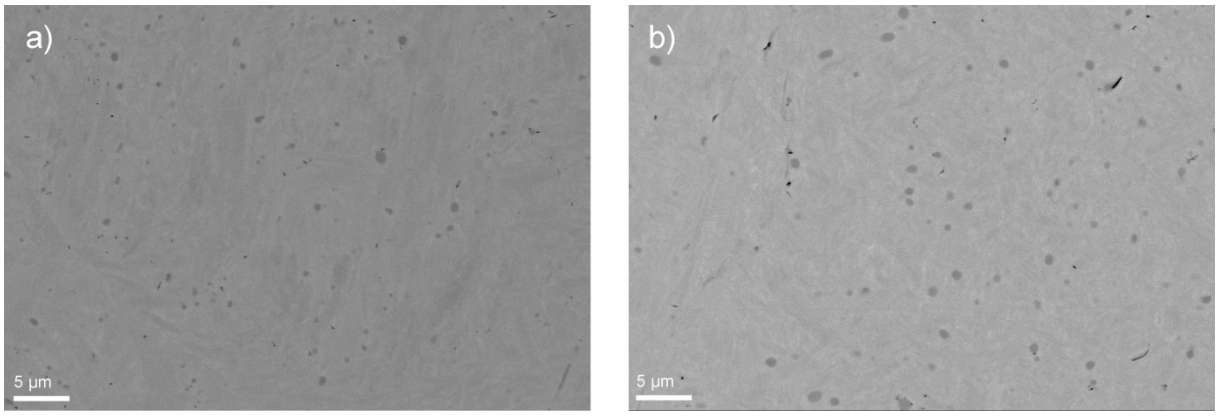

Figure 2: SEM micrographs (BSE) corresponding to the samples quenched with 6 K/s (λ = 0.5) (a) and 0.12 K/s (λ = 0.25) (b).

Precipitates at former austenite grain boundaries can be found with higher magnifications at specific sites of the slowly quenched sample as demonstrated in Figure 3. The TEM micrograph given in Figure 3a shows a carbide network along former austenite grain boundaries. The network seems to contain several separate elongated elements. EDX measurements (not shown here) revealed increased carbon contents and increased contents of carbide forming elements such as chromium, molybdenum and vanadium. Thus, the precipitates are carbides. The thicknesses of those elongated carbide structures are in the range of 100 nm. The bright regions coming along with the carbide network is most likely due to chromium depletion within those regions. The foils have been produced by electrochemical etching and those chromium depleted zones naturally experience an increased etching rate. The carbide structures have been proved by EDX to contain increased chromium contents which confirms this assumption. Figure 3b shows the occurrence of carbides at grain boundaries with a different morphology. Globular carbides with a diameter of approximately 50 nm are visible. Again, the carbides are accompanied by chromium depleted zones. Electron diffraction on the grain boundary carbide depicted in Figure 4a reveals that the carbide is a Fe_3C and that it has an orientation relationship to at least one of the adjacent matrix grains. From the diffraction pattern given in Figure 4b it could be concluded that the (-321) plane of the carbide is parallel to the (-200) plane of the martensite grain. The carbide is tilted in [111] zone axis which is parallel to the [012] direction of the martensite lattice. It must be noted that those grain boundary carbides were characterised exclusively in the slowly quenched specimen.

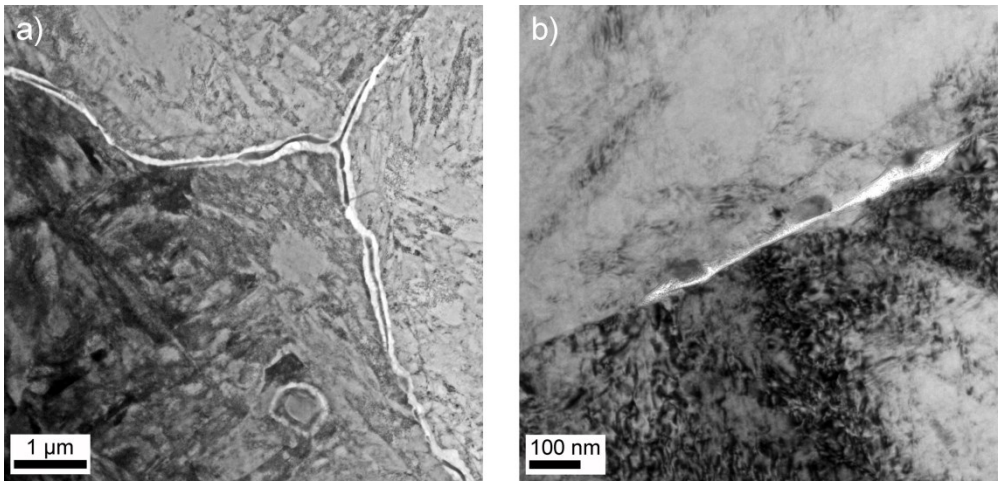

Figure 3: TEM micrographs of the slowly quenched sample (0.12 K/s, λ = 25) showing partly continuous carbide films (a) and discrete precipitates (b) along former austenite grain boundaries.

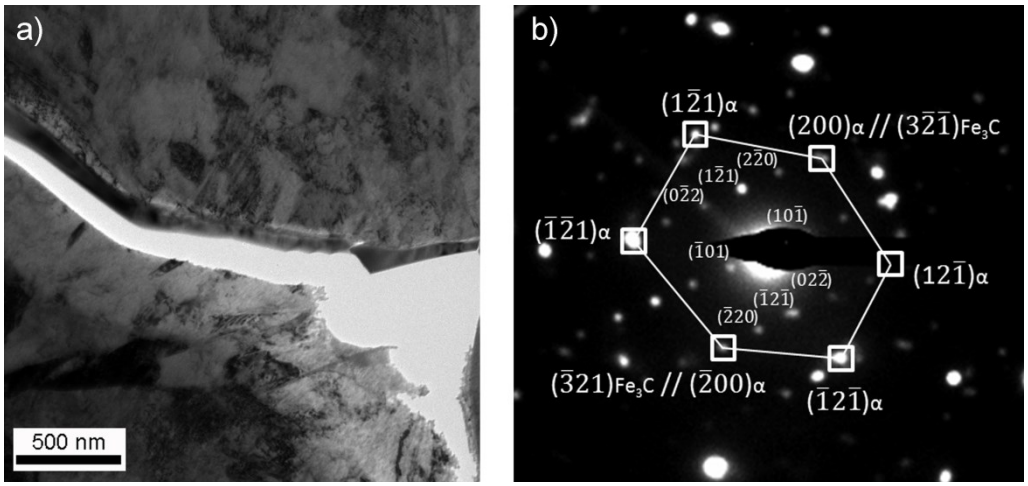

Figure 4: TEM micrograph showing an elongated grain boundary carbide in the slowly quenched sample (a); Corresponding indexed diffraction pattern (b).

Impact toughness

The observed microstructural distinctions between fast and slowly quenched samples lead to significant differences in impact energy and fracture behaviour. Results of the impact bending tests are summarized in Figure 5. In the as-quenched condition, shown as the filled columns, both samples show equal impact energies in the range of 20 J. After the two-step tempering treatment at 883.15 K (610°C) the impact values rise up in the case of the fast quenched sample to 180 J and in the slowly quenched sample to 110 J, which is clearly lower compared to the fast quenched sample. Figure 6 depicts the fracture surfaces corresponding to the as-quenched samples. From the low magnification images it is clearly visible that failure is dominated by cleavage fracture for both samples, but the fracture mechanism is transcrystalline in case of the fast quenched sample (Figure 6a) and inter-crystalline in case of the slowly quenched sample (Figure 6c). Analysis at higher magnification shows that the fracture surface of the fast quenched sample contains a lot of globular carbides in the size range of microns (Figure 6b). On the other hand, fern-like carbide structures occupy the inter-

crystalline fracture surfaces in case of the slowly quenched sample (Figure 6d). Those carbide structures can be found on the entire fracture surface. The assumption of those structures to correspond to carbides has been revealed by EDX in both cases. Figure 7 shows the fracture surfaces corresponding to the tempered samples. Failure is dominated by ductile fracture in both cases, but also small amounts of cleavage surfaces can be seen. A closer look onto those cleavage fracture surfaces displays the difference between fast and slowly quenched samples. In case of the fast quenched sample the cleavage surfaces are transcrystalline and very smooth, whereas in case of the slowly quenched sample the cleavage surface again corresponds to a grain boundary region containing the previously mentioned fern-like carbide structures.

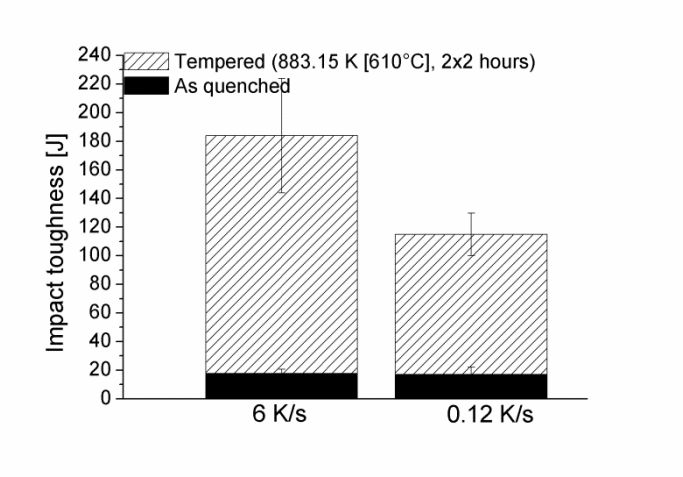

Figure 5: Results of the impact bending tests corresponding to the as-quenched and the tempered sample state.

Discussion

The martensitic chromium stainless steel X38CrMo16 is often exposed to cyclic impact loading during plastic mould processing. Therefore, sufficient impact toughness is required for a satisfying tool performance. Tool steel producers suffer from low impact toughness properties when hardening of the material occurs at low quenching rates, which are unavoidable for large dies. The microstructural features which are responsible for this loss in toughness are characterized. For this, microstructure and toughness properties of samples quenched with 6 K/s and 0.12 K/s (λ = 0.5 and 25) have been compared.

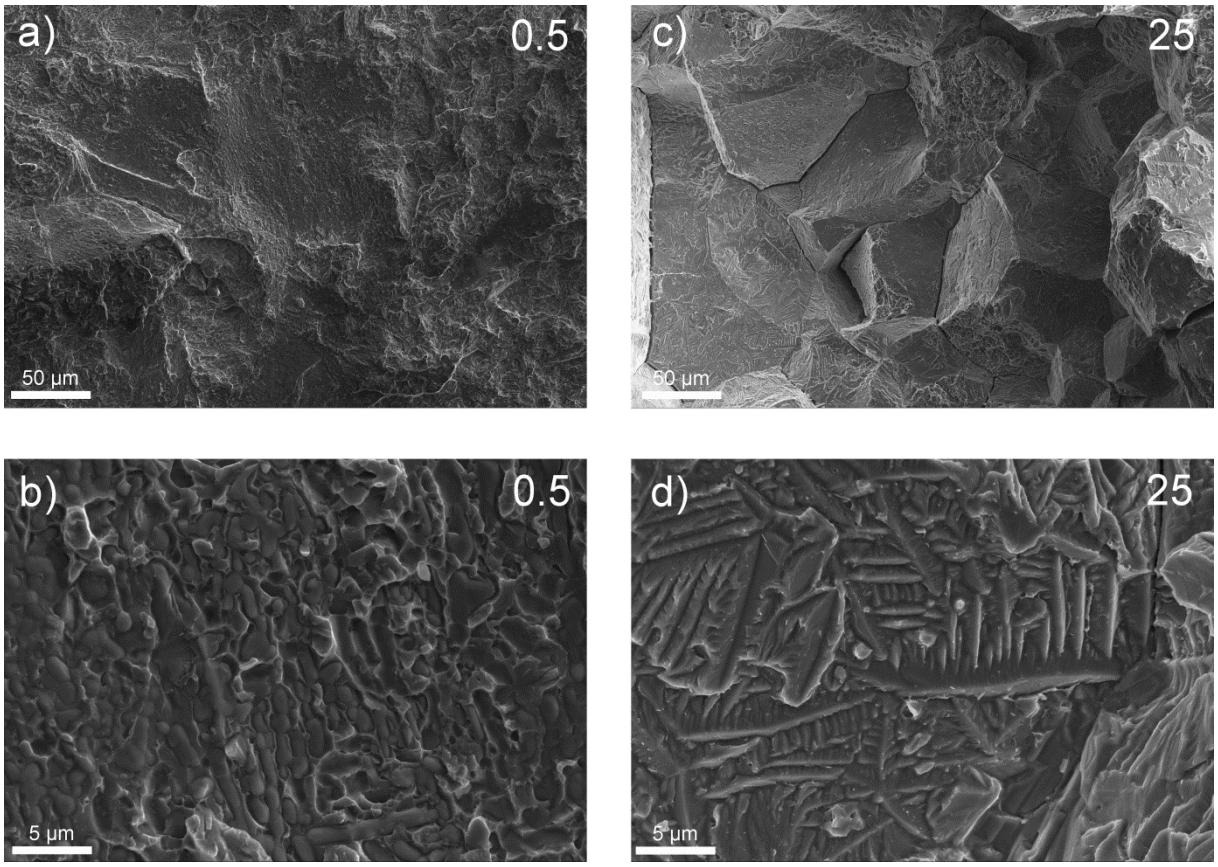

Figure 6: SEM micrographs of the fracture surfaces corresponding to the as-quenched samples. Overview of the fast quenched (6 K/s, λ = 0.5) sample (a); Detail of the corresponding sample (b); Overview of the slowly quenched (0.12 K/s, λ = 25) sample (c); Detail of the corresponding sample (d).

The martensite start temperature is 493.15 K (220°C) for both samples. Another change in volume can be observed at approximately 593.15 K (320°C) in case of the slowly cooled sample. This is most likely due to an increased martensite start temperature corresponding to regions which have been depleted in carbon during cooling of the austenite. Kulmburg proposed this so-called grain boundary martensite to be a result of formerly precipitated carbides at the grain boundaries. The grain boundary near regions deplete in carbon and carbide forming elements during the precipitation at the grain boundaries [20]. The lower amount of solute elements increases the martensite start temperature for these regions and causes the kink in the dilatometer curve. The heavily etched regions beneath the grain boundary carbides of the electro-polished TEM samples confirm this assumption. Due to the chromium enrichment of the carbides, which has been revealed by EDX measurements, the grain boundary near regions are not only depleted in carbon, but also in chromium. This chromium depletion causes an increased etching rate during the sample preparation. Therefore, the earlier formed grain boundary martensite could not be analysed by TEM. However, this was not the intention of the present work. The chromium enrichment of the carbides indicates that they have formed at increased temperatures where the chromium atoms are mobile, hence, significantly above the martensite start temperature. The chromium enrichment and the evidence of an orientation relationship to the matrix indicate that these grain boundary carbides have definitely formed in the austenitic phase during cooling. Additionally, the carbides have been attributed to cementite by diffraction experiments.

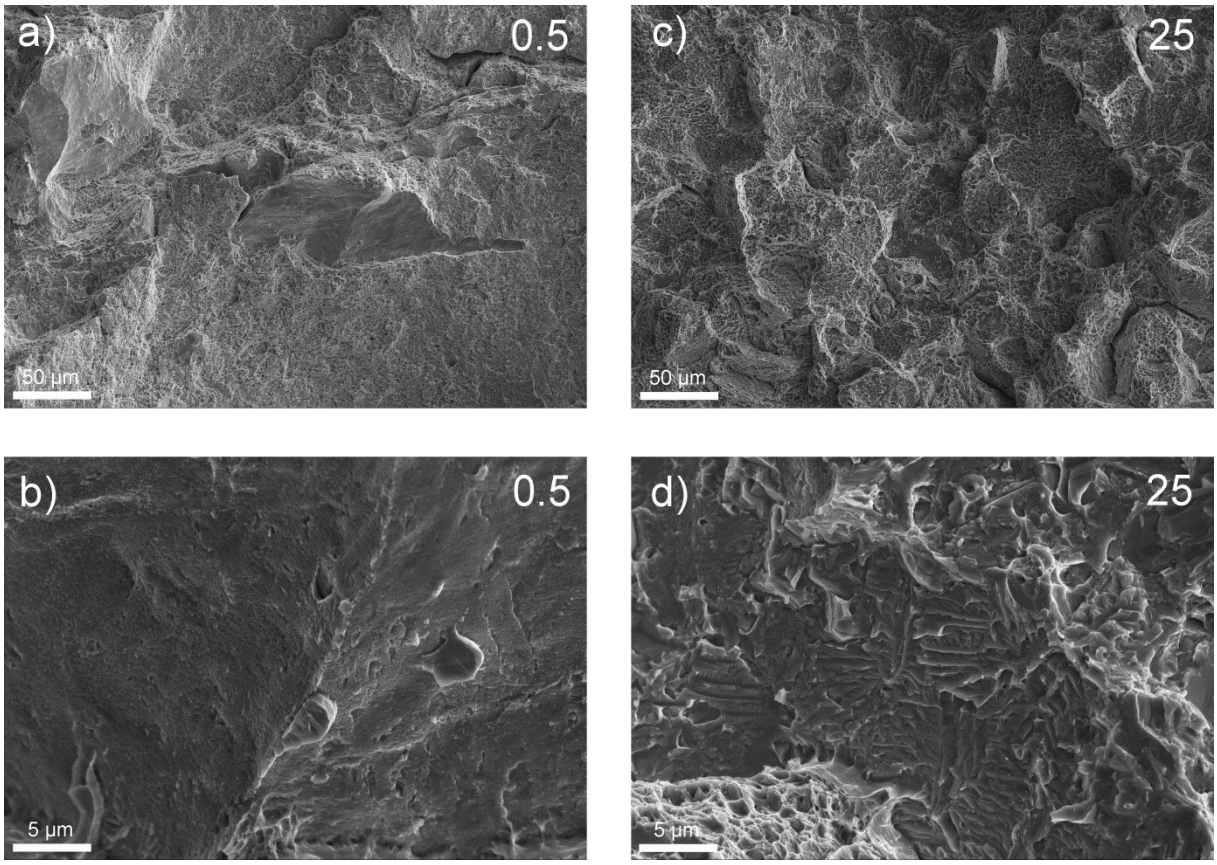

Figure 7: SEM micrograph of the fracture surface of the fast quenched (6 K/s, λ = 0.5) and tempered sample showing predominantly ductile fracture with small amounts of cleavage fracture (a); Detail of the corresponding cleavage fracture (b); SEM micrograph of the fracture surface of the slowly quenched (0.12 K/s, λ = 25) and tempered sample showing predominantly ductile fracture with small amounts of cleavage fracture (c); Detail of the corresponding cleavage fracture (d).

The pro-eutectoid cementite formation from austenite has been studied for decades. Several orientation relationships between austenite and pro-eutectoid cementite at grain boundaries have been published [21–23]. For convenience, those investigations have been predominantly performed on hypereutectoid high manganese austenitic steels. The orientation relationship found in this work is related to the martensitic matrix and the pro-eutectoid cementite which has already been formed in the austenite. For the moment, the evidence of an orientation relationship serves the purpose of the present work. An assessment of the orientation relationship presented here with respect to the typical orientation relationships given in literature will be part of future work.

The influence of those precipitates on the impact toughness is not relevant in case of the as-hardened samples. After hardening, the as-quenched martensite is heavily distorted, which generally leads to low impact values during impact bending testing. The overall stresses do also act on the grain boundaries. As they are already weakened by the grain boundary cementite the fracture is intercrystalline in case of the slowly quenched sample. However, due to the high stresses within the matrix also the fast quenched sample collapses at low impact energies, but the cleavage fracture is transcrystalline because the grain boundaries are not weakened in that case. The fracture surface corresponding to the slowly quenched specimen gives a deeper insight into the morphology of those carbides. The entire grain boundaries are covered by cementite structures which are described in literature as fernlike or dendritic pro-

eutectoid cementite [13]. Although these carbides are not visible in the common SEM micrographs, the inter-crystalline fracture surfaces nicely demonstrate their occurrence, which indicates that this cementite type grows predominantly in the grain boundary plane and not into the grains. The reason is that crystallographic constraints on cementite precipitate growth are more relaxed within the more open structure of the grain boundaries. This allows solid-state dendrites to form along them [14]. The investigations of Kral and Spanos demonstrate that most of the pro-eutectoid grain boundaries predominantly have this dendritic form even when they have been described as plates in earlier studies. This could be found out by a 3D-visualisation made possible by deep etching procedures [15,16]. This might also explain the variable form of appearance of the precipitates in the TEM investigations of the present work. Depending on the orientation of the dendritic structure in relation to the 2D-sample, the nature of the carbides can differ. When the brakes of the dendrite are cross-sectioned, singular globular particles occur in the 2D-micrograph. When the cross-section goes along a dendrite the carbide structure occurs as film or separate elongated particles.

Due to the stress relaxation of the martensitic matrix during tempering, the tempered samples show significantly higher impact energies. The fracture surfaces of the corresponding samples reveal a predominantly ductile fracture. For both cooling rates, small amounts of cleavage fracture occur. In case of the fast quenched sample these regions are smooth transcrystalline surfaces. In case of the slowly quenched sample the cleavage fracture surfaces correspond to grain boundaries which are decorated by dendritic pro-eutectoid cementite particles. Thus, weakening of the grain boundaries by those carbides becomes prominent for the failure in case of the tempered sample condition where the matrix is relaxed. This explains the significantly lower impact energies obtained by the impact tests of the slowly quenched sample compared to the fast quenched one. Retained austenite decomposition has not been considered for the interpretation since the volume fraction in the as-quenched material has been found to be lower than 3 percent for both cooling rates. In a similar hot-work tool steel such low amounts have been proposed not to influence the impact toughness [17].

Conclusions

Two different cooling rates have been applied to a plastic mould steel X38CrMo16 during hardening in order to correlate microstructural distinctions with impact toughness properties of the material. Following conclusions can be drawn:

1. Fernlike pro-eutectoid cementite precipitates at former austenite grain boundaries during quenching from austenitisation temperature in case of low cooling rates. Increased chromium contents and an orientation relationship to at least one of the adjacent matrix grains reveal that those carbides have formed at elevated temperatures, hence, directly from the austenite during cooling.
2. The occurrence of those carbides weakens the former austenitic grain boundaries. Consequently, amounts of intercrystalline cleavage lead to lowered impact toughness and insufficient performance of the fully heat treated material.
3. In the as-hardened material the grain boundary carbides do not significantly influence toughness. Although intercrystalline cleavage is obvious in case of the slowly quenched sample, impact values are on the same level as measured for the fast cooled sample. The pro-eutectoid carbides become the dominant factor regarding impact toughness not before the martensitic matrix is relaxed.

References

[1] G.A. Roberts, G. Krauss, R. Kennedy, Tool Steels, 5th ed., ASM International, Materials Park, OH, 1998.

[2] V.G. Gavriljuk, H. Berns: Proceedings of the 1998 5th International Conference on High Nitrogen Steels (HNS), Stockholm, 1998.

[3] H. Berns, V.A. Duz, R. Ehrhardt, V.G. Gavriljuk, Y.N. Petrov, A.V. Tarasenko: Materials Research and Advanced Techniques, 1997, vol. 88, pp. 109–116.

[4] H. Berns, S.N. Bugajchuk, V.A. Duz, R. Ehrhardt, V.G. Gavriljuk, Y.N. Petrov, I.A. Yakubzov: Steel Research, 1994, vol. 65, pp. 444–450.

[5] H. Berns, R. Ehrhardt: Steel Research, 1996, vol. 67, pp. 343–349.

[6] H. Jesperson: Metallurgia Italiana, 2009, vol. 101, pp. 55–60.

[7] S. Mayer, C. Scheu, H. Leitner, H. Clemens, I. Siller: BHM Berg- Und Hüttenmännische Monatshefte, 2007, vol. 152, pp. 132–136.

[8] K. Bungardt, O. Mülders, R. Meyer-Rhotert: Archiv Für Das Eisenhüttenwesen, 1966, vol. 37, pp. 381–389.

[9] E.M. Mahla, N.A. Nielsen: Transactions of the ASM, 1951, vol. 43, pp. 290.

[10] F.G. Wilson: Journal of the Iron and Steel Institute, 1971, vol. 209, pp. 126–130.

[11] U.E. Wolff: Transactions of the AIME, 1966, vol. 236, pp. 19.

[12] L.K. Singhal, J.W. Martin: Transactions of the AIME, 1968, vol. 242, pp. 814.

[13] G. Spanos, M.V. Kral: International Materials Reviews, 2009, vol. 54, pp. 19–47.

[14] M.V. Kral, G. Spanos: Acta Materialia, 2003, vol. 51, pp. 301–311.

[15] M.V. Kral, G. Spanos: Scripta Materialia, 1997, vol. 36, pp. 875–882.

[16] M.V. Kral, G. Spanos: Acta Materialia, 1999, vol. 47, pp. 711–724.

[17] C. Lerchbacher, S. Zinner, H. Leitner: Materials Science and Engineering A, 2013, vol. 564, pp. 163–168.

[18] S. Mayer: Doctoral Thesis, Department of Physical Metallurgy and Materials Testing, Leoben (2009).

[19] C. Lerchbacher, S. Zinner, H. Leitner: Metallurgical and Materials Transactions A, 2012, vol. 43, pp. 4989–4998.

[20] A. Kulmburg, F. Korntheuer: Journal of Heat Treatment and Materials, 1976, vol. 31, pp. 195–204.

[21] W. Pitsch: Acta Metallurgica, 1962, vol. 10, pp. 897–900.

[22] S.W. Thompson, P.R. Howell: Scripta Metallurgica, 1987, vol. 21, pp. 1353–1357.

[23] D.S. Zhou, G.J. Shiflet: Scripta Metallurgica Et Materialia, 1992, vol. 27, pp. 1215–1218.